

A Dissertation

entitled

Mitigating Biomechanical Complications of Growth Rods in Juvenile Idiopathic

Scoliosis

by

Aakash Agarwal

Submitted to the Graduate Faculty as partial fulfillment of the requirements for the

Doctor of Philosophy Degree in Biomedical Engineering

---

Dr. Vijay K. Goel, Committee Chair

---

Dr. Anand Agarwal, Committee Member

---

Dr. Sarit Bhaduri, Committee Member

---

Dr. Scott C. Molitor, Committee Member

---

Dr. Charles Armstrong, Committee Member

---

Dr. Patricia R. Komuniecki, Dean  
College of Graduate Studies

The University of Toledo  
May 2015

Copyright 2015, Aakash Agarwal

This document is copyrighted material. Under copyright law, no parts of this document may be reproduced without the expressed permission of the author.

An Abstract of  
Mitigating Biomechanical Complications of Growth Rods in Juvenile Idiopathic  
Scoliosis

by

Aakash Agarwal

Submitted to the Graduate Faculty as partial fulfillment of the requirements for the  
Doctor of Philosophy Degree in Biomedical Engineering

The University of Toledo  
May 2015

Growth rods are used to limit the progression of scoliosis without restraining the opportunity for spinal growth. However, major complications like rod breakage, screw loosening, and altered sagittal contour have been encountered. Out of all above, rod breakage is the most common complication with highest number of incidences reported in clinical literature. Thompson et al [1] reported the early 7 fractures in 28 patients with growth rods. More recently, Yang et al [2] presented a thorough retrospective review, where they found eighty-six rod fractures occurred in 49 of 327 total patients (49 of 327, 15%). While pedicle screws provide better anchorage, screw loosening does indeed occur.[3, 4] Some researchers also believe that the distraction forces applied are so high that these instead are stimulating growth rather than sustaining it.[5, 6] Suboptimal distraction could also lead to poor sagittal contours in juvenile patients.[7] Therefore, there is a need to optimize the distraction force and distraction frequency for sustained spinal growth, along with unaltered final sagittal contour, lower stresses on the rods and minimal loads at the screw-bone interface.

The current study hypothesizes that there exists an optimal distraction force that will sustain the growth of the spine, i.e. growth will be equal to normal spinal growth.

Furthermore this optimal distraction force produces minimum change in sagittal contours, and results in lower von Mises stresses on the rods and minimum force at the pedicle screw-bone interface at the end of distraction interval. The current study also hypothesizes that the optimal distraction force increases with increases in stiffness of the spine, and the optimal distraction force decreases with an increase in distraction frequency. In conjunction, the maximum stresses on the rod (at an optimal distraction force) decreases with increase in distraction frequency. Additionally, it hypothesizes that the spines with increased stiffness requires a higher frequency of distraction for the rods to be under similar stress conditions.

Based on the above hypotheses, the first objective of this study was to analyze the effect of magnitude of distraction forces on the T1-S1 growth, maximum von Mises stresses on the rods, sagittal contours, and load at the pedicle screw-bone interface. The second objective was to quantify the maximum von Mises stresses on the rod, at different distraction intervals, for a period of 24 months to analyze the change in stresses with variance in frequency of distraction.

To achieve these objectives, multiple representative scoliotic spine models were developed, and personalized growth rods were used as instrumentation. The material properties were adapted from literature, and subroutines consisted of mimicking Hueter Volkmann's principle and spinal auto-fusion. Simulation steps incorporated 6 months of growth under various distraction forces to analyze the effects of distraction force on the biomechanics of the spine with growth rods, and 24 months of growth under various intervals of distraction, to analyze the effects of distraction interval on propensity of rod fracture.

Results showed that an optimal distraction force existed for each model, at which the growth was sustained with minimum stresses on the rod, lower loads at screw-bone interface and unaltered sagittal contours. Additionally for all models, analyzing the frequency showed that the stresses on the rods were highest for 12-month distraction (2 distractions in 2 years) and lowest for 2-month distraction (12 distractions in 2 years). These results followed similar trends, with numerical values of optimal distraction forces at close proximity for various representative scoliotic spine models.

Furthermore, to elucidate the link between higher loads at the screw-bone interface with screw loosening, an *in vitro* study was performed. This study proved that the pull out strength of pedicle screws (4.5 mm diameter, 1.5 mm thread depth, and double lead) showed significant reduction after 6 months of fatigue at higher distraction forces compared to optimal distraction forces.

Next, a sensitivity study was performed by varying the material properties of the disc and hence altering the axial stiffness of a scoliotic spine model (Group 1A representative spine). It was found that the stresses on the rod increased with increases in axial stiffness of the spine, and consequently the required optimal frequency to achieve a factor of safety of 2 for growth rods (Ti6AL4V with 4.5mm diameter) increases alongside.

In conclusion, this study suggests that as the distraction forces vary so do its effect on loads at the screw-bone interface and stresses on the rods. The results of this study signify the importance of shorter distraction periods in reducing the stresses on the rods.

I would like to dedicate this work to my family, Dr. Vijay K Goel, Dr. Anand Agarwal, and all my friends who believed in me and have been there through thick and thin. I hope the results of this work would ultimately help in our unified goal of providing the young juvenile patients with better care and less morbidity. As Bob Brown had said “The future will either be green or not at all”

## **Acknowledgements**

First and foremost I express my sincere gratitude to my advisor, Dr. Vijay K Goel, whose expertise, constant support and guidance have allowed me to reach this point. Second, I would like to thank my committee members, Dr. Anand Agarwal, Dr. Scott Molitor, Dr. Sarit Bhaduri, and Dr. Charles Armstrong for their valuable suggestions during this period.

I would also like to thank Amanda Zakeri for working with me in my final year to help develop scoliotic models and David Dick for his assistance with *in vitro* tests. In addition to this, I am grateful to the department of bioengineering, industrial innovation and partnerships (IIP) grant, department of orthopedics, and Dr. Eda Ayan Yildirim for their financial support during different phases of my PhD program.

Finally I take the opportunity to express my profound gratitude to my parents, my uncle and aunt, and my brother for their unconditional moral support and belief in me. I would also like to thank Dr. Arvind Jayaswal for his continued clinical support all along.

## Table of Contents

Acknowledgements	vii
List of Tables	xii
List of Figures	xiii
<b>List of Abbreviations</b>	xxiii
<b>List of Symbols</b>	xxiv
1. Introduction	1
1.1 Rationale for Research.....	1
1.2 Outline.....	6
2. Juvenile Idiopathic Scoliosis	8
2.1 Anatomy of a Normal Spine.....	8
2.2 Functional Components of a Vertebra.....	14
2.3 Curves of Spine.....	15
2.4 Scoliosis.....	16
2.5 Treatment of Juvenile Idiopathic Scoliosis.....	18
3. Growth Rods and Occurrence of Fracture	22
3.1 Introduction.....	22
3.2 History of Fracture in Fusion-less Instrumentation.....	23
3.3 Growth Rod Fracture.....	24



3.4 Advent of non-invasive distractions.....	27
3.5 Summary.....	29
4. Materials and Method.....	32
4.1 Introduction.....	32
4.2 Novel Methodology for Finite Element Model Development.....	37
4.2.1 Normal Juvenile Spine.....	39
4.2.2 Representative Juvenile Scoliotic Models.....	42
4.2.3 Growth Rod Design and Instrumentation.....	48
4.2.4 Material Properties and Boundary condition.....	52
4.3 Incorporation of Growth modulation.....	57
4.4 Incorporation of Autofusion.....	58
4.5 Parametric study.....	62
4.5.1 Effect of Distraction Forces.....	62
4.5.2 Effect of Distraction Frequency.....	63
4.6 Sensitivity Study.....	65
4.7 <i>In Vitro</i> Experiment: Correlation of Loads to Screw Loosening.....	66
5. Results.....	73
5.1 Introduction.....	73
5.2 Effect of Distraction Force on Normal Juvenile Spine.....	73
5.3 Effect of Distraction Frequency on Normal Juvenile Spine.....	82
5.4 Effect of Distraction Force on Representative Juvenile Spines.....	89
5.5 Effect of Distraction Frequency on Representative Juvenile Spines.....	115
5.6 Sensitivity Study.....	122

5.7 <i>In vitro</i> evaluation of screw loosening.....	124
6. Discussion	125
6.1 Overview.....	125
6.2 Effect of distraction force.....	126
6.3 Effect of distraction frequency.....	128
6.4 Sensitivity Study.....	133
6.5 <i>In Vitro</i> Screw Loosening.....	135
6.6 Limitations.....	135
6.7 Conclusions.....	139
References	141
A. The Matlab Codes	158



## List of Tables

4.1 A comparison between the vertebral body and intervertebral disc heights of the scaled down model and the 3D reconstruction of a 9 year old juvenile CTs.....	39
4.2 The material properties used in the model for bone, ligament, intervertebral disc and instrumentation .....	52
4.3 The material constants for annular fibrosus, nucleus pulposus and ligaments used with Prony series for modeling viscoelastic behavior of the disc <sup>27, 28</sup> .....	54
4.4 The range of motion (degrees) of the present model with available literature data for 0.5Nm with no preload [72-74] .....	55
4.5 Follower load applied based on percentage increase in load from T1 to L5. ....	56
4.6 Different models simulated under dual growth rod instrumentation group.....	63
4.7 Distraction applied based on expected growth within the instrumented levels for the period between consecutive distractions [81] .....	64
5.1 The table below gives numerical value of forces in the rod (axial direction) with different distraction forces. Negative values are tensile forces and positives are compressive forces.....	82

## List of Figures

2-1 Side and back views of a normal spine showing the cervical, thoracic, lumbar, sacral and coccygeal regions. (Source: <a href="http://www.wpclipart.com/medical/anatomy/spine/spine_normal_views.jpg">http://www.wpclipart.com/medical/anatomy/spine/spine_normal_views.jpg</a> ) .....	9
2-2 Median sagittal section of a functional spinal unit showing different structural components including cancellous bone, cortical bone, ligaments and intervertebral disc. (Source: <a href="http://www.wikidoc.org/index.php/File:Gray301.png">http://www.wikidoc.org/index.php/File:Gray301.png</a> ).....	11
2-3 Posterior longitudinal ligaments at the thoracic region. Also a section cut shows the pedicle cross section. (Source: <a href="http://www.wikidoc.org/index.php/File:Gray302.png">http://www.wikidoc.org/index.php/File:Gray302.png</a> )...	14
2-4 Standing X-ray of a 7 year old patient showing scoliotic deformity.....	18
2-5 The X-ray shows mild scoliosis of a 4 year old patient kept under observation. ....	20
2-6 A 7 year old patient after dual growth rod instrumentation. The X-ray image shows the proximal and distal rods along with anchors (pedicle screws) and tandem connector (parallel).....	21
3-1 A 13 year old patient's X-ray showing magnetic growth rod implanted. This patient would not undergo invasive lengthening surgeries because this growth rod could be distraction non-invasively. ....	29
4-1 FE model of a normal juvenile spine after scaling and adjustment of vertebral body to intervertebral body heights. ....	41

4-2 FE model of a normal juvenile spine with altered kyphotic and lordosis curve. ....	42
4-3 Schematic showing projection vectors of the plum line (vertical line) onto the curve (S shaped curve) obtained from the polynomial equation in coronal plane. The magnitude and direction of this vector is given which could be deduced by simple trigonometry....	44
4-4 Schematic showing an example of an angular profile (change in angle with height) for the thoracic curve in coronal plane; the angles are measured in axial plane as showed. ....	46
4-5 Various juvenile idiopathic curves as classified by Robinson et al [70] and used for generating representative scoliotic models. ....	47
4-6 Instrumented normal juvenile spine model .....	49
4-7 Instrumented normal juvenile spine model with altered sagittal contours .....	49
4-8 The figure shows the region of tandem connector before and after distraction. The connector elements are modeled analytically. ....	49
4-9 Group 1A representative juvenile scoliotic FE model.....	50
4-10 Group 1B representative juvenile scoliotic FE model.....	50
4-11 Group 2 representative juvenile scoliotic FE model .....	51
4-12 Group 3 representative juvenile scoliotic FE model .....	51
4-13 Group 4 representative juvenile scoliotic FE model .....	52
4-14 Graphical presentation of force vs. number of distraction .[21].....	60
4-15 Graphical presentation of length vs. number of distraction .[21].....	61
4-16 The plot showing increase in stiffness due to autofusion at different period after instrumentation with dual growth rods. ....	62
4-17 The actuator applied the load along the rod to simulate the fatigue. ....	67

4-18 The in-vitro setup: 3-axes vice was mounted on top of x-y table top axes to establish proper orientation between rod and actuator. ....	68
4-19 The figure shows the superposition of sinusoidal loading and distraction force change due to growth for first 50 cycles as an example. ....	70
4-20 The figure shows the superposition of sinusoidal loading and distraction force change due to growth for last 50 cycles as an example. ....	72
4-21 Summary of the entire methodology. ....	72
5-1 Distraction forces (N) between the proximal and distal rods on each side before and after stress relaxation. The effective distraction force obtained after stress relaxation in soft tissue was less than the initial distraction force applied during the surgery. The maximum time period used was 83 minutes. ....	77
5-2 Distractions achieved (mm) in-between the proximal and distal rods on each side with different distraction forces. The distraction obtained increased with increase in distraction force. ....	78
5-3 The change in thoracic kyphosis (in degrees) after distraction and following 6 months of growth with respect to intact baseline for different distraction forces. The thoracic kyphosis decreased immediately after distraction and then recovered to varying extent. ....	78
5-4 The above figure shows the change in lumbar lordosis (in degrees) after distraction and following 6 months of growth with respect to intact baseline for different distraction forces. The lumbar lordosis decreased immediately after distraction and then recovered to varying extents with growth depending upon the initial distraction force. ....	79
5-5 Height increase across T1-S1 (in mm) during the growth period of 6 months following distraction with different distraction forces and its comparison with intact. GR	

125N provided height growth equal to intact exemplifying sustenance of growth. GR 150N, GR 175N and GR 200N showed higher growth than intact exemplifying stimulation of growth.....	80
5-6 Maximum von Mises stress (in MPa) in the growth rod after distraction (t=0) and after 6 months of growth (t=6 months) with different distraction forces. ....	81
5-7 Average load (N) at the screw-bone interface after distraction (t=0) and after 6 months of growth (t=6 months) with different distraction forces. The positive values correspond to caudal-cranial direction and the negatives in cranial-caudal direction. ....	81
5-8 The maximum von Mises stress on the rod for the period of 24 months with distraction every 12 months. The first curve is for the growth period from 1 <sup>st</sup> distraction (at 0 months) to 12 months (just before distraction). The second curve is for the growth period from 2 <sup>nd</sup> distraction (at 12 months) to 24 months (just before distraction) .....	84
5-9 The maximum von Mises stress on the rod for the period of 24 months with distraction every 6 months. The first curve, second curve, third curve and fourth curve are for the growth period 1 <sup>st</sup> distraction to 6 months, 2 <sup>nd</sup> distraction to 12 months, 3 <sup>rd</sup> distraction to 18 months and 4 <sup>th</sup> distraction to 24 months respectively.....	85
5-10 The maximum von Mises stress on the rod for the period of 24 months with distraction every 3 months. The first curve represents 1 <sup>st</sup> distraction and 3 months of growth following it. Each subsequent curve relates to the subsequent distraction and its growth period of 3 months.....	85
5-11: The maximum von Mises stress on the rod for the period of 24 months with distraction every 2 months. The first curve represents 1 <sup>st</sup> distraction and 2 months of	



growth following it. Each subsequent curve relates to the subsequent distraction and its growth period of 2 months..... 86

5-12: The graph shows the maximum von Mises stress on the rod immediately after distraction with different frequency of distraction for the duration of 24 months. For 12 monthly distraction there are two peaks (at 0 and at 12 months). For 6 monthly distraction there are four peaks (at 0, 6, 12, and 18 months). For 3 monthly distraction there are eight peaks (at 0, 3, 6, 9, 12, 15, 18, and 21 months). For 2 monthly distraction there are twelve peaks (at 0, 2, 4, 6, 8, 10, 12, 14, 16, 18, 20, and 22 months). ..... 86

5-13 The graph compares the highest value of the maximum von Mises stress on the rod seen with different frequency of distraction for the duration of 24 months. These highest value pertains to last distraction in each case. For 12 monthly distraction it is the distraction at 12<sup>th</sup> months. For 6 monthly distraction it is at 18<sup>th</sup> months. For 3 monthly distraction it is at 21<sup>st</sup> month. For 2 monthly distraction it is at 22<sup>nd</sup> month. .... 87

5-14 The graph shows the percentage increase in highest maximum von Mises stress by using cobalt-chromium and stainless steel with respect to titanium for different intervals of distraction. .... 88

5-15 The graph compares the factor of safety with different materials like titanium, cobalt-chromium and stainless steel for different intervals of distraction. The factor of safety was calculated as fatigue strength of the material divided by the highest maximum von Mises stress on the rod in 24 months. .... 89

5-16 Height increase across T1-S1 (in mm) during the growth period of 6 months following distraction for representative scoliotic model 1A. The data from non-scoliotic normal spine instrumented with growth rod is shown in red..... 91

5-17 The thoracic Cobbs's angle (in degrees) after distraction (t=0) and following 6 months (t=6 months) of growth for representative scoliotic model 1A.....	91
5-18 The kyphosis (in degrees) after distraction (t=0) and following 6 months (t=6 months) of growth for representative scoliotic model 1A. The data from non-scoliotic normal spine instrumented with growth rod is shown on the right.....	92
5-19 The lordosis (in degrees) after distraction (t=0) and following 6 months (t=6 months) of growth for representative scoliotic model 1A. The data from non-scoliotic normal spine instrumented with growth rod is shown on the right.....	92
5-20 Maximum von Mises stress (in MPa) in the growth rod after distraction (t=0) and after 6 months of growth (t=6 months) for representative scoliotic model 1A. The data from non-scoliotic normal spine instrumented with growth rod is shown on the right. ....	93
5-21 Average load (N) at the screw-bone interface after distraction (t=0) and after 6 months of growth (t=6 months) for representative scoliotic model 1A. The data from non-scoliotic normal spine instrumented with growth rod is shown on the right. ....	93
5-22 Height increase across T1-S1 (in mm) during the growth period of 6 months following distraction for representative scoliotic model 1B.....	95
5-23 The thoracic Cobbs's angle (in degrees) after distraction (t=0) and following 6 months (t=6 months) of growth for representative scoliotic model 1B.....	96
5-24 The kyphosis (in degrees) after distraction (t=0) and following 6 months (t=6 months) of growth for representative scoliotic model 1B. ....	96
5-25 The lordosis (in degrees) after distraction (t=0) and following 6 months (t=6 months) of growth for representative scoliotic model 1B. ....	96

5-26 Maximum von Mises stress (in MPa) in the growth rod after distraction (t=0) and after 6 months of growth (t=6 months) for representative scoliotic model 1B.....	97
5-27 Average load (N) at the screw-bone interface after distraction (t=0) and after 6 months of growth (t=6 months) for representative scoliotic model 1B.....	97
5-28 Height increase across T1-S1 (in mm) during the growth period of 6 months following distraction for representative scoliotic model 2. ....	99
5-29 The kyphosis (in degrees) after distraction (t=0) and following 6 months (t=6 months) of growth for representative scoliotic model 2. ....	100
5-30 The lordosis (in degrees) after distraction (t=0) and following 6 months (t=6 months) of growth for representative scoliotic model 2. ....	100
5-31 The thoracic Cobbs's angle (in degrees) after distraction (t=0) and following 6 months (t=6 months) of growth for representative scoliotic model 2.....	101
5-32 Maximum von Mises stress (in MPa) in the growth rod after distraction (t=0) and after 6 months of growth (t=6 months) for representative scoliotic model 2. ....	102
5-33 Average load (N) at the screw-bone interface after distraction (t=0) and after 6 months of growth (t=6 months) for representative scoliotic model 2.....	103
5-34 Height increase across T1-S1 (in mm) during the growth period of 6 months following distraction for representative scoliotic model 3. ....	104
5-35 The kyphosis (in degrees) after distraction (t=0) and following 6 months (t=6 months) of growth for representative scoliotic model 3. ....	105
5-36 The lordosis (in degrees) after distraction (t=0) and following 6 months (t=6 months) of growth for representative scoliotic model 3. ....	106

5-37 The thoracic Cobbs's angle (in degrees) after distraction (t=0) and following 6 months (t=6 months) of growth for representative scoliotic model 1B. ....	107
5-38 Maximum von Mises stress (in MPa) in the growth rod after distraction (t=0) and after 6 months of growth (t=6 months) for representative scoliotic model 3. ....	108
5-39 Average load (N) at the screw-bone interface after distraction (t=0) and after 6 months of growth (t=6 months) for representative scoliotic model 3. ....	109
5-40 Height increase across T1-S1 (in mm) during the growth period of 6 months following distraction for representative scoliotic model 4. ....	110
5-41 The kyphosis (in degrees) after distraction (t=0) and following 6 months (t=6 months) of growth for representative scoliotic model 4. ....	111
5-42 The lordosis (in degrees) after distraction (t=0) and following 6 months (t=6 months) of growth for representative scoliotic model 4. ....	112
5-43 The thoracic Cobbs's angle (in degrees) after distraction (t=0) and following 6 months (t=6 months) of growth for representative scoliotic model 4. ....	113
5-44 Maximum von Mises stress (in MPa) in the growth rod after distraction (t=0) and after 6 months of growth (t=6 months) for representative scoliotic model 4. ....	114
5-45 Average load (N) at the screw-bone interface after distraction (t=0) and after 6 months of growth (t=6 months) for representative scoliotic model 4. ....	114
5-46 The graph shows the maximum von Mises stress on the rod immediately after distraction with different frequency of distraction for the duration of 24 months (for representative scoliotic model 1A). For 12 monthly distraction there are two peaks (at 0 and at 12 months). For 6 monthly distraction there are four peaks (at 0, 6, 12, and 18 months). For 3 monthly distraction there are eight peaks (at 0, 3, 6, 9, 12, 15, 18, and 21	

months). For 2 monthly distraction there are twelve peaks (at 0, 2, 4, 6, 8, 10, 12, 14, 16, 18, 20, and 22 months). The data from non-scoliotic normal spine instrumented with growth rod is shown on the right. .... 116

5-47 The graph shows the maximum von Mises stress on the rod immediately after distraction with different frequency of distraction for the duration of 24 months (for representative scoliotic model 1B). For 12 monthly distraction there are two peaks (at 0 and at 12 months). For 6 monthly distraction there are four peaks (at 0, 6, 12, and 18 months). For 3 monthly distraction there are eight peaks (at 0, 3, 6, 9, 12, 15, 18, and 21 months). For 2 monthly distraction there are twelve peaks (at 0, 2, 4, 6, 8, 10, 12, 14, 16, 18, 20, and 22 months)..... 117

5-48 The graph shows the maximum von Mises stress on the rod immediately after distraction with different frequency of distraction for the duration of 24 months (for representative scoliotic model 2). For 12 monthly distraction there are two peaks (at 0 and at 12 months). For 6 monthly distraction there are four peaks (at 0, 6, 12, and 18 months). For 3 monthly distraction there are eight peaks (at 0, 3, 6, 9, 12, 15, 18, and 21 months). For 2 monthly distraction there are twelve peaks (at 0, 2, 4, 6, 8, 10, 12, 14, 16, 18, 20, and 22 months)..... 119

5-49 The graph shows the maximum von Mises stress on the rod immediately after distraction with different frequency of distraction for the duration of 24 months (for representative scoliotic model 3). For 12 monthly distraction there are two peaks (at 0 and at 12 months). For 6 monthly distraction there are four peaks (at 0, 6, 12, and 18 months). For 3 monthly distraction there are eight peaks (at 0, 3, 6, 9, 12, 15, 18, and 21

months). For 2 monthly distraction there are twelve peaks (at 0, 2, 4, 6, 8, 10, 12, 14, 16, 18, 20, and 22 months)..... 120

5-50 The graph shows the maximum von Mises stress on the rod immediately after distraction with different frequency of distraction for the duration of 24 months (for representative scoliotic model 4). For 12 monthly distraction there are two peaks (at 0 and at 12 months). For 6 monthly distraction there are four peaks (at 0, 6, 12, and 18 months). For 3 monthly distraction there are eight peaks (at 0, 3, 6, 9, 12, 15, 18, and 21 months). For 2 monthly distraction there are twelve peaks (at 0, 2, 4, 6, 8, 10, 12, 14, 16, 18, 20, and 22 months)..... 122

5-51 The graph shows the relation between the axial stiffness of Group 1A FE model and percentage correction obtained at that given stiffness with gravitational loads. .... 123

5-52 The graph established relationship between maximum allowed distraction interval (for maximum von Mises stress up to 255 MPa) on the rod for a given percentage of Cobb’s angle correction observed (related to axial stiffness) under gravitational loads. 124

## List of Abbreviations

FE.....	Finite Element
FEA.....	Finite Element Analysis
GR.....	Growth rod

## List of Symbols

%.....Percentage

MPa....Mega Pascal

mm .....Milimeter

N.....Newton



# Chapter 1

## Introduction

### 1.1 Rationale for Research

About 2.5% of children across all age groups have scoliosis. It has also been estimated that females are a high risk category with 1% of cases requiring surgical intervention.[8] Scoliosis Research Society defines scoliosis as a lateral deviation of the normal vertical line of the spine which, when measured by X-ray, is greater than ten degrees. Scoliosis consists of a lateral curvature of the spine with rotation of the vertebrae about axial axis. Scoliosis could result from multiple conditions including neuromuscular disorders, skeletal dysplasia, congenital anomalies, and developmental disorders (idiopathic).[9] Of all, idiopathic scoliosis is the most common deformity and it represents 80-85% of all scoliosis cases. The Scoliosis Research Society adopted a scoliosis classification system that is based on the age of onset: infantile scoliosis, 0 to 3; juvenile scoliosis, 3 to 9; and adolescent scoliosis, older than 9 years of age.[10, 11]

Progression of scoliosis in children poses a substantial challenge for spinal surgeons. These young patients are undergoing active growth; hence early fusion of any kind would stunt their growth and have an untoward effect on their quality of life. However, if left untreated a major curve progression is imminent, with chances of respiratory insufficiency. This has led to an advent of growth friendly surgical management of early

scoliosis. These growth friendly surgical treatment aim to avoid, delay or limit spinal fusion. They are classified as distraction-based, guided growth and compression-based techniques.[12-14]

Distraction-based dual growth rods are the most commonly used growth friendly surgical instrumentation.[15, 16] In a typical growth rod implant surgery, two rods (proximal and distal) are attached along the two lateral sides of the spine using pedicle screws. The proximal and distal rods are pushed apart to distract the spine, correcting the curve. This corrects the curve by about fifty percent at the time of the initial surgery. Thereafter the distal and proximal rods on each side are fixed using a tandem connector. A regular construct lengthening (at 6 months to a year) is continued for a period of 5-10 years of implantation (until the longitudinal growth of spine stops).[17] During such lengthening surgeries the proximal and distal rods at each side are distracted apart. The position of the rods after distraction is maintained using a tandem connector.[18]

Growth rod technique is not a single surgery technique. Several invasive distractions have to be followed after the main surgery. Due to this the child suffers extreme morbidity and discomfort. For example, a child who has been implanted with growth rod at an age of 5 would undergo 10-14 consecutive distraction surgeries. Moreover there have been many instances of failure.[19] The goal of this proposal will help in dissemination of key concepts which when put into clinical practice could lower the morbidity and complication rate.

With traditional growth rods, changing the frequency of distraction wasn't an option because of its invasive nature. A higher frequency of distraction (<6months) will put the patient into high risk of complication. A lower frequency of distraction (>1 year)

lowers the growth potential. However with the arrival of magnetic growth rods in the spine industry, the serial distractions could be achieved non-invasively. Therefore we would also investigate the potential of increased frequency of distraction and how it could affect the growth rod fracture propensity among the patient.

Growth rod fractures occur in 15% of patients treated with growing rods.[17, 20, 21] While pedicle screws provide better anchorage, screw loosening does indeed occur.[3, 4] Thompson report 29% (2 out of 7 patients) complication of rod breakage with growth rods.[18] Klemme reported 12 rod breakage in 67 patients.[22] In 2005 Akbarnia reported 2 rod breakage among 23 patients.[7] Yang et al found that the risk of rod fracture increases with single rods, stainless steel rods and smaller diameter rods. They also found that rod fracture was more prevalent among patient's preoperative ability of ambulation.[20] Nevertheless, rod fracture also occurred in non-ambulatory patients. The mean time report for rod fracture was  $25 \pm 21$  months and the mean time after distraction was  $5.8 \pm 3$  months. Hence fracture could occur either early or at a later stage.[20] This high incidence of rod fracture is attributed to the fact that growth rods are non-fusion implants, and therefore goes through long cycles of loading and unloading.

Some researchers also believe that the distraction forces applied are so high that it instead is stimulating growth rather than sustaining it.[5] Excessive distraction could lead to poor sagittal balance and other complication in juvenile patients, including rod fractures. Sakai et al presented a case study where they report observation of 8.3-mm gap between T11-T12 immediately after distraction. This space was remarkably wider than the adjacent disc spaces, raising the suspicion of a distraction phenomenon (severance of union between soft and hard tissue), which was confirmed with computed tomography.[23]

There also exists a predicament of decision making on frequency of lengthening: shorter intervals of lengthening versus longer intervals of lengthening (less number of lengthening).[24] With conventional growth rods, the frequency is limited to 6 months due to reasons of trauma to patient.[17] However with recent advent of magnetically controlled growing rod (MCGR) there has been a potential to change the gold standard for treatment of scoliotic growing spine. [25, 26] The major advantage of MCGR is that the distractions following the initial surgery is noninvasive. Hence frequency of distraction can be increased without causing discomfort to the patient.[25] This presents an opportunity and applicability for inclusion of distraction frequency as a variable in our research.

The overall goals of this project are I) modeling and analyzing the effect of distraction force on T1-S1 height sustenance, sagittal contours, load at screw-bone interface and stresses on the rods and II) modeling and analyzing the effect of distraction frequency on stresses on the rods with optimal distraction forces. As a first step, a normal juvenile spine model will be utilized in order to address the hypotheses of this study. This will help us in finding pitfalls in the current modeling process and establish a solid base for extending the analysis on multiple representative scoliotic spine models. Multiple representative scoliotic spine models will be produced using a novel and efficient method of generating representative scoliotic spine finite element models. Analysis on multiple representative models will also help in establishing a relationship, if any exists, between the type of curve and the desired magnitude and frequency of distraction. Sensitivity analysis will then be conducted to identify the effect of variance in spinal stiffness on the stresses generated on rods for sustained growth.

Juvenile idiopathic scoliotic has a longer duration of treatment compared to any other kind of spinal pathology or disorder. To add to this, the patients involved are very young and this increases the risk of complications. Therefore, it is unethical to undertake clinical trial on these patients without a thorough base. Doing cadaveric testing on juvenile spines is not feasible due to unavailability of pediatric spines. Furthermore, *in vivo* studies on pigs and sheep also suffer from inherent disadvantages like absence of scoliosis. Scoliosis could be produced in animals but the biomechanics of the scoliotic curve during growth will be very different from humans due to different loading conditions, anatomical differences and differences in hard and soft tissue properties. In contrast to all above, computational modeling is a cost effective and versatile tool to model and analyze the goal of this project. It also allows parametric studies to establish the relationship between the different parameters and their effect on the output. The scoliotic spines vary tremendously in the type of curve and geometry. Furthermore scoliotic spines with the same curvature could have different levels of flexibility in different patients. Therefore biomechanical result from using a single patient specific scoliotic spine finite element model may not be useful for other kinds of curves. This implies that different representative finite element models would be required to represent different kinds of scoliotic curves. Hence we have proposed to use multiple representative finite element models to achieve the goal of the project holistically.

We have two specific aims, each with multiple hypotheses to test:

**Specific Aim 1: Analyze the effect of distraction forces on T1-S1 height sustenance, load at bone-screw interface and stresses on the rods.**

Hypothesis 1.1: There exists an optimal distraction force that will sustain the growth of the spine, i.e. growth will be equal to normal spinal growth.

Hypothesis 1.2: The optimal distraction force produces minimum change in sagittal contours, and results in lower von Mises stresses on the rods and minimum force at the pedicle screw-bone interface at the end of distraction interval.

Hypothesis 1.3: The optimal distraction force increases with increases in stiffness of the spine.

**Specific Aim 2: Analyze the effect of distraction frequencies on optimal distraction force and stresses on the rods.**

Hypothesis 2.1: The optimal distraction force decreases with increase in distraction frequency.

Hypothesis 2.2: The maximum stresses on the rod (at an optimal distraction force) decreases with increase in distraction frequency.

Hypothesis 2.3: Spines with increased stiffness requires a higher frequency of distraction for the rods to be under similar stress condition.

## **1.2 Outline**

The second chapter of this dissertation provides a brief description of the anatomy of a normal spine, juvenile idiopathic scoliosis and the surgical treatment method using growth rods. It provides the information base required to continue with the literature review, finite element model description, results and discussion.

Chapter three presents a literature review of growth rod complication and the possible causes that has been proposed. To begin the chapter, the reader is given an introduction to the current review of complications associated with the growth rod in juvenile scoliotic patients. Then, review of research that focuses on the causes and proposed solutions for these complication.

The fourth chapter continues with the thoracolumbar juvenile scoliotic spine model development and validation. This includes a complete description of methods used to build the model and relevant assignment of materials, subroutines and the type of validation carried out.

The results for this study are presented in the fifth chapter.

Chapter six includes a thorough discussion of all the results. It also provides the limitations of this study and conclusion that follow from the results and discussion presented in the preceding sections.

## **Chapter 2**

### **Juvenile Idiopathic Scoliosis**

#### **2.1 Anatomy of a Normal Spine**

The spine has distinct five regions: cervical, thoracic, lumbar, sacral and coccygeal. There are 7 cervical vertebrae (C1-C7) in the neck, 12 thoracic vertebrae (T1-T12) in the chest, and 5 lumbar vertebrae (L1-L5) in the abdomen, 5 sacral (fused S1-S5) vertebrae in the pelvis (that form the sacrum) and 4 coccygeal vertebrae in the “tail bone” (that form the coccyx) (Figure 2-1). A typical vertebra can be divided into two basic regions, a vertebral body and a vertebral arch. The bone in both regions is composed of an outer layer of compact bone and a core of trabecular bone. The shell of compact bone is thin on the surface of the vertebral body and is thicker in the vertebral arch and its processes. [27]



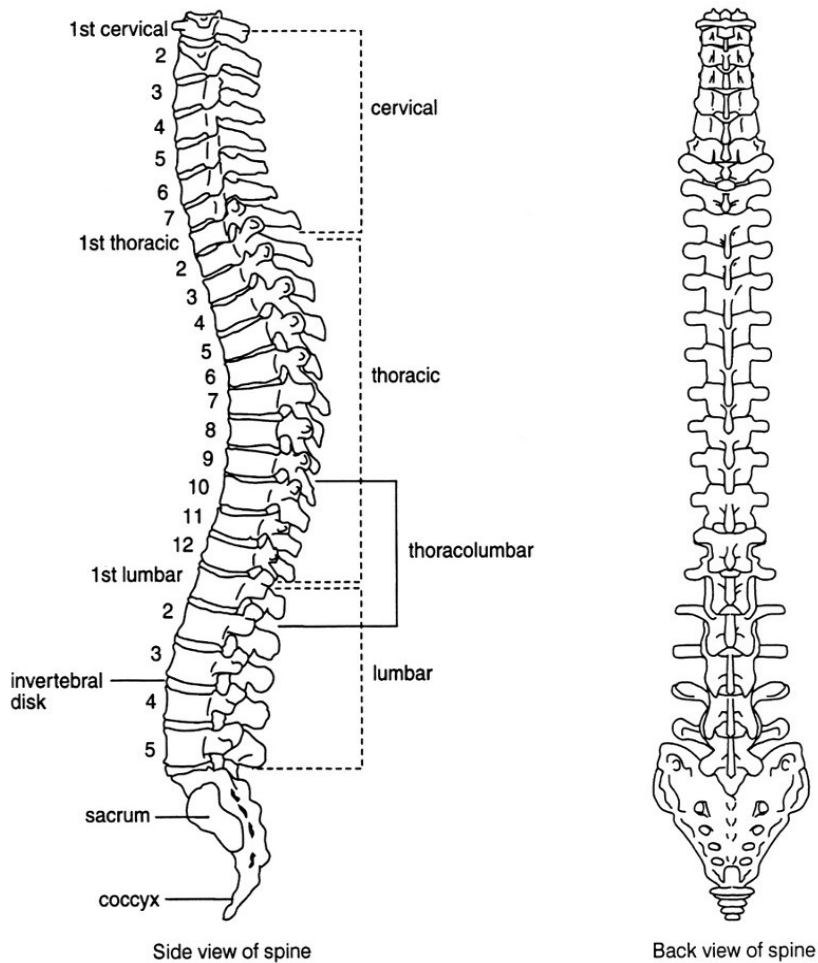


Figure 2-1: Side and back views of a normal spine showing the cervical, thoracic, lumbar, sacral and coccygeal regions. (Source: [http://www.wpclipart.com/medical/anatomy/spine/spine\\_normal\\_views.jpg](http://www.wpclipart.com/medical/anatomy/spine/spine_normal_views.jpg))

The vertebral body is the large anterior portion of a vertebra that acts to support the weight of the human frame. The vertebral bodies are connected to one another by fibrocartilaginous intervertebral discs. The vertebral bodies, combined with their intervening discs, create a flexible column or pillar that supports the weight of the trunk and head. The vertebral bodies also must be able to withstand additional forces from contraction of the axial and proximal limb muscles. The transverse diameter of the

vertebral bodies increases from C2 to L3. This is due to the fact that each successive vertebral body is required to carry a slightly greater load.[28] There is variation in the width of the last two lumbar vertebrae, but the width steadily diminishes from the first sacral segment to the apex (inferior tip) of the coccyx. Most vertebral bodies are concave posteriorly (in the transverse plane) where they help to form the vertebral foramina. Small foramina for arteries and veins appear on the front and sides of the vertebral bodies. Posteriorly there are small arterial foramina and one or two large, centrally placed foramina for the exiting basivertebral veins (Figure 2-2).[29] The vertebral (posterior) arch has several unique structures. These include the pedicles, laminae, superior articular, inferior articular, transverse, and spinous processes. The pedicles create the narrow anterior portion of the vertebral arch. They are short, thick, and rounded and attach to the posterior and lateral aspects of the vertebral body. They also are placed superior to the midpoint of a vertebral body. Because the pedicles are smaller than the vertebral bodies, a groove, or vertebral notch, is formed above and below the pedicles. These are known as the superior and inferior vertebral notches, respectively. The laminae are continuous with the pedicles. They are flattened from anterior to posterior and form the broad posterior portion of vertebral arch uniting with the spinous process posteriorly, completing the vertebral foramen. The spinous process of each vertebra projects posteriorly and often inferiorly from the laminae. The size, shape, and direction of this process vary greatly from one region of the vertebral column to the next. The spinous processes throughout the spine function as a series of levers both for muscles of posture and for muscles of active movement. Most of the muscles that attach to the spinous processes act to extend the vertebral column. Some muscles attaching to the spinous processes also rotate the vertebrae

to which they attach. Lateral to the spinous processes are the vertebral grooves. These grooves are formed by laminae in the cervical and lumbar regions. They are much broader in the thoracic region and are formed by both the laminae and transverse processes. The left and right vertebral grooves serve as gutters. These gutters are filled with the deep back muscles that course the entire length of the spine.

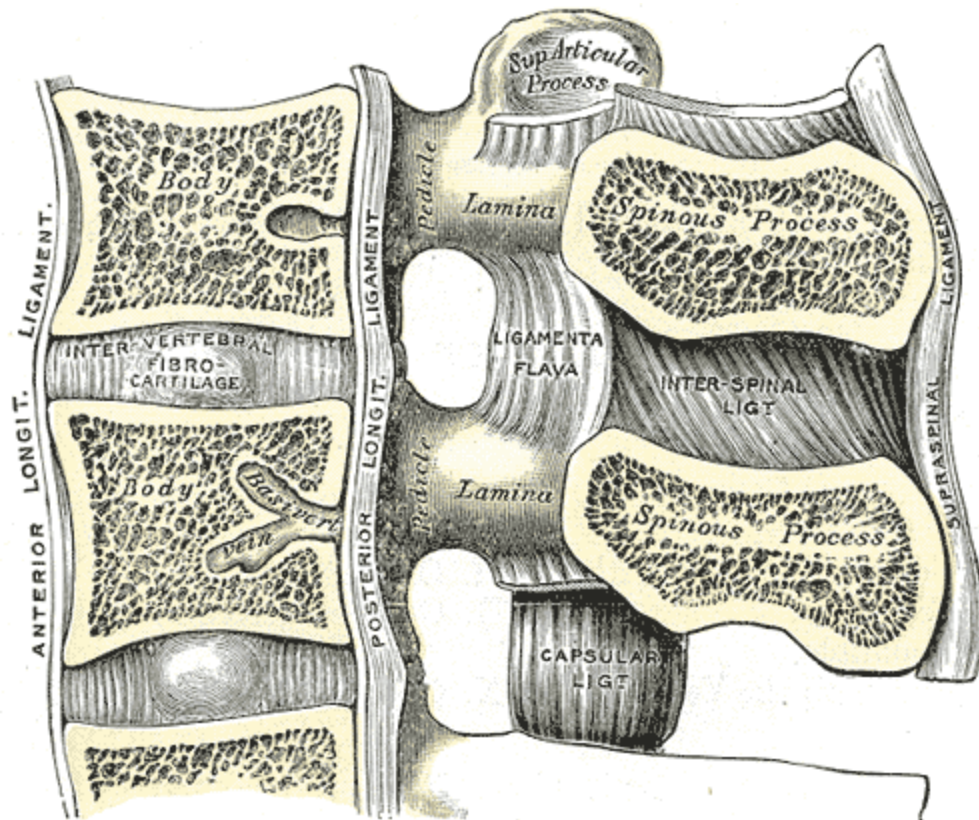


Figure 2-2: Median sagittal section of a functional spinal unit showing different structural components including cancellous bone, cortical bone, ligaments and intervertebral disc. (Source: <http://www.wikidoc.org/index.php/File:Gray301.png>)

The vertebral foramen is the opening within each vertebra that is bounded by the structures discussed thus far. Therefore the vertebral body, the left and right pedicles, the left and right laminae, and the spinous process form the borders of the vertebral foramen

in a typical vertebra. The size and shape of the vertebral foramina vary from one region of the spine to the next, and even from one vertebra to the next. The vertebral canal is the composite of all of the vertebral foramina. This region houses the spinal cord, nerve roots, meninges, and many vessels. The transverse processes project laterally from the junction of the pedicle and the lamina (pediculolaminar junction). The transverse processes serve as muscle attachment sites and are used as lever arms by spinal muscles. The muscles that attach to the transverse processes maintain posture and induce rotation and lateral flexion of single vertebrae and the spine as a whole. The superior articular processes project superiorly, and the articular surface (facet) faces posteriorly. The inferior articular processes (zygapophyses) and facets project inferiorly and the articular surface (facet) faces anteriorly. Adjoining zygapophyses form zygapophyseal joints (Z joints), which are small and allow for limited movement. Mobility at the Z joints varies considerably between vertebral levels. The Z joints also help to form the posterior border of the intervertebral foramen.

Ligaments of the spine act to carry tensile forces that resist excessive motion, thus stabilizing the spine. The anterior longitudinal ligament (ALL), posterior longitudinal ligament (PLL), capsular ligaments (right and left CL), ligamentum flavum (LF) and the interspinous ligament (ISL) are of particular biomechanical interest. Anatomical locations of these ligaments reveal that any type of rotational motion will produce a tensile force in at least one of these ligaments. The ALL is a continuous ligament which originates as a band attached to the inferior surface of the occiput and ends at the first segment of the sacrum. It is firmly attached to the anterior surface of the vertebral bodies and may be loosely attached to the intervertebral discs as well. The lateral edges are blended with the

periosteum. Tension in the ligament develops when the spine is in extension. The PLL is also a continuous ligament which originates at the occiput and runs down the posterior aspect of the vertebral column from within the neural canal before terminating at the coccyx. The PLL is similar to the ALL in that it is firmly attached to the vertebral bodies. However, the PLL is also firmly attached to the intervertebral disc (Figure 2-3). The articular facets are surrounded by the right and left capsular ligaments (CLs) which enclose the joint cavities. The CLs serve to stabilize the articulation of the adjacent facets, thereby reducing excessive separation of the surfaces. The ligamentum flavum (LF) is an extremely elastic ligament. It has also been called the 'yellow ligament', which is due to its relatively high elastin fiber content when compared to other spinal ligaments. The LF is a flat band that spans the space between the laminae of adjacent vertebrae. Biomechanically, this ligament acts to resist flexion. The interspinous ligament (ISL) bridges the gap between adjacent spinous processes while the supraspinous ligament (SSL) runs over the spinous processes (Figure 2-2).[30]

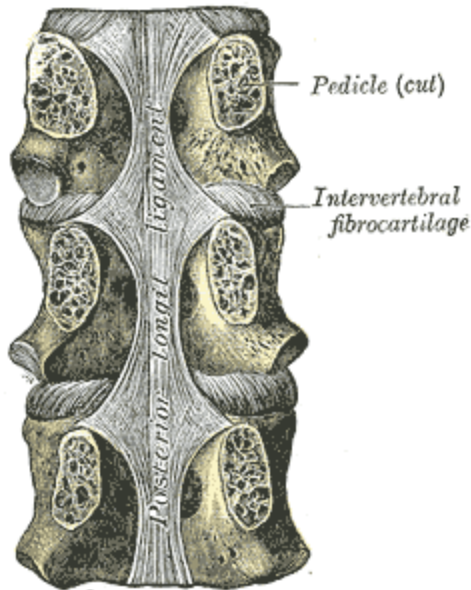


Figure 2-3: Posterior longitudinal ligaments at the thoracic region. Also a section cut shows the pedicle cross section. (Source: <http://www.wikidoc.org/index.php/File:Gray302.png>)

## 2.2 Functional Components of a Vertebra

Each region of a typical vertebra is related to one or more of the functions of the vertebral column (support, protection of the spinal cord and spinal nerve roots, and movement). In general, the vertebral bodies help with support, whereas the pedicles and laminae protect the spinal cord. The superior and inferior articular processes help determine spinal movement by the facing of their facets. The transverse and spinous processes aid movement by acting as lever arms upon which the muscles of the spine act. The posterior arches also act to supports and transfer weight, and the articular processes of the cervical region form two distinct pillars (left and right) that bear weight. [31-33]

## 2.3 Curves of Spine

The spine develops four anterior to posterior curves, two kyphoses and two lordoses. Kyphoses are curves that are concave anteriorly, and lordoses are curves that are concave posteriorly. The two primary curves are the kyphoses. These include the thoracic and pelvic curvatures. They are referred to as primary curves because they are seen from the earliest stages of fetal development.[34] The thoracic curve extends from T2 to T12 and is created by the larger superior to inferior dimensions of the posterior portion of the thoracic vertebrae. The pelvic curve extends from the lumbosacral articulation throughout the sacrum to the tip of the coccyx. The concavity of the pelvic curve faces anteriorly and inferiorly. The two secondary curves are the cervical lordosis and lumbar lordosis. These curves are known as secondary or compensatory curves because even though they can be detected during fetal development, they do not become apparent until the postnatal period. The cervical lordosis begins late in intrauterine life but becomes apparent when an infant begins to lift his or her head from the prone position (approximately 3 to 4 months after birth). This forces the cervical spine into a lordotic curve. The cervical lordosis is further accentuated when the small child begins to sit upright and stabilizes his or her head, while looking around in the seated position. This occurs at approximately 9 months of age. The action of the erector spinae muscles, pulling the lumbar spine erect in order to achieve the position necessary for walking, creates the posterior concavity known as the lumbar lordosis. The lumbar lordosis therefore develops approximately 10 to 18 months after birth as the infant begins to walk upright. The lumbar lordosis extends from T12 to the lumbosacral articulation. The region between L3 and the lumbosacral angle is more prominently lordotic than the region from T12 to L2. Following infancy, the lumbar

lordosis is maintained by the shape of the intervertebral discs and the shape of the vertebral bodies. Each of these structures is taller anteriorly than posteriorly in the lumbar region of the spine. The kyphoses and lordoses of the spine, along with the intervertebral discs, help to absorb the loads applied to the spine. These loads include the weight of the trunk, along with loads applied through the lower extremities during walking, running, and jumping. In addition, loads are applied by carrying objects with the upper extremities, the pull of spinal muscles, and the wide variety of movements that normally occur in the spine. The spinal curves, acting with the intervertebral discs, dissipate the increased loads that would occur if the spine were shaped like a straight column.[35]

## **2.4 Scoliosis**

Scoliosis is a deformity of the trunk, mainly characterized by a lateral deviation (of more than 10 degrees) of the spinal column in combination with axial rotations of the vertebrae (Figure 2-4). These axial rotations of the vertebrae are towards the convexity of the curve. In more than 80% of cases, a specific cause is not known. Such cases are termed “idiopathic”, meaning “of undetermined cause”. This is particularly common in adolescent girls. Idiopathic scoliosis is typically called “infantile” in children 0-3 years old, “juvenile” in children 4-10 years old, “adolescent” in adolescents 11-18 years old, and “adult” in patients over 18 years old. Conditions known to cause spinal deformity are congenital spinal column abnormalities (present at birth – called congenital scoliosis), neurologic disorders (neuromuscular scoliosis), genetic conditions, and many other causes. Early onset scoliosis is a lateral (side-to-side) curve of the spine that is diagnosed before the age of 10. There are several different types of early onset scoliosis, mostly these include:



infantile idiopathic scoliosis, juvenile idiopathic scoliosis and congenital Scoliosis. Juvenile idiopathic scoliosis is a type of scoliosis that is first diagnosed between the ages of 4 and 10. This category makes up about 10% to 15% of all idiopathic scoliosis in children. At the younger end of the spectrum, boys are affected slightly more than girls and the curve is often left-sided. Towards the upper end of the age spectrum, the condition is more like adolescent idiopathic scoliosis, with a predominance of girls and right-sided curves. The severity of scoliosis is often quantified by the Cobb angle. The Cobb angle is a unit of measurement for interpretation of scoliosis curves in a radiographic projection of the spine. In practice, a line is drawn along the superior end plate of the superior end vertebra, and then another line is drawn along the inferior end plate of the inferior end vertebra. The angle between these two lines (or lines drawn perpendicular to them) is measured as the Cobb angle. In S-shaped scoliosis there are two adjacent curves where the lower end vertebra of the upper curve represents the upper end vertebra of the lower curve.

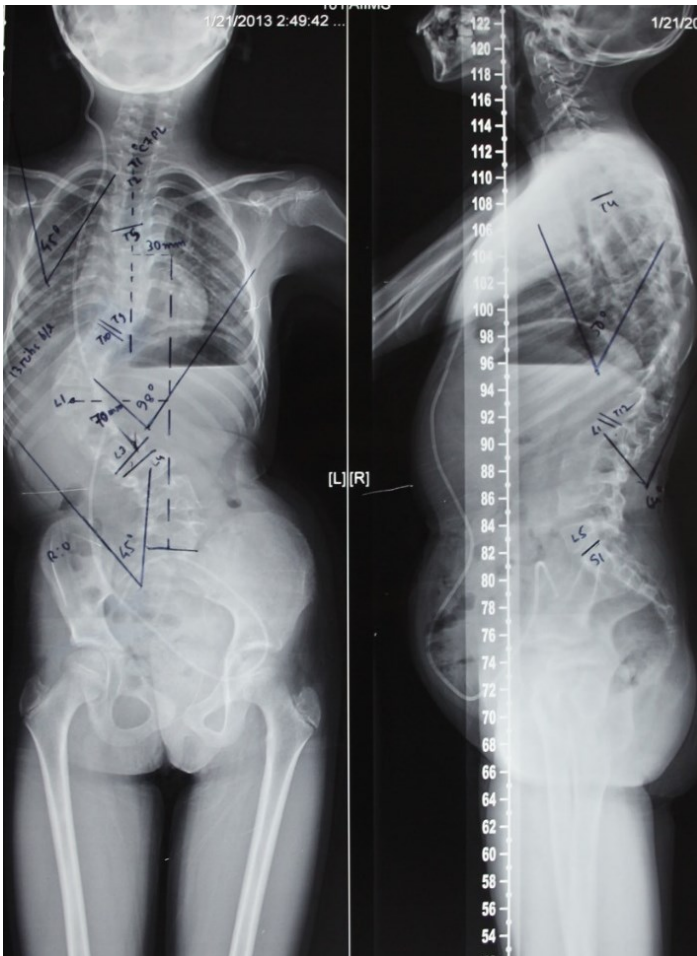


Figure 2-4: Standing X-ray of a 7 year old patient showing scoliotic deformity.

## 2.5 Treatment of Juvenile Idiopathic Scoliosis

The clinical treatment of scoliosis depends on the severity of the curve (the Cobb angle), the remaining growth (age) and the progression of the curve (increase of the Cobb angle). In mild cases (Cobb angle < 25 degrees) with little curve-progression the patient is simply monitored, or treatment consists of physiotherapy and exercises. Although the benefits of physical therapy and exercise seem intuitive, it has not been shown that this

treatment alters the natural history of scoliosis. In mild and moderate scoliosis (40 degrees > Cobb angle > 25 degrees) with progression of the curve, bracing is considered a proper treatment to limit progression of the scoliosis (Figure 2-5). When Cobb-angles exceed 40 degrees and the curve is progressive, surgery is considered to be the usual standard to limit the progression of scoliosis, along with substantial correction of the existing curve. These juvenile patients are undergoing active growth; hence early fusion of any kind would stunt their growth, and have untoward effect on their quality of life. However, as mentioned earlier, if left untreated, a major curve progression is imminent with chances of respiratory insufficiency. This led to an advent of growth friendly surgical management of early scoliosis. These growth friendly surgical treatment aim to avoid, delay or limit spinal fusion. They are classified as distraction-based (i.e., growth rods, vertical expandable prosthetic titanium rib [VEPTR; Synthes, West Chester, PA]), guided growth (i.e., Luque trolley, Shilla), and compression-based techniques (i.e., tethers, staples). Distraction-based dual growth rods are the most commonly used growth friendly surgical instrumentation. A typical growth rod fixation has two foundations- proximal and distal, where limited fusion is performed. Either pedicle screws or hooks are used at each foundation. Each of the foundation has rods spanning towards the other which are connected to each other near thoracolumbar junction. The rods are connected using tandem connectors, which help in distraction during serial surgeries until a final fusion is performed (Figure 2-6).



Figure 2-5: The X-ray shows mild scoliosis of a 4 year old patient kept under observation.

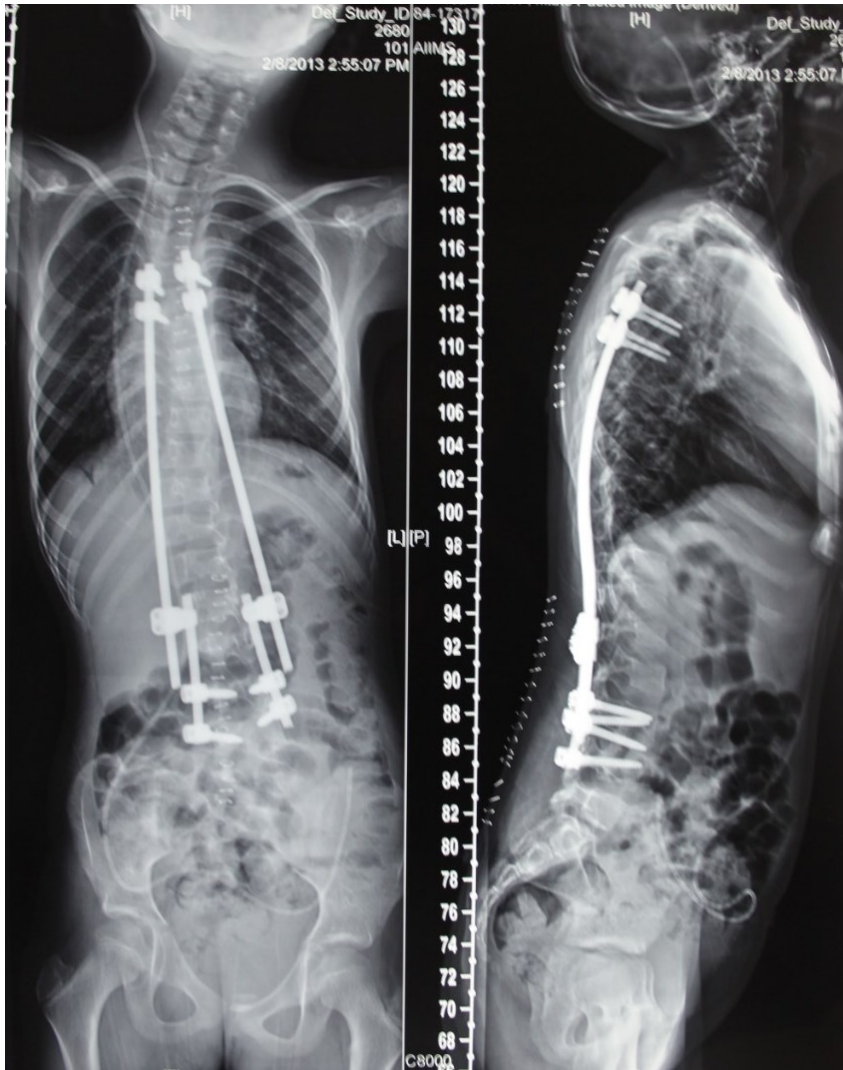


Figure 2-6: A 7 year old patient after dual growth rod instrumentation. The X-ray image shows the proximal and distal rods along with anchors (pedicle screws) and tandem connector (parallel).

## Chapter 3

### Growth Rods and Occurrence of Fracture

#### 3.1 Introduction

Juvenile idiopathic scoliotic patients are at a high risk of rapid curve progression and pulmonary insufficiency. [36, 37] Historically spinal fusion has been considered the gold standard, however recent reports have indicated that patients who undergo spinal fusion at this age develop functional and cosmetic limitations, impaired respiratory functions and a reduced quality of life. [38, 39] These led to an increased emphasis on treatments that prevent deformity progression yet allow continued spinal growth and thoracic development.

Growth rods have been used for several decades in deformity correction, along with provision for spinal growth until the patient has reached an appropriate size or age when a definitive fusion surgery is carried out. Even though the concept of growth rod has been there for a long time, the use of dual growth rods has only recently been popularized by Akbarnia et al [40-42], Thompson et al [1], and Breakwell et al.[43] In a typical dual growth rod surgery, the rods are attached along both sides of the spine above and below the curve using pedicle screws. The rod is then extended to correct the curvature until the surgeon feels enough compression in the rod to stop the adjustment. The curve can usually be corrected by fifty percent at the time of the initial surgery. For this, a patient must

undergo an invasive surgery, however the consecutive lengthening surgery includes exposing the tandem connectors through a small midline incision, loosening either the cranial or the caudal tandem-connector set screws, and distracting the two rods within the connector. This lengthening process is continued for a period of 5-10 years of implantation, until the point where patient has reached his or her growth limit. At present, the general consensus is to lengthen the rods every 6 months regardless of curve progression.

### **3.2 History of Fracture in Fusion-less Instrumentation**

In one of the first outcome studies reported by Moe et al [44], describing the use of segmental instrumentation without apical fusion, there were six instances of rod fractures that occurred in four patients. In this series of 20 patients, rod breakage occurred twice in two patients and once in the other two patients. They noted that the breakages occurred more commonly with thinner-threaded Harrington rods, and advised on the use of thicker Moe-modified Harrington rods with a central smooth portion. However, the prior conclusion about threaded Harrington rods has not been consistent. Klemme et al [45] reported 12 instances of rod breakage: seven involving Moe-modified Harrington rods, four with threaded and standard distraction Harrington rods, and one involving the Cotrel-Dubousset rods. In addition, it was noted that the survival time of Harrington rods was longer than the Moe-modified Harrington rods (20.5 months vs. 12 months), which contradicts Moe's findings.[44, 45] Rod fractures were common at the junction between the central smooth portion and the threaded or ratcheted portion of either rod.[45] Klemme *et al* deemed rod failures in general clinically benign, and advised against preemptive rod exchange to prevent rod failure. Furthermore, they advised postoperative bracing to limit bending moments on the rods. Mineiro and Weinstein further explored the topic in their

study of 11 patients undergoing subcutaneous rod placement with either Moe or Harrington rods.[46] Ten fractures occurred in eight patients with Moe rods, with all the fracture sites occurring in the threaded segment. Three fractures occurred in one patient and two fractures occurred in another. The authors hypothesized that stress risers are inherent in the rod design, such as the nut stripping the threads, and are contributing to the failures. The authors did not find any correlation with number of surgical procedures, rod bending, age, or magnitude/flexibility of the major scoliosis curve. One patient that did not have a failure with Moe rods was not ambulatory. The authors hypothesized that preemptive rod exchange could prevent rod failure; however, they added that this may increase wound complications.

### **3.3 Growth Rod Fracture**

Dual growth rods were first used in growing rod constructs in 1998 by Akbarnia and McCarthy. [40, 41] They used two separate stainless steel segments connected by a tandem connector housing. Thompson et al [1] compared the single versus dual constructs of submuscular growing rods with or without a short apical fusion in 28 consecutive patients. There were a total of seven fractures in seven patients. No differences in fracture rates were detected between the various types of constructs.[43] Dual Isola rods constructs were further studied by Akbarnia et al.[41] In a series of 23 patients, two single-rod breakages occurred in two patients. Both rod breakages were treated during lengthening procedures. Skaggs et al [47] later analyzed the same database for anchor data between 1998 and 2008. He reported that for the 896 pedicle screws, there were 22 (2.4%) complications directly related to the screw: acute loss of fixation (4), migration (14), breakage (1), skin breakdown (2), and unspecified loss of fixation (1). Of the 867 hooks,



there were 60 (6.9%) complications: acute loss of fixation (35), migration (22), and unspecified loss of fixation (3). However, there were no complications involving neurologic or vascular injury directly related to a hook or screw.

More recently Yang et al [2] presented a thorough retrospective review of 327 patients between 1990 to 2008 analyzing risk factors for growth rod fracture. They saw that eighty-six rod fractures occurred in 49 of 327 total patients (49 of 327, 15%). The mean time to fracture after initial insertion was  $25 \pm 21$  months, whereas the mean time to fracture after lengthening was  $5.8 \pm 3$  months after the previous lengthening. The most common fracture locations were above or below the tandem connectors (34 of 86). Other locations were adjacent to anchors (12 of 86) and cross-links. When anchors were examined as a whole, the rod fracture rate was 12% in constructs made of entirely hooks. In constructs entirely made of screws, the rod fracture rate was 9%. In a hybrid construct of screws and hooks, the rod fracture rate was 10%. As these were not statistically different, this indicated that the rod fracture occurred independent of the type of anchor used. Patients who were independently ambulatory preoperatively also had a higher fracture rate, although rod fractures also occurred in non-ambulatory patients (21%, 38 of 180 vs. 9 of 91, 8.7%). This also implies that just high cyclic loading is not the sole cause leading to failure of growth rods. From a 'strength of material' perspective, stainless steel rods had a higher fracture rate than titanium rods (58 of 198, 29% vs. 19 of 108, 18%). They also found that the patients who didn't have rod fracture had significantly larger mean rod diameter than the patients with rod fracture (4.8 mm vs. 4.1 mm). Besides the growth rods, there is an increasing inclination towards the use of pedicle screws instead of hooks as anchor in these surgeries. In one particular study, [48] using immature porcine spine to

better correlate the results with juvenile spine, the authors found that the pedicle screw constructs were significantly more stable than laminar hooks. Even from a theoretical point of view, an increased stability at the anchor points with use of pedicle screws may allow for delivery of greater distraction forces at the each lengthening surgery. A previous study by the same group examined this by placing a bonded strain gage at the tip of distractor tool and by running the signal through custom amplification. They found that the use of pedicle screws allowed for significantly greater distraction force application ( $416 \pm 101\text{N}$ ) than hooks ( $349 \pm 100\text{N}$ ). As the pedicle dimensions in these patients are smaller than adult, there has not been a general consensus for use of pedicle screws as anchor in these patients.

The high complication rate associated with treatment using growth rod has been attributed to the long duration of treatment and the number of procedures required during the treatment period. The magnitude of mechanical stress in these implants are of high importance as the spines are instrumented without fusion. Therefore the instrumentation construct incurs continued loading and micromotion, making the implants prone to fatigue and mechanical failure.

Sakai et al [49] recently coined the termed ‘distraction phenomenon’, where they found 8.3-mm gap after distraction due to circumferential detachments of the vertebral body from the endplate. It may have occurred due to the fact that the distraction force was too high for the patient’s spine to withstand.

Another important finding suggests that the patients undergoing growth rod surgery surpass the normal growth rate. Experiments on quadruped straight spines have shown higher growth-plate height with distraction compared to control.[50] Another study

showed that the vertebral body heights in the distraction group were significantly higher than normal, and therefore it was speculated that the distraction forces might be stimulating the apophyseal growth of axial skeleton via Hueter-Volkman principle.[51]

### **3.4 Advent of non-invasive distractions**

One of the major disadvantages of traditional growing rod systems is the requirement for multiple surgical procedures to lengthen the rods as the patient grows.[52] Considering that rod lengthening is performed approximately every 6 months, it is not uncommon for a child to undergo as many as 10-15 operations during their growing rod treatment.[21] Besides leading to psychological and physical trauma, it also results in social disadvantage (absence from school and other activities) and economic burden (multiple surgeries).[53, 54] With technological advances over recent years, magnetic growth rod has entered the market with recent reports corroborating its safety and efficacy at short-term follow-ups.[55-57] This system present the possibility of numerous distraction at any chosen interval without an invasive procedure making lengthening surgery an outpatient operation. Cheug et al [56], on 2-year results of MCGR surgery in 2012, described 2 patients with scoliosis who had significant improvement in major curve magnitude (overall mean, 57% correction) and acceptable gain in T1-S1 spinal height (overall mean, 46 mm). One patient experienced loss of distraction related to magnetic device issue, which ultimately resulted in a surgical revision to exchange the device and restore curve correction and spinal height. The same patient experienced a superficial surgical site infection that was treated with medical management. Dannawi et al. [57], later in 2013, reported a series of 34 patients with minimum 1-year follow-up. Mean major curve correction was 41% and overall gain in spinal height was 44 mm. There were 2 patients

with rod breakages, 2 with superficial surgical site infections, 2 with loss of distraction, 1 with a hook pullout, and 1 with prominent implants. Akbarnia et al. [55] also published a study in 2013 describing the results of 14 magnetic growth rod patients with a mean follow-up of 10 months (range, 6-18 months). At latest follow-up the major curve corrected an average of 48% and spinal height increased an average of 9 mm for single rod constructs and 20 mm for dual rod constructs. Complications included superficial surgical site infection and prominent implants. Partial loss of distraction was noted in 14 of 68 noninvasive lengthening surgeries for the entire cohort. Hickey et al. [58] studied clinical and radiographic outcomes in 8 magnetic growth rod patients with minimum 23-month follow-up. Major curve correction averaged 43% for primary magnetic growth rod patients and 44% for patients who were converted from traditional growth rods to magnetic growth rods. Annual spinal growth was 6 mm/year for primary patients and 12 mm/year for converted patients. Typical complications associated with growing rod surgery occurred, such as anchor failure and rod breakage.

The pronounced benefits of magnetic growth rods are non-invasive distractions and better height retention by proposing frequent distraction (Figure 3-1). The unapparent benefit of magnetic rod could be the reduction of maximum stresses on the rod (and hence reduction in rod fracture rate) by frequent smaller distraction instead of major ones at duration greater than 6 months. However this unapparent benefit has not been researched or proposed before. The resultant consequence of this is the occurrence of rod breakage and screw pullout even in patient implanted with magnetic growth rods.[57, 59]

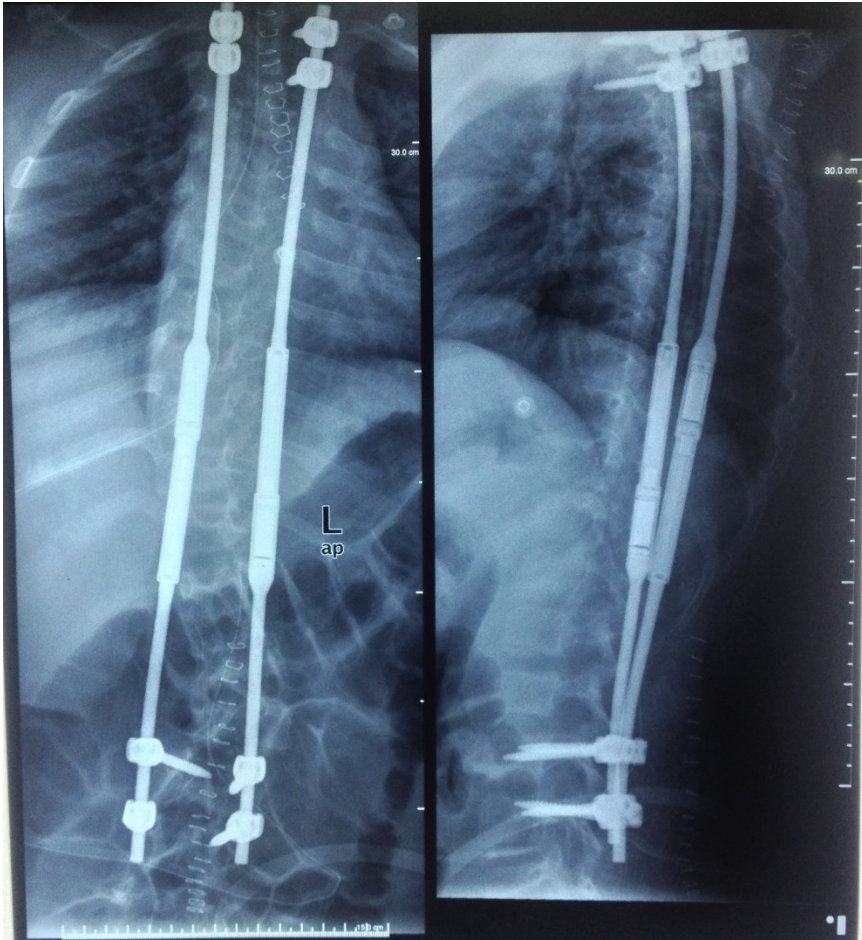


Figure 3-1: A 13 year old patient's X-ray showing magnetic growth rod implanted. This patient would not undergo invasive lengthening surgeries because this growth rod could be distraction non-invasively.

### 3.5 Summary

In summary, growth rods are the current standard for correcting and limiting the progression of scoliosis in juvenile growing patients. However, rod breakage is a usual complication with a rate of 15% or higher.[1, 40, 41, 43, 45, 46, 60] These complications are commonly addressed during routine lengthening or at cost of additional unplanned

surgeries. Moreover in patients with fractures, many cases of skin breakdown and deep wound infections at the rod fracture were reported.[2] All these require surgical debridement and antibiotic treatment. Beside rod replacement, these procedures tend to cause both psychological and physical trauma to the patient, provided their juvenile age at the time of surgery. Many factors have been identified that might help in better decision making to mitigate rod fracture.[20] Nevertheless, nothing substantial has been proposed and the occurrence of rod breakage still stand as one of the major complication seen with the patients undergoing growth rod implantation. Evidence from the literature points towards the fact that the distraction forces applied during these lengthening procedures are arbitrary and in most cases substantially high.[49, 51]

An ideal situation would be where the growth rod ‘grows’ (distracts) with the spine, but given the limitation of the conventional growth rods, there is a certain rate at which lengthening is undertaken. The usual standard for traditional growth rod is about 6 months. Therefore the distraction required for these cases should be equal to the expected growth in 6 months period for the patient. The forces produced would be proportional to the stiffness of the patient soft tissues (ligaments and disc). Therefore there is an inherent limitation on how much distraction is possible given the strength of these soft tissues. However increasing the frequency of distraction, i.e. shortening the distraction interval reduces the amount by which a spine has to be distraction. This isn’t really an option with the convention growth rod system given their invasive nature, although this could be achieved with noninvasive technologies like magnetic growth rod. There are no data or study that looks at how magnitude of various distraction forces and distraction frequencies

affect the propensity of growth rod fracture. The current study undertakes this goal with the previously mentions specific aims.

# Chapter 4

## Materials and Method

### 4.1 Introduction

This section describes in detail the methodology used for development of both normal and multiple representative scoliotic juvenile spine models. It further explains the incorporation of growth modulation, patient specific growth rod instrumentation, and the procedure for simulation of autofusion in these models. This is then followed by parametric study, analyzing the effect of distraction magnitude on T1-S1 height gain, sagittal contours, maximum von Mises stresses on the growth rods and screw-bone interface loading, and the effect of frequency of distraction on the maximum von Mises stresses on growth rods. The effect of high screw-bone interface loading on screw loosening was also verified using an *in vitro* experimental setup and is described at the later part of this section.

Several different FE models of the thoracolumbar spine have been used to study etiology and progression of idiopathic scoliosis. Besides the aforementioned application, they have also been used to analyze the mechanical response to bracing and surgery. For instance, beam element models simulating optimal surgical correction of scoliosis using Harrington distraction rods have been reported.[61-63] Spinal stiffness had an important role in predicting the nature and magnitude of corrective forces. Noone et al. later had developed a spinal column FE model where they applied traction to calculate the model



stiffness.[64] This helped them determine the optimal set of forces for gaining optimal correction of the spinal deformity. More recently, representative simple beam element model was used to simulate a cantilever method for scoliosis correction.[65] All these models could be classified into beam element models and volumetric element models. Beam element models are constitutive spring structures including rigid bodies, which are connected by joints and constraints, while volumetric models are composed of solid elements and shell elements.[66, 67] The elements used in volumetric models can be categorized into first order and second order, depending upon the number of nodes on the element; triangular element is 3-noded, while the higher order version of such an element is 6-noded. Beam element models fail to capture the complexity of 3D surface geometries, and it is impractical to include cortical structure, growth plates, and internal organs to such models. In contrast to beam-element models, volumetric element models better represent the spinal and scoliotic anatomy. The typical solid elements used are tetrahedral and hexahedral elements. Tetrahedral elements can be automatically generated using currently available meshing techniques. Although accommodating of any complex anatomical geometry, and therefore reducing the computational time and cost, they are theoretically less accurate than hexahedral elements. However, generating hexahedral elements using traditional methods is time consuming and expensive.[68] Currently there are several volumetric FE models that are composed of either tetrahedral elements [69], hexahedral elements [67, 70-76], or both [77-82], for scoliosis application. However, these volumetric FE models of spine developed are simplified and fail to mimic the exact geometry of the spinal components.

Anatomically accurate FE models are essential in order to investigate complex surgical procedures, as well as bracing techniques. Although it is valid to assume an anatomically complex geometry of the spine to be a stack of cylinders connected by layers of soft elements, it is not practical to simulate conditions such as relative over-growth of the vertebral body over the posterior elements on such simplified models. Also, due to the simplicity of the aforementioned volumetric models, accommodation of other soft tissue such as facet joints, ligaments, etc. is impractical. This further limits the investigation of the biomechanics of scoliotic spines. Developing separate patient-specific FE models for each individual that are geometrically robust with good quality hexahedral elements is computationally expensive and time intensive. In order to tackle such issues, tetrahedral elements that can be automatically generated to conform to complex geometries are preferred. However, as high-quality hexahedral elements are theoretically more accurate compared to tetrahedral elements, the former is preferred for FE analysis.[83, 84] In order to avoid the time intensive process of patient-specific FE modeling, a generalized model which can be morphed to accommodate subject-specific geometries have been developed for the pediatric brain [85], rat caudal vertebra [86, 87], femur [88, 89], vertebral centrum [90] and pelvis [91]. Such models use morphing algorithms to enable rapid development of age- and subject-specific FE models.[92] Recently, Lalonde et al. morphed a detailed FE model of a 32 years old thoracolumbar spine (T1-L5), including intervertebral discs and ligaments to a 10 years old and 82 years old spines using interpolation process.[80] Morphing of the generic FE mesh can distort the elements in the FE model causing degradation of element quality and generating poor simulation results. For more complex

anatomical structures, the nodes of distorted elements are adjusted through a time intensive manual process to refine mesh quality.

Material property and mechanical behavior are other characteristics along with the geometrical features that differentiate the younger population from adults. However, in the currently available FE studies on adolescent subjects the material property of adult was assigned to the spinal components due to lack of available data on adolescent specimens. Usually, a generalized FE model of a skeletally normal osteo-ligamentous adult thoracolumbar spine would be validated using material properties and *in vitro* experimental data obtained from adult cadaveric spines.[93-95] However, validating FE models of scoliotic spines against cadaveric range of motion data is not feasible due to the variations in the severity and type of deformity in each scoliotic patient.[96-100] Therefore most of the patient specific FE models used in scoliosis research were validated against the theories governing the etiology of scoliosis, except one where surgical technique was investigated on the validated thoracolumbar spine model.[69, 70, 77] Similarly, generalized FE models of scoliotic spines were validated against different hypotheses pertaining to etiology and progression of scoliosis deformity and simulated for bracing conditions.[67, 71, 79] Unavailability of cadaveric osteoligamentous scoliotic spine range of motion data that can be used to validate the FE models against is a drawback. Although *in vivo* experiments can be conducted on a specific scoliotic patient from whom the geometry can be obtained to develop the FE model, validating scoliosis patient-specific FE models is not feasible, due to the current difficulties involved in obtaining the joint reaction forces for every scoliotic patient. As a result, most of the personalized, scoliotic FE models were validated by simulating bracing techniques and patient-positioning.[72, 74]

Scale factors constitute another method used to make generalized model for younger patients. These scale factors have been used in the design and development of pediatric crash test dummies and pedestrian dummies (physical and numerical surrogates) for various ages between 6 months and 15 years.[101-103] Scaling techniques have also been incorporated into FE models of cervical spine developed referencing the CT images of a 10 year old child.[104] GJM Meijer et al validated a FE model of an adult female thoracolumbar spine that was geometrically scaled and deformed to obtain a 10 years AIS model.[105] To our knowledge, Abolaeha et al. is the only study in literature that simulated a surgical technique for juvenile subjects suffering from Early Onset Scoliosis (EOS), however there were no posterior elements, ligaments and facet joints in this model.[73]

Additionally, growth modulation in FE have been used for various studies with focus on etiology of scoliosis, efficacy of fusionless instrumentation and effects of various factors on scoliotic curve progression. Stokes et al developed a finite element model of the spine to investigate the initiation of the scoliosis curvature due to asymmetric loading.[106] Villemure et al developed an FE model that was intended to study the vertebral growth and growth modulation introducing a mathematical growth model into the FEM.[107] This study included scoliosis curve progression over a period of 24 months comparing the analysis results with radiograph scans. Fok in 2009 studied growth model in 3D utilizing the growth model developed by Villemure et al and Stokes et al, and studied the wedge angle generated by the model.[69, 106, 107]

## 4.2 Novel Methodology for Finite Element Model Development

Finite element model generation is a cumbersome process, and it takes a huge amount of time to generate and validate a new model. Typically for a juvenile spine it requires reconstruction of an entire 3D model of the spine from the computerized tomography (CT) data of a patient or a cadaver using specialized image reconstruction software.[108] Then this reconstructed 3D model is meshed using specialized meshing software. The two most common mesh modules used for the models are hexahedral and tetrahedral. The next and final steps are mesh refinement and validation of the newly generated finite element model with established *in vitro* or *in vivo* data.

Tetrahedral elements can be generated using automated tools available in different software but it has limited use in the analysis of spine models. Single hexahedral element (also known as voxelated meshes) is not practical due to its computational expenses and could also lead to erroneous data due to surface edge discontinuities. Hexahedral meshes perform better for finite element analysis but are much more difficult to generate specially at corners and edges of the solid model. This method of generating a finite element model suffers from multiple disadvantages. First and foremost, it limits the number of models that can be generated in a reasonable amount of time. Secondly, this process is unpractical for application where a general anatomy is not established and consists of huge variations (e.g. scoliotic spine deformity).

Other than the above mentioned conventional way of generating a finite element model, many researchers in the field have used different contemporary methodology as described next.

Little et al [109, 110] used series of elliptical and cubic equations to define the outer profile of endplates which was then used to extrapolate the outer profile of vertebral bodies using second order polynomial equation. Intervertebral disc were then interpolated between the outer profiles of endplates. The disadvantages were its very simplified vertebral body geometry and presence of rigid bodies and linear beams for posterior elements. O'Reilly et al [90] morphed a parametric FE model using landmark-based algorithm to automatically generate patient specific FE models for two motion segments of spine. They showed that mesh morphing is a viable method but it had several limitations. These limitations were difficulty in morphing the soft tissue (IVD) accurately by using CT data alone and the method could only morph the vertebral body of the central vertebra of a two motion segment spine. Clearly this technique could not be used for scoliotic spine model generation as it has complicated soft and hard tissue geometry. Gesbert et al [111] used splines to define the contours lines in sagittal and frontal radiographs, which allowed them to reconstruct spine as a curved beam. Then this curved beam representing spine was segmented using certain assumptions to limit the volume ratio of IVDs to vertebrae. This method does allow a quick retrieval of the shape of spine but it is very idealistic and may produce incredulous results for clinical application.

Due to the limitations and inefficiency in producing hexahedral mesh of scoliotic spine, many key researchers are using relatively simplified geometry and some even use tetrahedral-mesh FE model for their novel research.[69, 72, 79]

#### 4.2.1 Normal Juvenile Spine:

This section describes the method used to create a normal juvenile spine, which was later used as a foundation to produce multiple representative juvenile scoliotic spines. In this process, a CT of a typical 9 year old juvenile patient was taken, and the vertebral body and intervertebral height were recorded. To record the heights, the set of CTs with 0.5 mm slice thickness was imported in MIMICS (Materialize Inc., Leuven, Belgium) software. The 2D image data was then processed and edited to construct the three dimensional geometry of T1-S1 spine. The powerful segmentation tools of this software allowed easy segmentation, resulting in T1-S1 3D geometry that was used to query the heights.

Next a validated T1-S1 normal adult spine model [112] was scaled down to 71% of its original size to represent a juvenile size, based on literature data.[113] However the vertebral body to intervertebral height ratio of an adult is very different to a juvenile spine. For this reason, the mesh of this scaled down normal spine finite element model was altered, using ABAQUS (Dassault Systèmes, Simulia Inc., Providence, RI), to personalize the vertebral body and intervertebral body height to that of the recorded heights from juvenile CT data (Table 4.1) (Figure 4-1 & Figure 4-2).

Table 4.1: A comparison between the vertebral body and intervertebral disc heights of the scaled down model and the 3D reconstruction of a 9 year old juvenile CTs.

	3D geometry (mm)	Scaled down FE (mm)	Change made (mm)	

T1	8.74	11.34	-2.6	Reduced
T1-T2 Disc	5.41	3.05	2.36	Added
T2	8.92	12.53	-3.61	Reduced
T2-T3 Disc	4.05	2.81	1.24	Added
T3	9.24	12.61	-3.37	Reduced
T3-T4 Disc	5.18	2.01	3.17	Added
T4	9.42	13.01	-3.59	Reduced
T4-T5 Disc	4.29	2.02	2.27	Added
T5	9.72	13.01	-3.29	Reduced
T5-T6 Disc	4.64	2.22	2.42	Added
T6	10.26	13.97	-3.71	Reduced
T6-T7 Disc	3.62	2.18	1.44	Added
T7	10.75	14.61	-3.86	Reduced
T7-T8 Disc	4.45	2.4	2.05	Added
T8	11.66	15.01	-3.35	Reduced
T8-T9 Disc	4.57	2.31	2.26	Added
T9	12.05	15.49	-3.44	Reduced
T9-T10 Disc	4.91	2.22	2.69	Added
T10	12.28	16.2	-3.92	Reduced
T10-T11 Disc	4.94	2.41	2.53	Added
T11	14.33	17.1	-2.77	Reduced



T11-T12 Disc	4.36	3.77	0.59	Added
T12	15.14	18.23	-3.09	Reduced
T12-L1 Disc	5.1	4.58	0.52	Added
L1	15.58	19.12	-3.54	Reduced
L1-L2 Disc	5.9	5.75	0.15	Added
L2	17.47	19.53	-2.06	Reduced
L2-L3 Disc	6.4	8.67	-2.27	Reduced
L3	17.5	18.64	-1.14	Reduced
L3-L4 Disc	8.25	7.08	1.17	Added
L4	17.72	18.63	-0.91	Reduced
L4-L5 Disc	8.8	10.1	-1.3	Reduced
L5	18.49	18.17	0.32	Added
L5-S1 Disc	11.53	10.12	1.41	Added
S1	5.4	5.1	0.3	Added



Figure 4-1: FE model of a normal juvenile spine after scaling and adjustment of vertebral body to intervertebral body heights.



Figure 4-2: FE model of a normal juvenile spine with altered kyphotic and lordosis curve.

#### 4.2.2 Representative Juvenile Scoliotic Models.

This section describes the novel method used to generate multiple finite element scoliotic spine model with high overall geometric accuracy. In this approach we used the above described normal juvenile spine element as a template. The desired scoliotic spine was generated by using two custom script (MATLAB, Natick, MA UNITED STATES) that carried out the following operations: 1. lateral shift to create coronal deformity and 2. axial rotation to create axial deformity.

##### **Lateral shift**

In the lateral shift technique we started with forming a polynomial equation of the form  $X = f(Z) = a_1 + a_2Z + a_3Z^2 + a_4Z^3 + \dots + a_nZ^{n-1}$ , where  $X$  is the lateral shift (from the plum line),  $Z$  is the height (along the length of the thoracolumbar spine),  $a_1, a_2, \dots, a_n$  are the coefficients of the equation and  $n-1$  is the order of the equation. The curves defined by this polynomial equation were used as the base for projection of the normal spine finite element model. The order of the polynomial equation depends on the type of curve generated and is described shortly.

The boundary conditions, for which the values of  $X$ ,  $dX/dZ$  (only if it is zero), and  $Z$  were taken from the literature [114], were substituted in the above equation to derive the coefficients of the above polynomial equation. These boundary conditions constitute of inflection points (point of maxima and minima of the curve) and the points at which the curve crosses the plum line, i.e.  $X=0$ . We followed the convention where left lateral shift was considered negative  $X$  and right lateral shift as positive  $X$ . In clinical terms the points of maxima will be the apical vertebral translation (AVT) of the right curves and the points of minima would be the AVT of the left curves.

The nodes constituting the finite element model of the normal juvenile spine has its 3D global coordinate predefined with  $Z_{node}$  (where the subscript represents the node number) representing its axial position along the spine. We used this  $Z_{node}$  and substituted it in the equation that we obtained to calculate its lateral shift  $X_{node}$ . Thereafter, to project the nodes on this curve such that it generates a scoliotic spine with both vertebral and intervertebral disc wedging, a projection vector ( $\mathbf{V}_{node}$ ) perpendicular to the curve was defined. This projection vector  $\mathbf{V}_{node}$  makes an angle  $\Theta_{node}$  with the lateral shift line, where  $\tan(\Theta_{node}) = (dX/dZ)_{node}$ .  $\mathbf{V}_{node} = X_{node}(\cos^2(\Theta_{node}))\mathbf{i} + X_{node}(\cos(\Theta_{node})\sin(\Theta_{node}))\mathbf{j}$ , deduced by simple trigonometry as described schematically in the figure below (Figure 4-3).

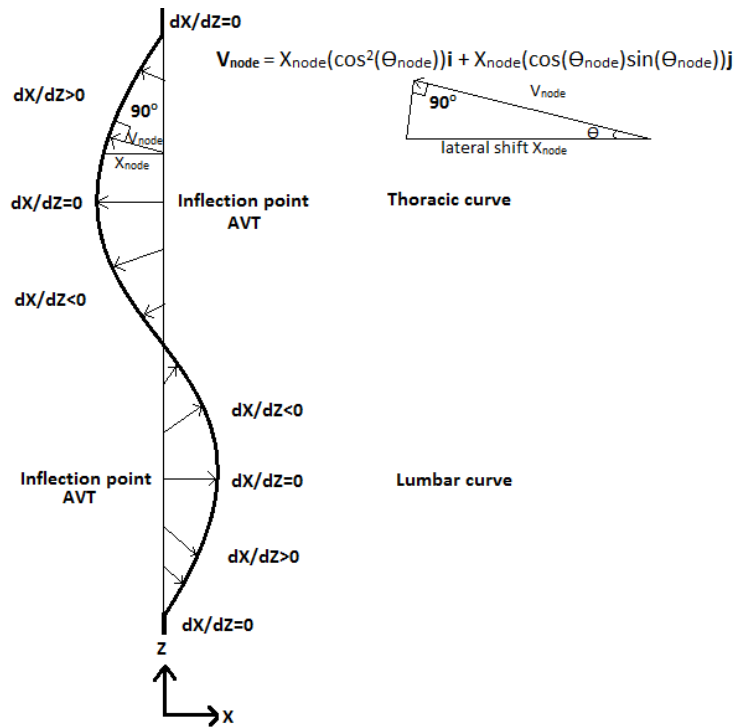


Figure 4-3 Schematic showing projection vectors of the plum line (vertical line) onto the curve (S shaped curve) obtained from the polynomial equation in coronal plane. The magnitude and direction of this vector is given which could be deduced by simple trigonometry.

### Axial rotation

In axial rotation technique, intervertebral discs (IVDs) and the vertebrae were rotated about the axis tangential to the sagittal profile line and passing through the center of the vertebral body or IVDs at that region. The angles of rotation for spine were taken from the literature.[114] The angular profile generated is shown in Figure 4-4. It shows that the angle changes from 0 to  $\phi_1$  for the superior IVD over the first truly rotated vertebra. Then the angle changes from  $\phi_1$  to  $\phi_2$  for the IVD between first and second axially rotated vertebrae and this profile reverses after the apex vertebral rotation (AVR) has been reached ( $\phi_5$  in this case).  $\phi_1$  and  $\phi_2$  are the whole axial rotation of first and second vertebra

respectively and  $\phi_5$  is the AVR. The apical vertebra mostly coincides with inflection regions.[115]

To achieve this, the nodes constituting the vertebral body and IVD were rotated in axial plane (more precisely the plane which intersects perpendicular to the sagittal contour profile) about the center of the vertebral body and center of IVD respectively. The initial position of the node is represented by vector  $\mathbf{R}_{\text{node}}$  (where the subscript represents the node number). This vector was then multiplied by a function that changed its direction by desired angles at each level while keeping its magnitude constant. This was achieved by resolving the vector into its components  $\mathbf{R}_{\text{node}(\mathbf{i})}$  and  $\mathbf{R}_{\text{node}(\mathbf{j})}$ .  $\mathbf{R}_{\text{node}(\mathbf{i})}$  was multiplied by  $\cos(\arctan(\mathbf{R}_{\text{node}(\mathbf{j})}/\mathbf{R}_{\text{node}(\mathbf{i})})+\phi_{\text{node}})$  and  $\mathbf{R}_{\text{node}(\mathbf{j})}$  by  $\sin(\arctan(\mathbf{R}_{\text{node}(\mathbf{j})}/\mathbf{R}_{\text{node}(\mathbf{i})})+\phi_{\text{node}})$  to form the new vector  $\mathbf{R}'_{\text{node}}=\mathbf{R}_{\text{node}(\mathbf{i})}\cos(\arctan(\mathbf{R}_{\text{node}(\mathbf{j})}/\mathbf{R}_{\text{node}(\mathbf{i})})+\phi_{\text{node}})+\mathbf{R}_{\text{node}(\mathbf{j})}\sin(\arctan(\mathbf{R}_{\text{node}(\mathbf{j})}/\mathbf{R}_{\text{node}(\mathbf{i})})+\phi_{\text{node}})$ , deduced by using simple trigonometry as shown in Figure 4-4.  $\phi_{\text{node}}$  was constant for all the nodes constituting the same vertebra. For the nodes constituting IVDs,  $\phi_{\text{node}}$  was variable and was defined as the functions of their position in Z-coordinate (i.e. the axial position)  $Z_{\text{node}}$ . For all IVDs above the AVR,  $\phi_{\text{node}} = (\phi_{\text{superior}} - \phi_{\text{inferior}}) (1 - (Z_{\text{node}} - Z_{\text{min}})/(Z_{\text{max}} - Z_{\text{min}}))$ , where  $\phi_{\text{superior}}$  is angular rotation of the vertebra superior to the IVD,  $\phi_{\text{inferior}}$  is angular rotation of the vertebra inferior to the IVD,  $Z_{\text{min}}$  and  $Z_{\text{max}}$  are the minimum and maximum of all Z-coordinates of the index IVD respectively. Similarly,  $\phi_{\text{node}} = (\phi_{\text{inferior}} - \phi_{\text{superior}}) ((Z_{\text{node}} - Z_{\text{min}})/(Z_{\text{max}} - Z_{\text{min}}))$  for all IVDs below AVR (Figure 4-4).

The MATLAB scripts used for axial rotation and coronal plane deformity has been compartmentalized in this study, but in theory there must exists a relationship between the two. As previously pointed out by Stokes et al, the natural history and the precise

relationships between scoliotic deformities in different planes is less well-known.[116] This subjects the current approach to a two-step process with independent inputs taken from literature.

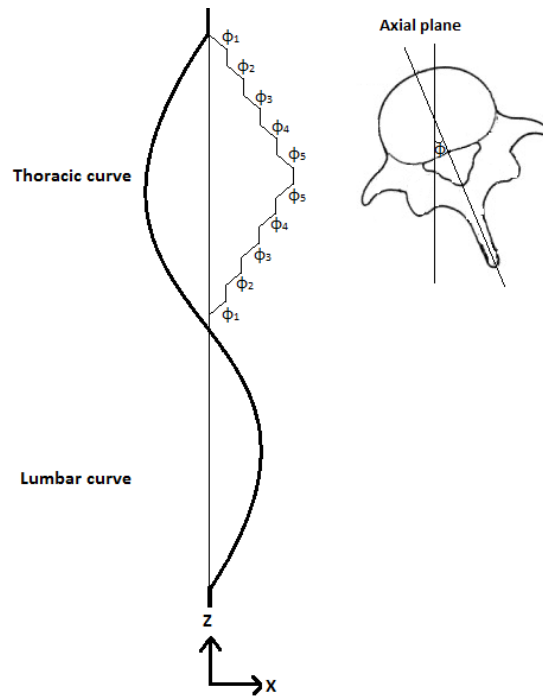


Figure 4-4: Schematic showing an example of an angular profile (change in angle with height) for the thoracic curve in coronal plane; the angles are measured in axial plane as showed.

Robinson et al [114] reviewed the medical records and radiographs of 109 consecutive patients who had juvenile idiopathic scoliosis and classified them into four major groups based on the curve pattern. 1(a) Group 1A: single mid-thoracic curve with the apex usually at the eighth thoracic vertebra, 1(b) Group 1B: major mid-thoracic curve with the apex usually at the eighth thoracic vertebra and a secondary minor lumbar curve, 3. Group 2: single thoracic curve with the apex usually at the ninth or tenth thoracic level, 4. Group 3:

single thoracolumbar curve with the apex at the twelfth thoracic level, 5. Group 4: major lumbar curve with the apex at the second or third lumbar level and a secondary minor thoracic curve. The above described technique were used to generate all of these 5 curve types as shown in figure below (Figure 4-5).

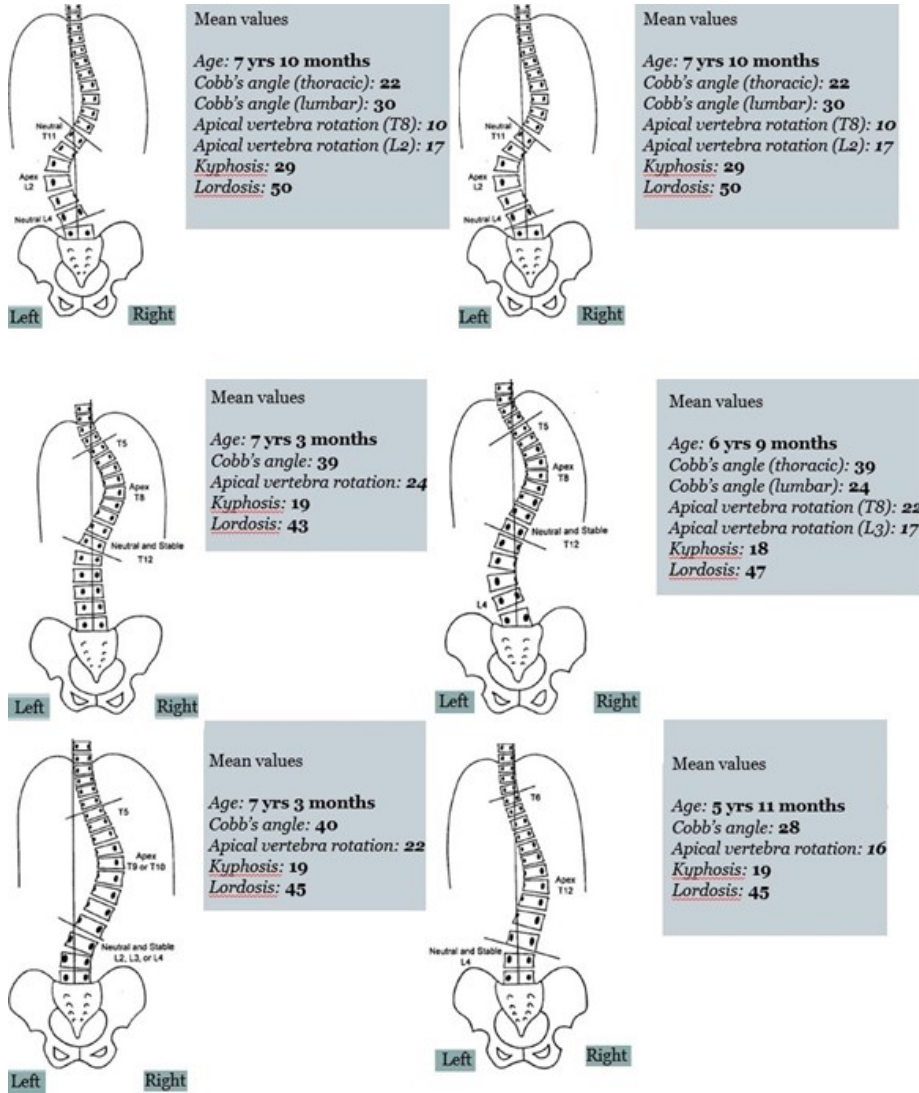


Figure 4-5: : Various juvenile idiopathic curves as classified by Robinson et al [114] and used for generating representative scoliotic models.

### 4.2.3 Growth Rod Design and Instrumentation

Growth rod instrumentation for each model was meticulously designed using Solidworks (Dassault Systèmes SolidWorks Corporation, Waltham, MA). First, the surface geometry of the spine model was transferred from Abaqus to Solidworks in form of STL file format. This surface cloud information was then used in Solidworks to help in proper placement of pedicle screws and assigning appropriate shape to the rods to account for the sagittal contour of each model. Thereafter, the complete growth rod instrumentation geometry was imported in Abaqus for modeling and simulation.

Growth rods were simulated in the FE spine models (normal and scoliotic) with eight 4.5 mm titanium alloy (Ti6Al4V) pedicle screws and four 4.5 mm titanium alloy (Ti6Al4V) rods (two distal and two proximal) (Figure 4-6, Figure 4-7, Figure 4-8, Figure 4-9, Figure 4-10, Figure 4-11, Figure 4-12, Figure 4-13). Four out of eight pedicle screws were anchored bilaterally at the pedicles of the upper two vertebral foundation, the rest were placed bilaterally at the pedicles of the lower two vertebral foundation. The pedicle screws were kinematically coupled to the pedicles via bushings in all three degrees of freedom. The proximal rods were tied bilaterally to the respective ipsilateral proximal pedicle screws and distal rods to ipsilateral distal pedicle screws. The tandem connection was simulated by kinematically coupling the ipsilateral free ends of the rods in all three degrees of freedom. For the sake of comparison, all the models were instrumented with an initial (pre distraction) Cobb angle of  $35^\circ$ , kyphosis of  $38^\circ$ , and lordosis of  $39^\circ$ .





Figure 4-6: Instrumented normal juvenile spine model



Figure 4-7: Instrumented normal juvenile spine model with altered sagittal contours

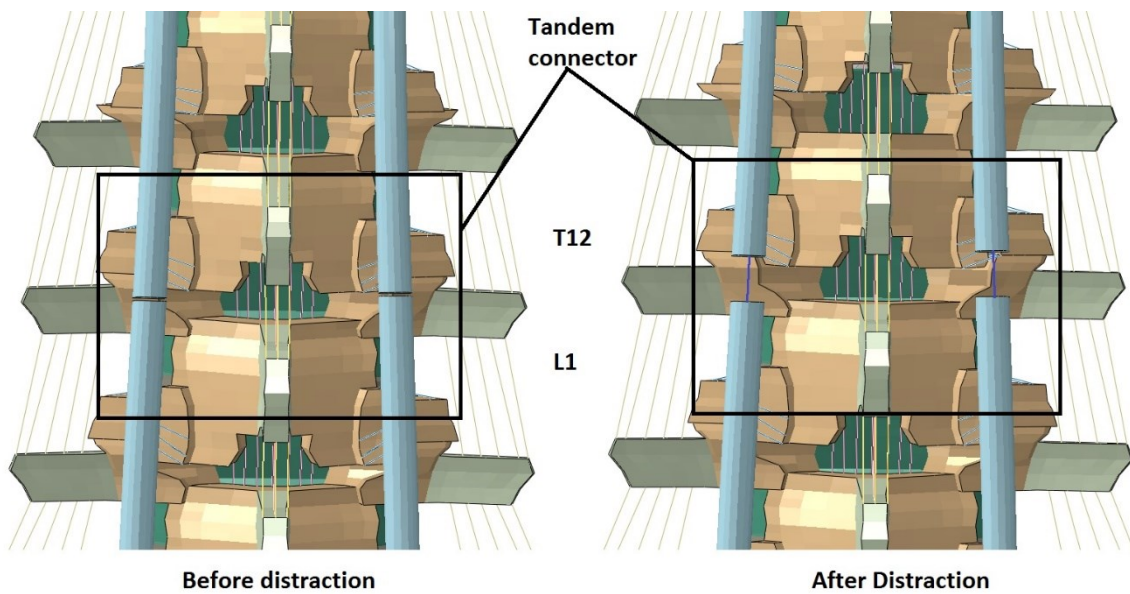


Figure 4-8: The figure shows the region of the tandem connector before and after distraction. The connector elements are modeled analytically.

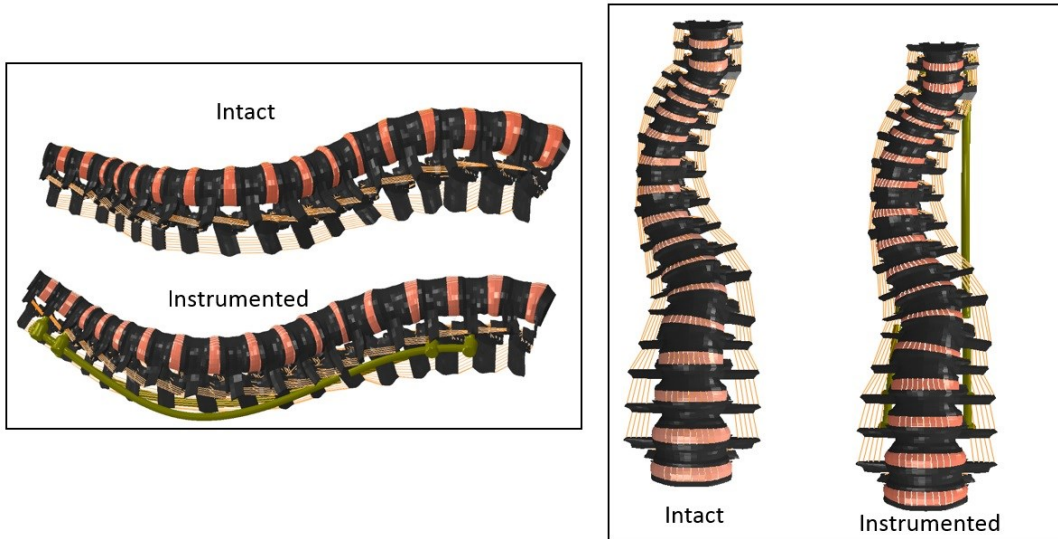


Figure 4-9: Group 1A representative juvenile scoliotic FE model

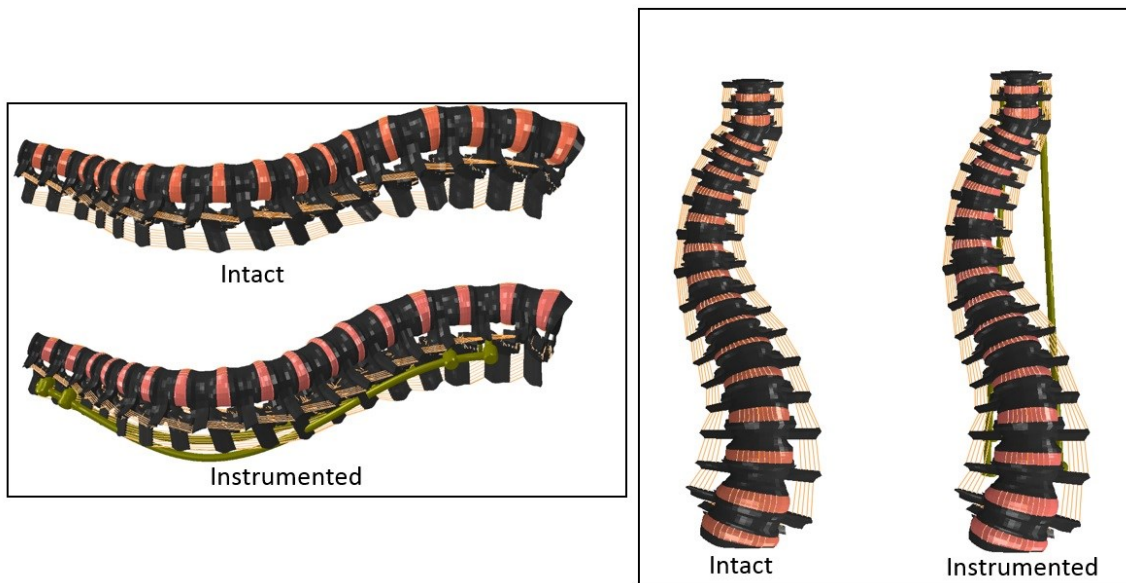


Figure 4-10: Group 1B representative juvenile scoliotic FE model



Figure 4-11: Group 2 representative juvenile scoliotic FE model



Figure 4-12: Group 3 representative juvenile scoliotic FE model



Figure 4-13: Group 4 representative juvenile scoliotic FE model

#### 4.2.4 Material Properties and Boundary condition

Following the development of the normal and representative scoliotic juvenile FE model, all the meshed regions were assigned appropriate material properties (Table 4.2 & Table 4.3). As scoliotic spine are atypical and vary in curve type and flexibility, there are no experimental data available to validate the generated representative spines. However for the normal juvenile spine there is limited data available (FE data) for comparison of the motion. The comparison is shown in Table 4.4.

Table 4.2: The material properties used in the model for bone, ligament, intervertebral disc and instrumentation

<b>Component</b>	<b>Element formulation</b>	<b>Modulus (MPa)/Poisson's ratio</b>
<b>Cortical bone</b>	Isotropic, elastic hex elements (C3D8)	75/0.29[117-120]
<b>Cancellous bone</b>	Isotropic, elastic hex elements (C3D8)	75/0.29[117-120]
<b>Growth plate</b>	Isotropic, elastic hex elements (C3D8)	25/0.4[119]
<b>Posterior bone</b>	Isotropic, elastic hex elements (C3D8)	200/0.25[117-120]
<b>Nucleus</b>	Isotropic, elastic hex elements (C3D8H)	1/0.4999[117-120]
<b>Annulus (ground)</b>	Neo-Hookean, hex elements (C3D8)	C10=0.348, D1=0.3[121]
<b>Annulus (fiber)</b>	Rebar	357–550[121]
<b>Apophyseal joints</b>	Nonlinear soft contact, GAPPUNI elements	12,000[121]
<b>Ligaments</b>	Tension-only, truss elements (T3D2)	90% of the adult ligament values[119, 121]
<b>Ti Pedicle screws</b>	Isotropic, elastic hex elements (C3D8)	115000/0.3

<b>Ti Growth rods</b>	Isotropic, elastic hex elements (C3D8), 4.5mm diameter	115000/0.3
-----------------------	---	------------

Table 4.3: The material constants for annular fibrosus, nucleus pulposus and ligaments used with Prony series for modeling viscoelastic behavior of the disc <sup>27, 28</sup>

	<b>Annular Matrix</b>	<b>Annular fibers</b>	<b>Ligament</b>	<b>Nucleus</b>
<b>Shear relaxation modulus (G(t))</b>	0.399	0.062	0.7045	0.638
	0.000	0.042	0.107	0.156
	0.361	0.065	0.076	0.120
	0.108	0.15	0.1102	0.0383
				0
<b>Bulk relaxation modulus (K(t))</b>	0.399	0	0	0
	0.300	0	0	0
	0.149	0	0	0
	0.150	0	0	0
				0
<b>Relaxation time constant (sec)</b>	3.45	1	1	0.141
	100	10	10	2.21
	1000	100	80	39.9
	5000	700	500	266
				500

Table 4.4: The range of motion (degrees) of the present model with available literature data for 0.5Nm with no preload [118-120]

	Combined flexion- extension		Combined lateral bending		Combined axial rotation	
	Literature	Present model	Literature	Present model	Literature	Present model
L1-L2	2.39	2.19	1.31	1.43	1.19	1.31
L2-L3	1.65	1.52	1.67	1.59	1.54	1.61
L3-L4	1.47	1.56	1.13	1.23	0.88	1.12
L4-L5	1.32	1.58	2.02	2.18	1.44	1.56

Shi et al simulated two distinct spinal loading techniques in their recent study and reported no significant differences in the growth modulation output. The two approaches were: gravitational and follower load. Under the gravitational approach, the loading direction was maintained axially to simulate forces which, when coupled with T1 restricted in the transverse plane and L5 constrained in all degrees of freedom, provided appropriate spinal stability.[81] In the other loading technique, the follower load was alternatively simulated in a fashion that the resultant forces from cumulative loads on each vertebra was maintained tangential to the curvature of the spine in the sagittal plane and remained axial in the coronal plane. In former, the vector direction of gravitational loading approach remained constant throughout the analysis whereas the directional vector in follower load method changed itself in order to maintain tangential loading in sagittal contours. Based



on their results and analysis, follower load technique was chosen and simulated to account for the load at different vertebral levels due to upper body mass and muscle contraction. Schultz et al had reported that the spine is loaded with 14 % body weight at T1, following a 2.6 % body weight increase between succeeding vertebrae.[122] The given proportions were used to calculate the follower load for the current 9 year old patient’s spine with a mean weight of 22 Kg as shown in Table 4.5. Boundary condition consisted of restraining the inferior surface of S1 vertebra in all degrees of freedom based on previously approved methodology for growth simulation in FE.[81]

Table 4.5: Follower load applied based on percentage increase in load from T1 to L5.

22 Kg & 9 years old	Percentage of weight (%)	Weight (Kg)	Load (N)
T1	14.0	3.1	30.2
T2	16.7	3.7	36.0
T3	19.4	4.3	41.8
T4	22.1	4.9	47.6
T5	24.8	5.4	53.4
T6	27.5	6.0	59.2
T7	30.1	6.6	65.0
T8	32.8	7.2	70.8
T9	35.5	7.8	76.6
T10	38.2	8.4	82.4
T11	40.9	9.0	88.2



T12	43.6	9.6	94.0
L1	46.3	10.2	99.8
L2	49.0	10.8	105.6
L3	51.7	11.4	111.4
L4	54.4	12.0	117.2
L5	57.0	12.5	123.0

### 4.3 Incorporation of Growth modulation

Unlike adult spine, a juvenile spine has a certain rate of longitudinal growth. It is attributed to the vertebral growth plates consisting of superior and inferior epiphyseal plates. In the present models, these were modeled near the two ends of each vertebra using isotropic and elastic hexahedral elements. The pressure change was sensed at the growth plate, while new bone was added to the bone layers adjacent to it.[81] The mean growth strain rate for 9 year old patient's spine is 0.035 for 6 months period. However the growth strain rate gets altered in such patients due to growth rods and distraction forces. This altered growth rate was captured in the finite element model using the empirical equation provided by Villemure et al.[123] Essentially the equation describes the Hueter-Volkman principle of growth modulation, which is expressed in their empirical equation below:

$$G = G''[1 + \beta(\sigma - \sigma'')] ]$$

where G is the actual growth strain, G'' is the mean baseline growth strain (at a given age),  $\sigma$  is actual compressive stress on the growth plate (in MPa),  $\sigma''$  is the mean baseline stress on the growth plate for the intact spine (in MPa) and  $\beta$  is equal to  $1.5\text{MPa}^{-1}$  for vertebrae. For intact model, G is equal to G''. G'' is equal to 0.035 per 6 months for a 9 year old child

spine, as per the published literature.[14, 69] Integration of this growth modulation into the FE model was done by means of thermal expansion, converting the growth strains (calculated from above equation for each element) into thermal loads and applying those across the nodes.[24] The thermal loads were determined using the following relation:

$$\delta T = \varepsilon / \alpha$$

Where,  $\delta T$  is the thermal load for the iteration,  $\varepsilon$  is the thermal strain (growth strains) for the iteration, and  $\alpha$  is an arbitrary number representing the coefficient of thermal expansion.

#### **4.4 Incorporation of Autofusion**

The spines instrumented with growth rods exhibit diminished lengthening with subsequent distractions.[24] It was also shown that the forces required to achieve distraction increase with subsequent distraction.[24] This is attributed to autofusion at the spinal segments and is an important aspect that was included in the current models. It was incorporated in the models by increasing the stiffness of the spine as a function of time, using the available data (Figure 4-14 & Figure 4-15) on diminished lengthening on subsequent distractions, as shown in Figure 4-16.[24] The data pertain to increase in distraction force with subsequent distraction surgery. The duration between each distraction was 6 months. The data was presented as distraction versus months following surgery with #1 for 1<sup>st</sup> distraction, over a period of 24 months at 6-monthly interval. The stiffness was calculated based on the mean values of distraction forces and the corresponding distractions. The mean value of distraction forces were 143 N, 102 N, 170 N, 201 N, and 373 N at 0, 6, 12, 18 and 24 months, respectively. The corresponding mean

values of distraction were 17 mm, 10 mm, 11 mm, 9 mm, and 8 mm, respectively. Stiffness was calculated as distraction force divided by distraction; 8.4 N/mm, 10 N/mm, 15.4 N/mm, 22.2 N/mm and 46.3 N/mm at 0, 6, 12, 18 and 24 months, respectively. These values were used to find a polynomial equation establishing a relation between stiffness and the time after implantation. The percentage increase in stiffness at each time point was found and incorporated into the spine model by increasing the modulus of elasticity of nucleus pulposus and annulus fibrosus. The slopes of increase in the longitudinal stiffness of the spine (in tension) with respect to the Young's modulus ( $\text{N}/\text{mm}^2$ ) of the nucleus pulposus and the shear modulus ( $\text{N}/\text{mm}^2$ ) of the annulus fibrosus were calculated, these were  $0.55 \text{ mm}^{-1}$  and  $7.2 \text{ mm}^{-1}$  respectively. Thus the necessary increase in stiffness was achieved by using the above given slopes to calculate the required absolute increase of modulus values for nucleus pulposus and annulus fibrosus.

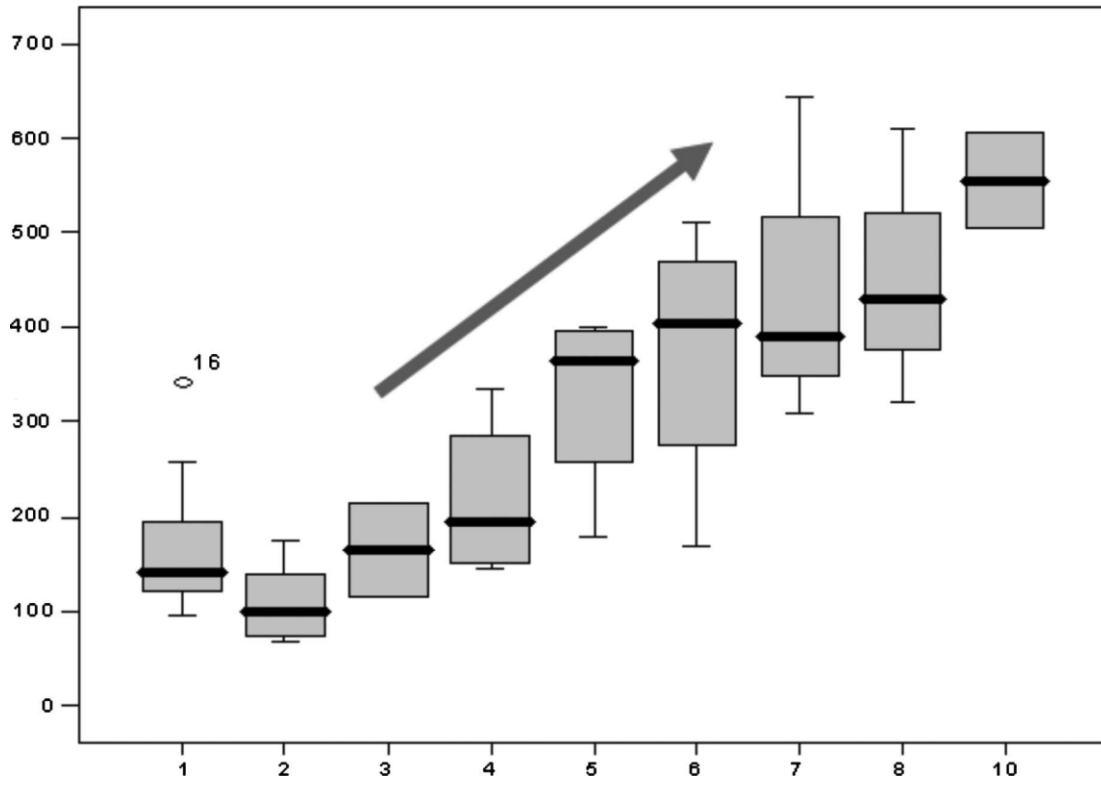


Figure 4-14: Graphical presentation of force vs. number of distraction .[24]

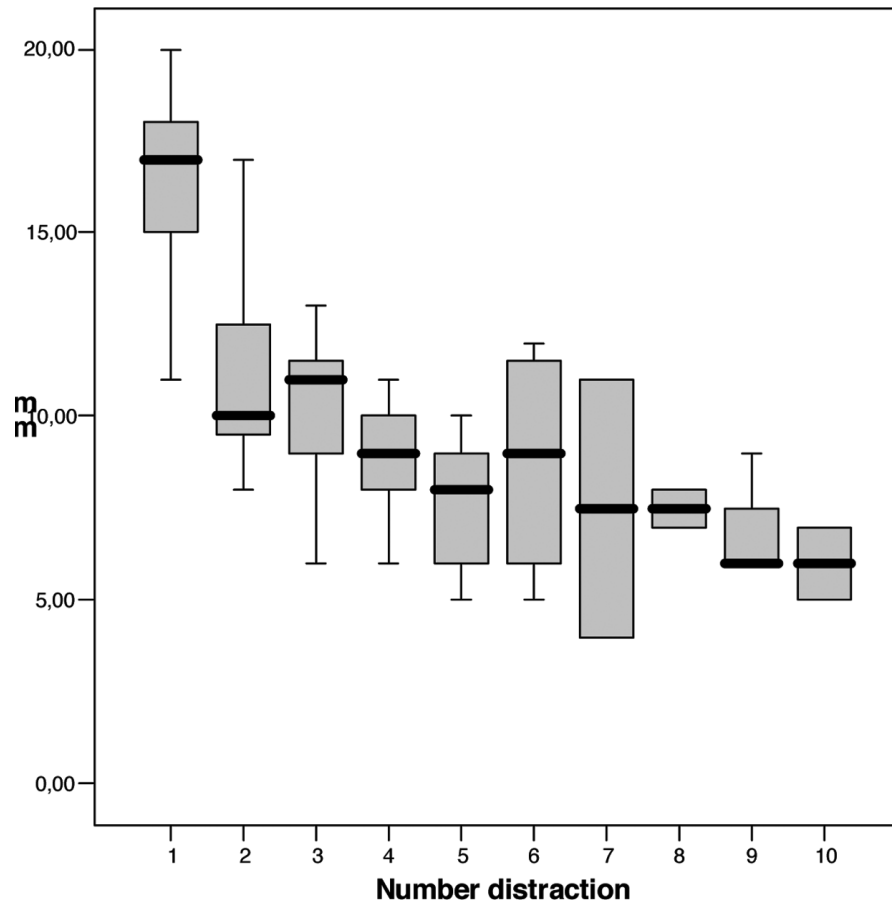


Figure 4-15: Graphical presentation of length vs. number of distraction .[24]

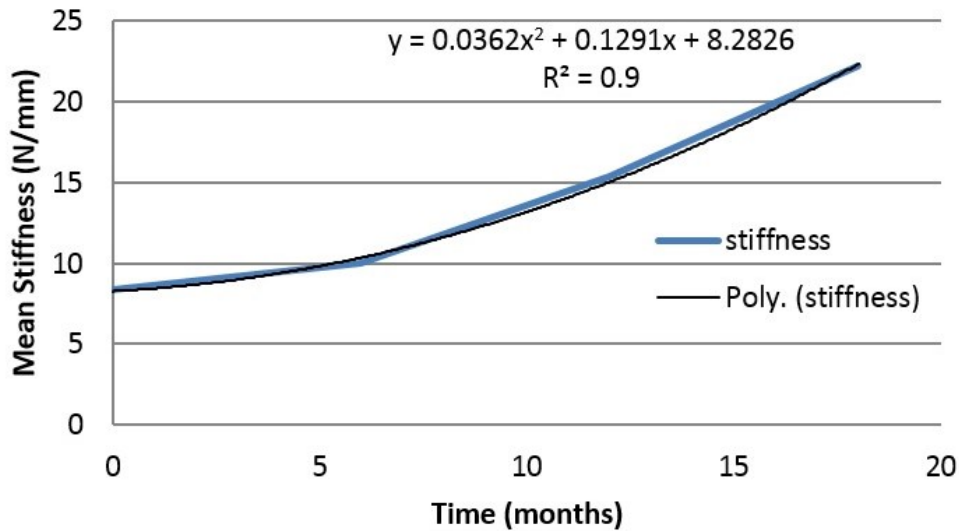


Figure 4-16: The plot showing increase in stiffness due to autofusion at different period after instrumentation with dual growth rods.

#### 4.5 Parametric study

##### 4.5.1 Effect of Distraction Forces

As mentioned earlier despite many advantages of growth rod systems, there have been many instances of failure.[19] Rod fractures occur in 15% of patients treated with growing rods.[17, 20, 21, 124] It has been established that pedicle screws provides for a better anchor, however there has been incidences of screw loosening cited in the literature.[3, 4] Some researchers also believe that the distraction forces applied are so high that, instead of sustaining growth, it is stimulating it.[5, 6] Suboptimal distraction could also lead to poor sagittal contours in juvenile patients.[7] Hence there is a need for studies to optimize the distraction force for sustained growth of the spine, along with unaltered final sagittal contour and lower stresses on the rods. Therefore a parametric study was

undertaken to elucidate the effects of distraction forces on the T1-S1 height gain, change in sagittal contours, change in Cobb angle (not applicable for normal juvenile spine model), maximum von Mises stresses on the rods and screw-bone interface loads. For each model 8 different cases were simulated with distraction forces varying from 25 N at each side (50 N total) to 200N at each side (400 N total) (Table 4.6). These magnitudes of distraction forces used are within the range reported in the literature.[24] These cases were then simulated for 6 months of growth using growth modulation in FE as described previously.

Table 4.6: Different models simulated under dual growth rod instrumentation group

<b>Dual growth rod instrumented models</b>	<b>Distraction force per rod ( N)</b>	<b>Total distraction force ( N)</b>
<b>GR 25N</b>	25	50
<b>GR 50N</b>	50	100
<b>GR 75N</b>	75	150
<b>GR 100N</b>	100	200
<b>GR 125N</b>	125	250
<b>GR 150N</b>	150	300
<b>GR 175N</b>	175	350
<b>GR 200N</b>	200	400

#### 4.5.2 Effect of Distraction Frequency

With the recent advent of non-invasive growth rods, there is a possibility of numerous distractions based on patient's requirement and surgeon's assessment. This new

technology makes it feasible to distract rods at shorter intervals without causing discomfort to the patient.[25] A parametric study was performed to analyze the effect of distraction frequency on the maximum von Mises stress generated on the rods. Four cases with different distraction time intervals were simulated over a 24 month period. The simulation cases included: (a). 2 distractions (at time 0 and at time 12 months) at 12 months period for 24 months, (b). 4 distractions (at time 0, at time 6 months, at time 12 months, and at time 18 months), (c). 8 distractions (at time 0, at time 3 months, at time 6 months, at time 9 months, at time 12 months, at time 15 months, at time 18 months, and at time 21 months), and (d). 12 distractions (at time 0, at time 2 months, at time 4 months, at time 6 months, at time 8 months, at time 10 months, at time 12 months, at time 14 months, at time 16 months, at time 18 months, at time 20 months, and at time 22 months). For comparison the distraction magnitude at each case was based on expected normal growth within the instrumented level for the period between consecutive distractions as shown in Table 4.7.

Table 4.7: Distraction applied based on expected growth within the instrumented levels for the period between consecutive distractions [125]

<b>Distraction required (mm)/Optimal distraction force (N)</b>	<b>Frequency of distraction (months)</b>
11.6/250	12
5.8/125	6
2.9/63	3
1.93/32	2



## 4.6 Sensitivity Study

Juvenile scoliotic spine varies in curve type and curve rigidity. The issue of curve type has been addressed by the use of multiple representative scoliotic spines to demonstrate similar trends in the effect of distraction forces and frequency. This section describes the methodology implemented to address the effect of curve rigidity on the distraction frequency with optimal distraction force. The study was performed by varying the stiffness of the spine and applying distraction up to a maximum stress of 255 MPa. Thereafter, for each model (with different stiffness, 8.2 N/mm, 12.5 N/mm, 13.8 N/mm, 14.7 N/mm, 16.2 N/mm, 18.2 N/mm, 20.2 N/mm, 21.9 N/mm, 23.1 N/mm, 25.5 N/mm), the highest distraction interval was correlated to the growth interval as shown in the table above to find the optimal distraction interval. 255 Mpa was chosen to keep the factor of safety equal to two, as the fatigue strength of titanium is 510 MPa. The stiffness was varied by increasing the modulus of elasticity of nucleus pulposus and annulus fibrosus. As described in a previous section, the slopes of increase in longitudinal stiffness of spine (in tension) with respect to the Young's modulus ( $\text{N/mm}^2$ ) of nucleus pulposus and shear modulus ( $\text{N/mm}^2$ ) of annulus fibrosus were  $0.55 \text{ mm}^{-1}$  and  $7.2 \text{ mm}^{-1}$  respectively. Beside this the change in Cobb angle correction by gravity (to simulate unconstrained traction) was also recorded for each model to establish a relationship between mathematically calculated stiffness and clinically measurable parameters.

#### 4.7 *In Vitro* Experiment: Correlation of Loads to Screw Loosening

Rod breakage and screw loosening are two chief complications associated with growth rod instrumentation in juvenile scoliotic spine. Rod breakage was evaluated with maximum von Mises stresses on the rod, which is a direct indicator of yielding of growth rods. However, screw loosening was evaluated with screw-bone interface loads and is an indirect predictor of screw loosening. Therefore, to better translate the results from FE, an *in vitro* experiment was performed.

Six vertebrae with T-scores of -0.8 (normal bone) were chosen for this experiment. All vertebrae (T1, T2, T3, T4, T10 and T11, these were the largest of all) were intentionally chosen from a single thoracic spine specimen to reduce the variability in bone mineral density that might have occurred otherwise. Each vertebra was cleaned of excess soft tissues and a 2.5 mm hole was drilled in both of the pedicles of each vertebra. This was followed by insertion of 4.5 mm Ti6AL4V pedicle screws. A single 5.5 mm Ti6AL4V rod was then attached to each pedicle screw and the assembly was tightened to a torque of 10 Nm. Thereafter the vertebrae were potted using bondo and fiber resin (1:1), and mounted on the MTS machine. The specimen was gripped using a 3 axes vice, which in turn was mounted on an X-Y table on top of MTS load cell (Figure 4-17 & Figure 4-18).

Screw-bone interface loads for 150 N (Group 1-optimal distraction force) and 400 N (Group 2-high distraction force) of total distraction force and 6 months of growth (normal juvenile spine instrumented with growth rods) were taken from FE results and each load profile was super-positioned with  $\pm 0.75$  Nm ( $\pm 14$  N with a moment arm of 53 mm) of sinusoidal motion at 5 Hz for 1.25 million cycles. The resultant load profiles were then

discretized into 125 steps with each step consisting of 1000 cycles (Figure 4-19 & Figure 4-20). Each group consisted for 6 samples (i.e. 3 vertebrae).



Figure 4-17: The actuator applied the load along the rod to simulate the fatigue.



Figure 4-18: The in-vitro setup: 3-axes vice was mounted on top of x-y table top axes to establish proper orientation between rod and actuator.

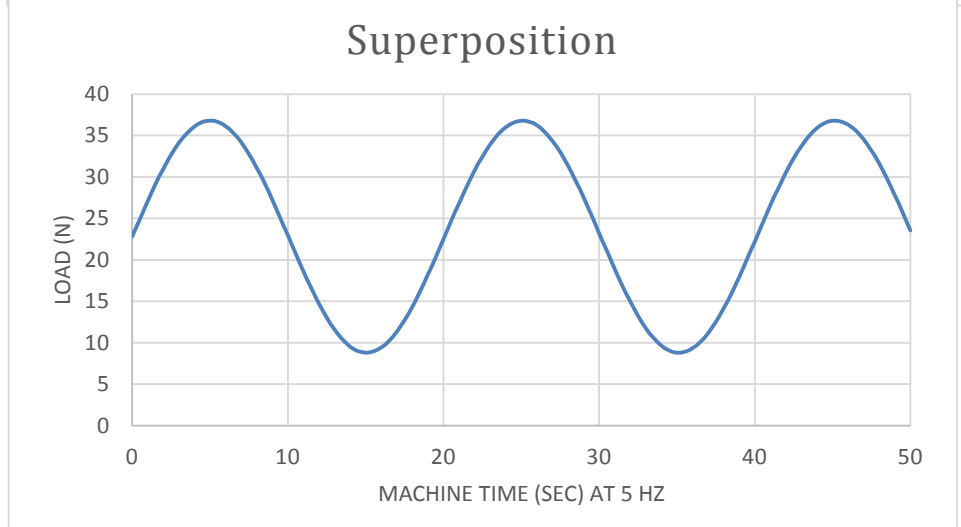
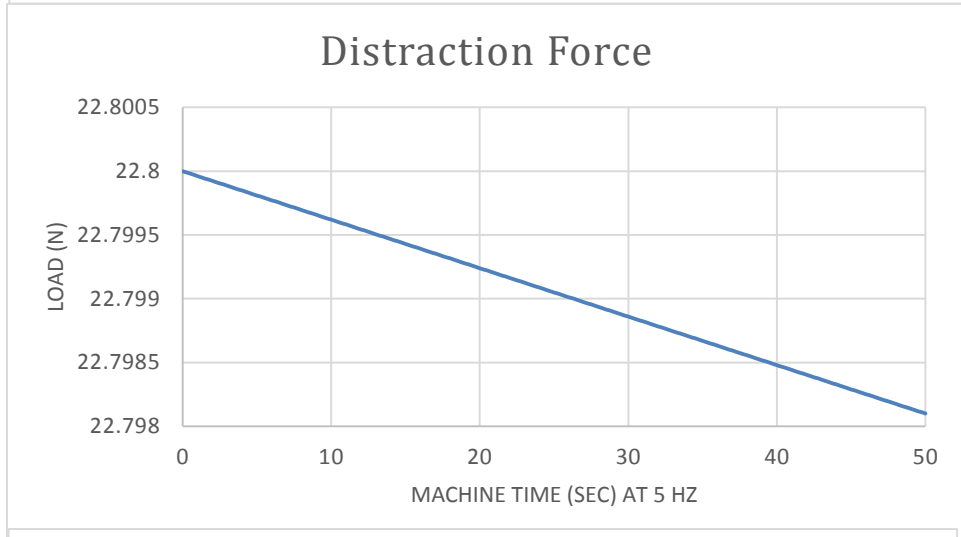
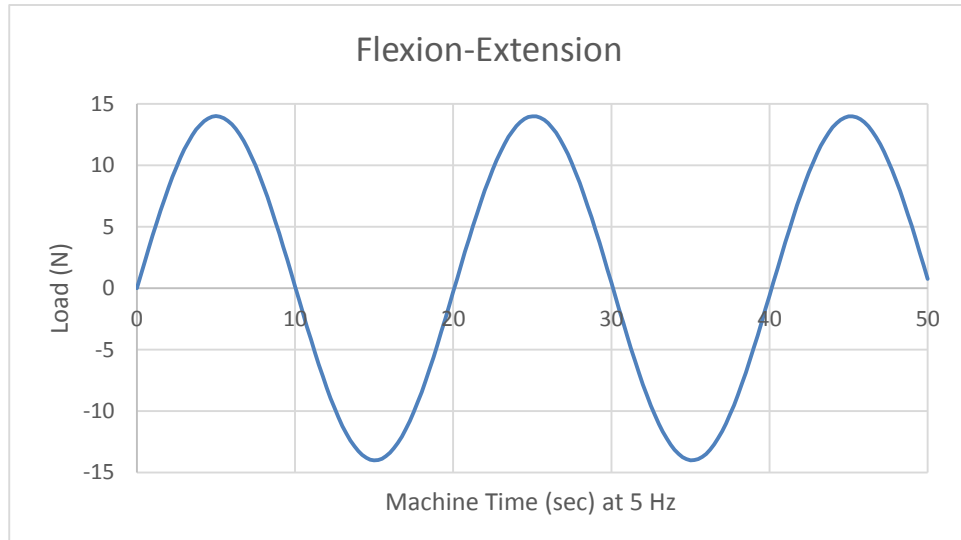


Figure 4-19: The figure shows the superposition of sinusoidal loading and distraction force change due to growth for first 50 cycles as an example.

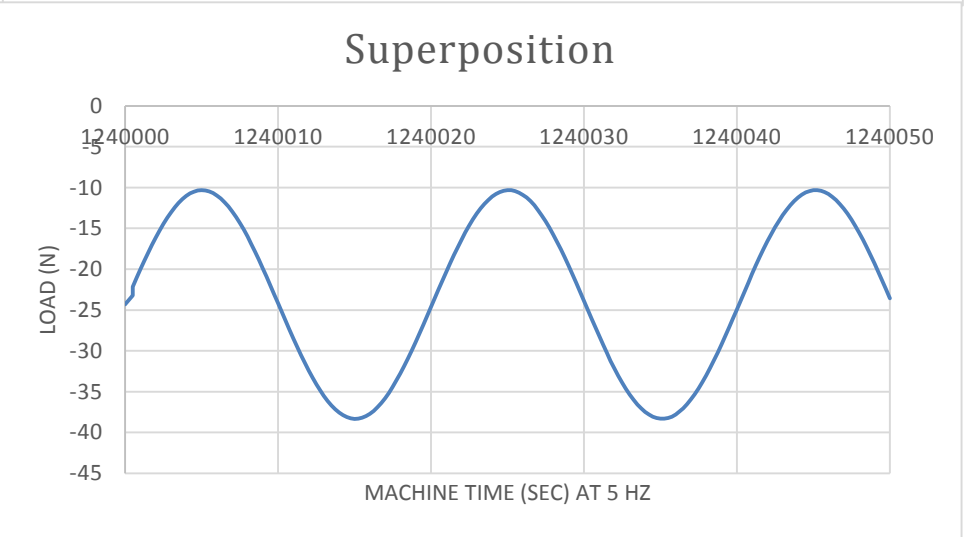
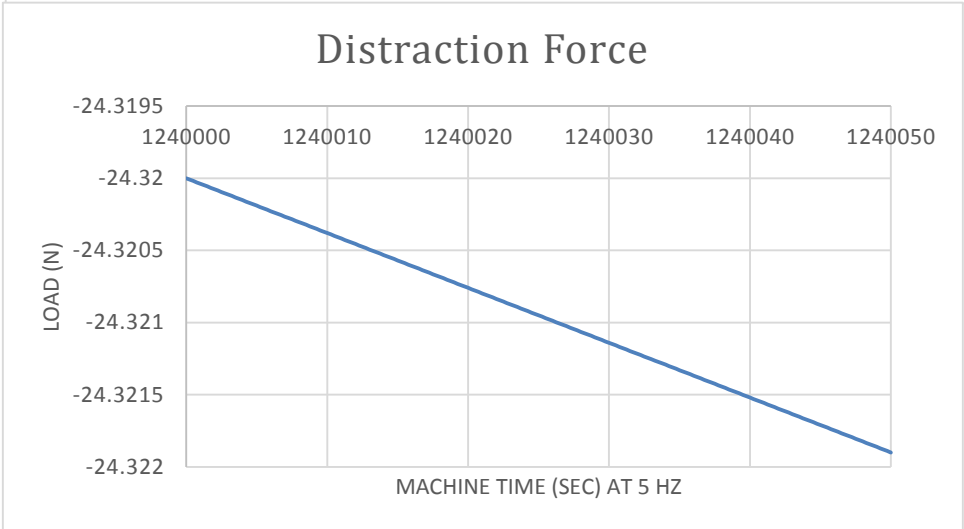
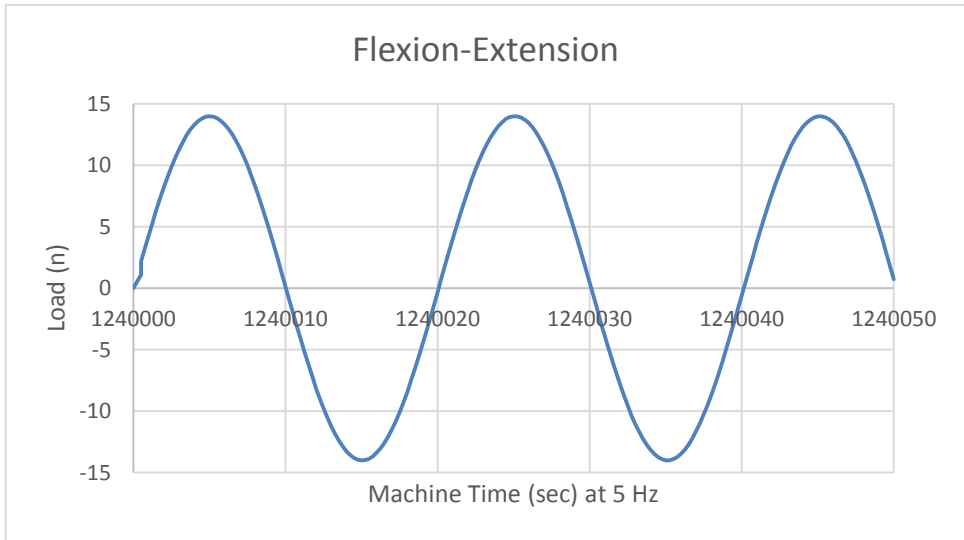


Figure 4-20: The figure shows the superposition of sinusoidal loading and distraction force change due to growth for last 50 cycles as an example.

After 1.25 million cycle the pedicle screws were pulled out in a direction collinear to the axis of the screw (at a rate of 5mm/min). The peak pull out forces for each group were recorded and unpaired t-tests were performed between group 1 (optimal distraction force) and group 2 (high distraction force).

Figure 4-21 provides the summary of the entire methodology involved in this study.

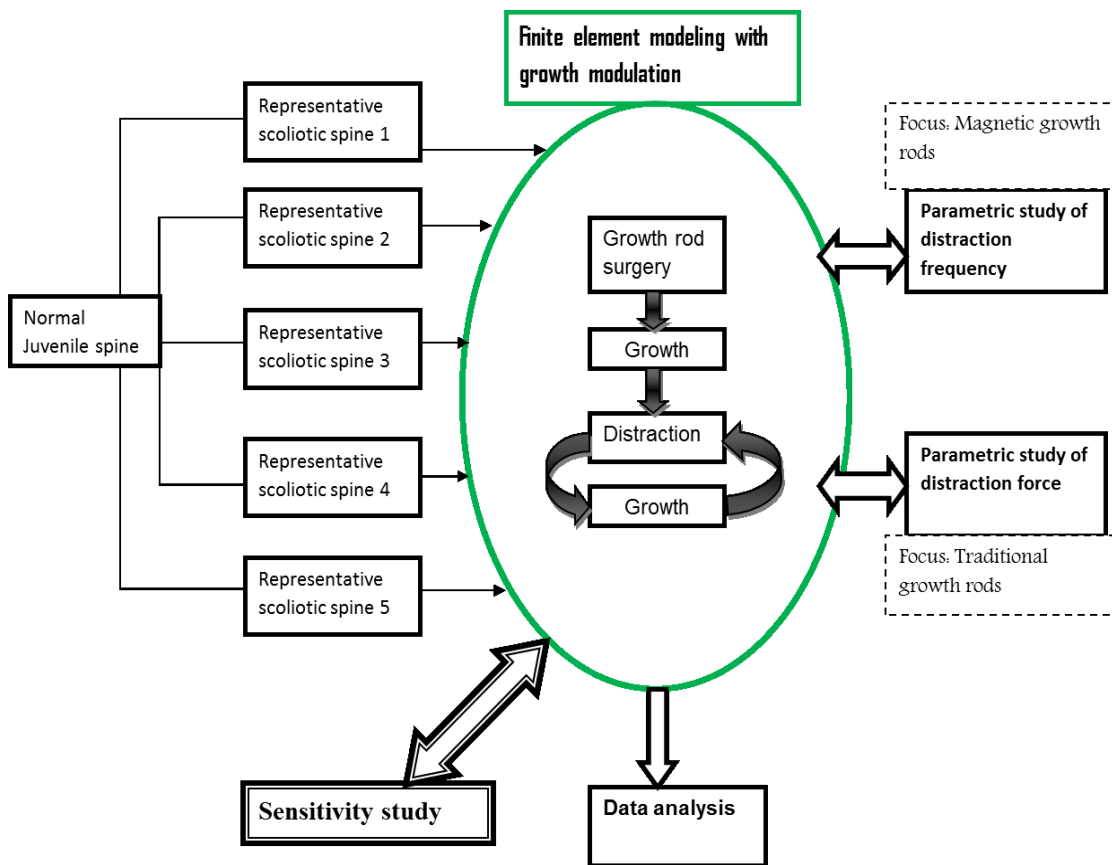


Figure 4-21: Summary of the entire methodology.



# Chapter 5

## Results

### 5.1 Introduction

The first step of this project was to analyze the normal juvenile spine model instead of a scoliotic spine to isolate the effects on spinal growth, sagittal contours, and maximum von Mises stresses on the rods arising from different distraction forces and frequencies, thus producing results independent of the severity of deformity and curve rigidity. The first section presents results from this analysis. The second section in this chapter proceeds with the analysis of the objectives using multiple representative scoliotic spine models. The third section presents the results of *in vitro* study and sensitivity analysis.

### 5.2 Effect of Distraction Force on Normal Juvenile Spine

In brief, the normal juvenile spine was instrumented with growth rods via pedicle screws as anchors. Multiple cases, varying in magnitude of distraction forces, were simulated for 6 months of growth and the results were then analyzed. It was seen that the actual distraction force decreased by 15.4-16.5 % for all the models in the time frame of 83 minutes. This was expected as these models incorporated viscoelasticity and therefore allowed stress relaxation (Figure 5-1). The distraction obtained increased uniformly in increments of 1.1-1.2 mm from 50 N to 400 N of distraction force with 50 N distraction

force providing 1.4 mm and 400 N distraction force exhibiting 9.0 mm of distraction (Figure 5-2). Thoracic kyphosis (T4-T12) decreased by 2.3<sup>0</sup>, 3.0<sup>0</sup>, 3.4<sup>0</sup>, 3.8<sup>0</sup>, 4.0<sup>0</sup>, 4.2<sup>0</sup>, 4.3<sup>0</sup>, and 4.4<sup>0</sup> with 50 N, 100 N, 150 N, 200 N, 250 N, 300 N, 350 N, and 400 N of distraction force respectively from intact baseline value (pre-distraction) (Figure 5-3). Lumbar lordosis (L1-L5) decreased by 1.4<sup>0</sup>, 2.2<sup>0</sup>, 2.9<sup>0</sup>, 3.5<sup>0</sup>, 4.0<sup>0</sup>, 4.4<sup>0</sup>, 4.8<sup>0</sup>, and 5.1<sup>0</sup> with 50 N, 100 N, 150 N, 200 N, 250 N, 300 N, 350 N, and 400 N of distraction force respectively from intact baseline value (pre-distraction) (Figure 5-4). The maximum von Mises stress on the rod after distraction was 78.6 MPa, 111.8 MPa, 144.6 MPa, 176.1 MPa, 207.7 MPa, 239.5 MPa, 269.5 MPa, and 301.1 MPa with 50 N, 100 N, 150 N, 200 N, 250 N, 300 N, 350 N, and 400 N of distraction force respectively (Figure 5-6). The average load (in caudal-cranial direction) exerted on the T3 and T4 vertebrae by the pedicle screws after distraction was 22.8 N, 34.7 N, 46.1 N, 57.2 N, 68.2 N, 79.0 N, 89.8 N, and 100.5 N with 50 N, 100 N, 150 N, 200 N, 250 N, 300 N, 350 N, and 400 N of distraction force respectively (Figure 5-7). Similar loads were exerted on L4 and L5 vertebrae but in opposite direction (Figure 5-7).

A second set of data was collected after the simulation period equivalent to 6 months of growth. It was found that the thoracic kyphosis (T4-T12) increased by 4.3<sup>0</sup>, 4.2<sup>0</sup>, 3.9<sup>0</sup>, 3.2<sup>0</sup>, 2.6<sup>0</sup>, 2.1<sup>0</sup>, 1.7<sup>0</sup>, and 1.4<sup>0</sup> with 50 N, 100 N, 150 N, 200 N, 250 N, 300 N, 350 N, and 400 N of distraction force respectively after 6 months of growth following distraction (the increase is relative to post-distraction) (black arrows, Figure 5-3). Lumbar lordosis (L1-L5) increased by 5.6<sup>0</sup>, 5.6<sup>0</sup>, 5.3<sup>0</sup>, 4.7<sup>0</sup>, 4.2<sup>0</sup>, 3.7<sup>0</sup>, 3.4<sup>0</sup>, and 3.2<sup>0</sup> with 50 N, 100 N, 150 N, 200 N, 250 N, 300 N, 350 N, and 400 N of distraction force respectively after 6 months of growth following distraction (the increase is relative to post-distraction)

(black arrows, Figure 5-4). The thoracic kyphosis and lumbar lordosis did not change after growth for the intact model. T1-S1 height increased by 4.5 mm, 5.6 mm, 6.7 mm, 7.6 mm, 8.6 mm, 9.6 mm, 10.6 mm, and 11.2 mm with 50 N, 100 N, 150 N, 200 N, 250 N, 300 N, 350 N, and 400 N of distraction force after 6 months of growth (Figure 5-5). For intact spine the T1-S1 height increased by 8.6mm (Figure 5-5). The maximum von Mises stress on the rod after growth was 114.5 MPa, 63.2 MPa, 28.7 MPa, 38.7 MPa, 58.2 MPa, 79.4 MPa, 99.8 MPa, and 114.9 MPa with 50 N, 100 N, 150 N, 200 N, 250 N, 300 N, 350 N, and 400 N of distraction force respectively (Figure 5-6). The average load (in caudal-cranial direction) exerted on the T3 and T4 vertebrae by the pedicle screws after growth were -24.8 N, -10.9 N, 0.0 N, 9.0 N, 18.5 N, 28.4 N, 37.9 N, and 45.5 N with 50 N, 100 N, 150 N, 200 N, 250 N, 300 N, 350 N, and 400 N of distraction force respectively (Figure 5-7). Similar loads were exerted on L4 and L5 vertebrae but in opposite direction (Figure 5-7).

The above analysis was performed with the initial T4-T12 kyphosis and L1-L5 lordosis of  $17.5^{\circ}$  and  $21.1^{\circ}$  respectively (intact baselines). These values of kyphosis and lordosis are lower than normal baseline and hence the entire analysis was repeated after changing the intact T4-T12 kyphosis and L1-L5 lordosis to  $30^{\circ}$  and  $35^{\circ}$  respectively. This was undertaken to verify the uniformity in trends. It was seen that the thoracic kyphosis (T4-T12) decreased by  $2.9^{\circ}$ ,  $4.3^{\circ}$ ,  $5.2^{\circ}$ ,  $5.8^{\circ}$ ,  $6.6^{\circ}$ ,  $7.4^{\circ}$ ,  $8.1^{\circ}$ , and  $9.3^{\circ}$  with 50 N, 100 N, 150 N, 200 N, 250 N, 300 N, 350 N, and 400 N of distraction force respectively from intact baseline value (pre-distraction). Lumbar lordosis (L1-L5) decreased by  $-4.5^{\circ}$ ,  $5.5^{\circ}$ ,  $6.1^{\circ}$ ,  $6.9^{\circ}$ ,  $7.6^{\circ}$ ,  $8.9^{\circ}$ ,  $10.0^{\circ}$ , and  $11.0^{\circ}$  with 50 N, 100 N, 150 N, 200 N, 250 N, 300 N, 350 N, and 400 N of distraction force respectively from intact baseline value (pre-distraction). The

maximum von Mises stress on the rod after distraction was 103.4 MPa, 141.5 MPa, 164.3 MPa, 210.8 MPa, 232.3 MPa, 269.1 MPa, 288.9 MPa, and 315.4 MPa with 50 N, 100 N, 150 N, 200 N, 250 N, 300 N, 350 N, and 400 N of distraction force respectively. The average load (in caudal-cranial direction) exerted on the T3 and T4 vertebrae by the pedicle screws after distraction was 23.4 N, 35.4 N, 46.7 N, 57.7 N, 68.4 N, 79.2 N, 89.5 N, and 100.1 N with 50 N, 100 N, 150 N, 200 N, 250 N, 300 N, 350 N, and 400 N of distraction force respectively. Similar loads were exerted on L4 and L5 vertebrae but in opposite direction.

Thoracic kyphosis (T4-T12) increased by 8.2°, 7.9°, 6.9°, 6.0°, 5.0°, 4.6°, 4.1°, and 3.3° with 50 N, 100 N, 150 N, 200 N, 250 N, 300 N, 350 N, and 400 N of distraction force respectively after 6 months of growth following distraction (the increase is relative to post-distraction). Lumbar lordosis (L1-L5) increased by 10.8°, 9.8°, 9.0°, 7.7°, 6.6°, 6.1°, 5.9°, and 5.1° with 50 N, 100 N, 150 N, 200 N, 250 N, 300 N, 350 N, and 400 N of distraction force respectively after 6 months of growth following distraction (the increase is relative to post-distraction). The thoracic kyphosis and lumbar lordosis did not change after growth for the intact model. T1-S1 height increased by 4.8 mm, 5.9 mm, 6.8 mm, 8.0 mm, 8.9 mm, 10.1 mm, 11.0 mm, and 11.9 mm with 50 N, 100 N, 150 N, 200 N, 250 N, 300 N, 350 N, and 400 N of distraction force after 6 months of growth. For intact spine the T1-S1 height increased by 8.6mm. The maximum von Mises stress on the rod after growth was 216.3 MPa, 169.0 MPa, 111.0 MPa, 91.7 MPa, 75.1 MPa, 110.4 MPa, 137.2 MPa, and 170.5 MPa with 50 N, 100 N, 150 N, 200 N, 250 N, 300 N, 350 N, and 400 N of distraction force respectively. The average load (in caudal-cranial direction) exerted on the T3 and T4 vertebrae by the pedicle screws after growth were -31.4 N, -23.3 N, 10.6 N, -7.2 N, 15.0

N, 32.7 N, 42.4 N, and 50.4 N with 50 N, 100 N, 150 N, 200 N, 250 N, 300 N, 350 N, and 400 N of distraction force respectively. Similar loads were exerted on L4 and L5 vertebrae but in opposite direction.

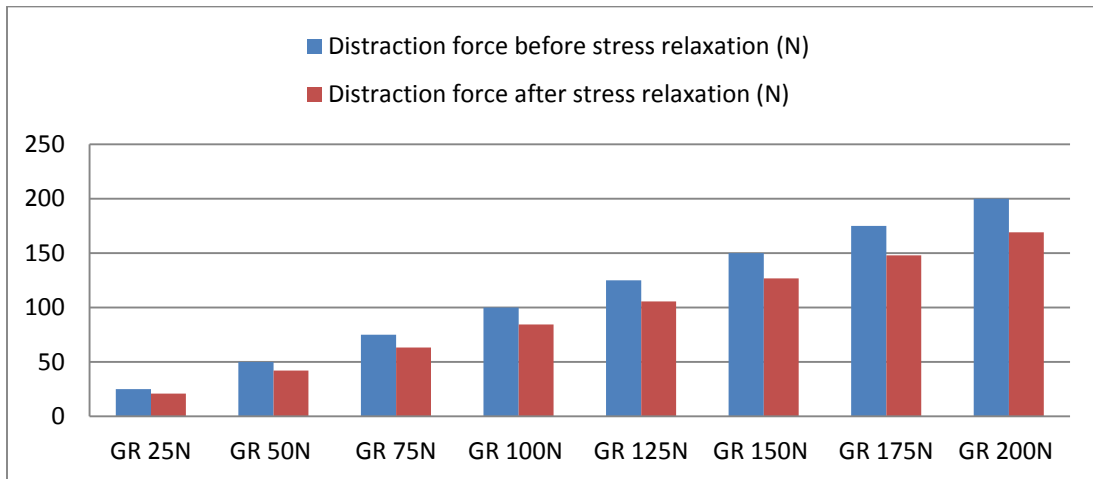


Figure 5-1: Distraction forces (N) between the proximal and distal rods on each side before and after stress relaxation. The effective distraction force obtained after stress relaxation in soft tissue was less than the initial distraction force applied during the surgery. The maximum time period used was 83 minutes.

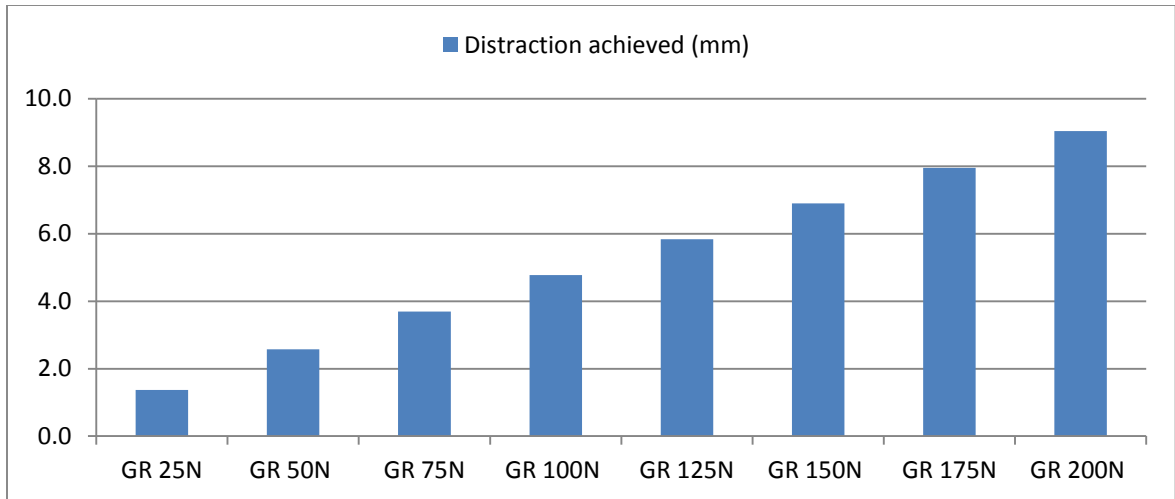


Figure 5-2: Distractions achieved (mm) in-between the proximal and distal rods on each side with different distraction forces. The distraction obtained increased with increase in distraction force.

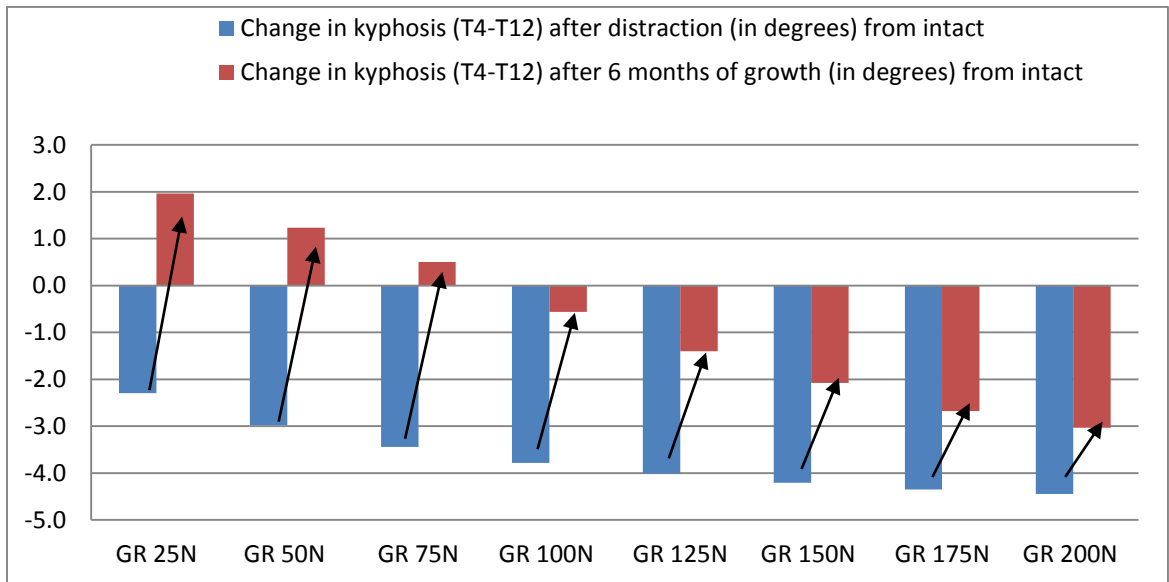


Figure 5-3: The change in thoracic kyphosis (in degrees) after distraction and following 6 months of growth with respect to intact baseline for different distraction forces. The

thoracic kyphosis decreased immediately after distraction and then recovered to varying extent.

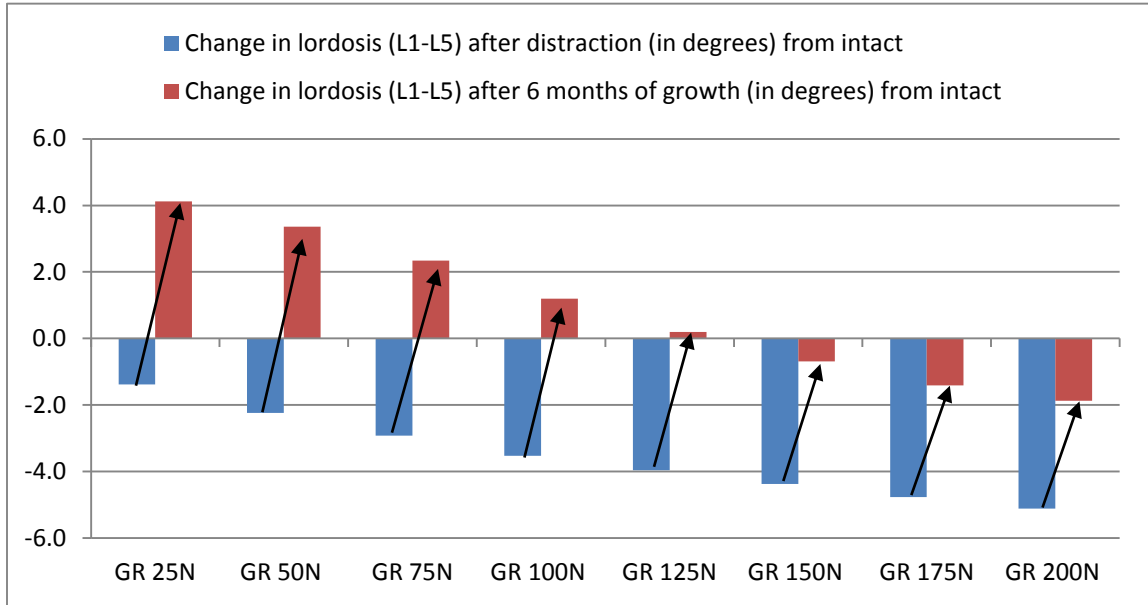


Figure 5-4: The above figure shows the change in lumbar lordosis (in degrees) after distraction and following 6 months of growth with respect to intact baseline for different distraction forces. The lumbar lordosis decreased immediately after distraction and then recovered to varying extents with growth depending upon the initial distraction force.

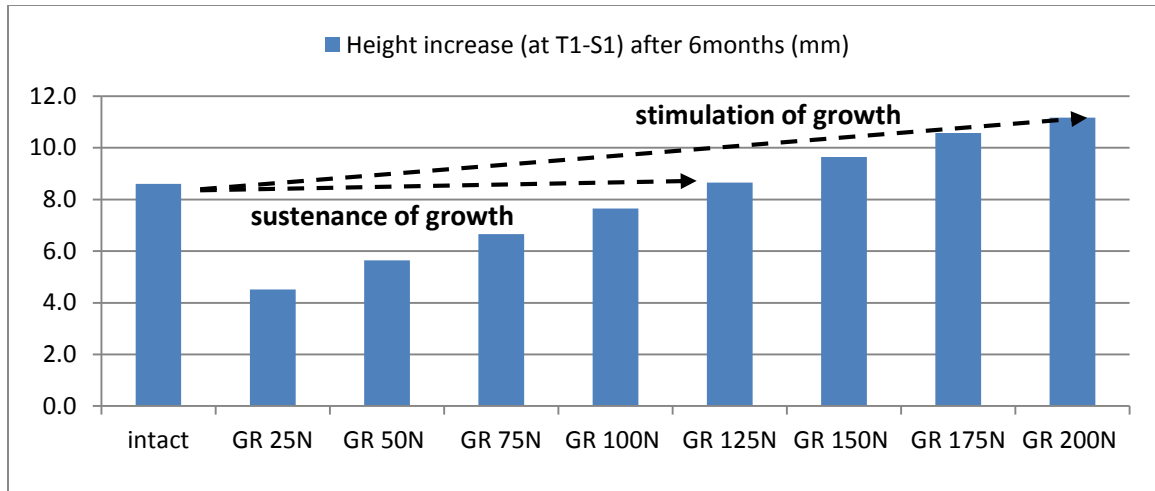


Figure 5-5: Height increase across T1-S1 (in mm) during the growth period of 6 months following distraction with different distraction forces and its comparison with intact. GR 125N provided height growth equal to intact exemplifying sustenance of growth. GR 150N, GR 175N and GR 200N showed higher growth than intact exemplifying stimulation of growth.



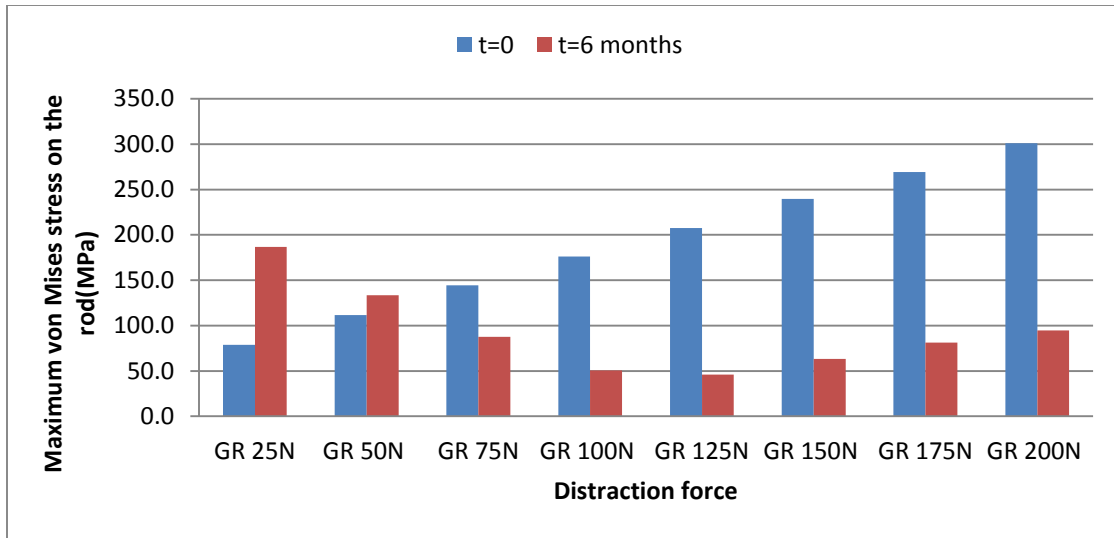


Figure 5-6: Maximum von Mises stress (in MPa) in the growth rod after distraction (t=0) and after 6 months of growth (t=6 months) with different distraction forces.

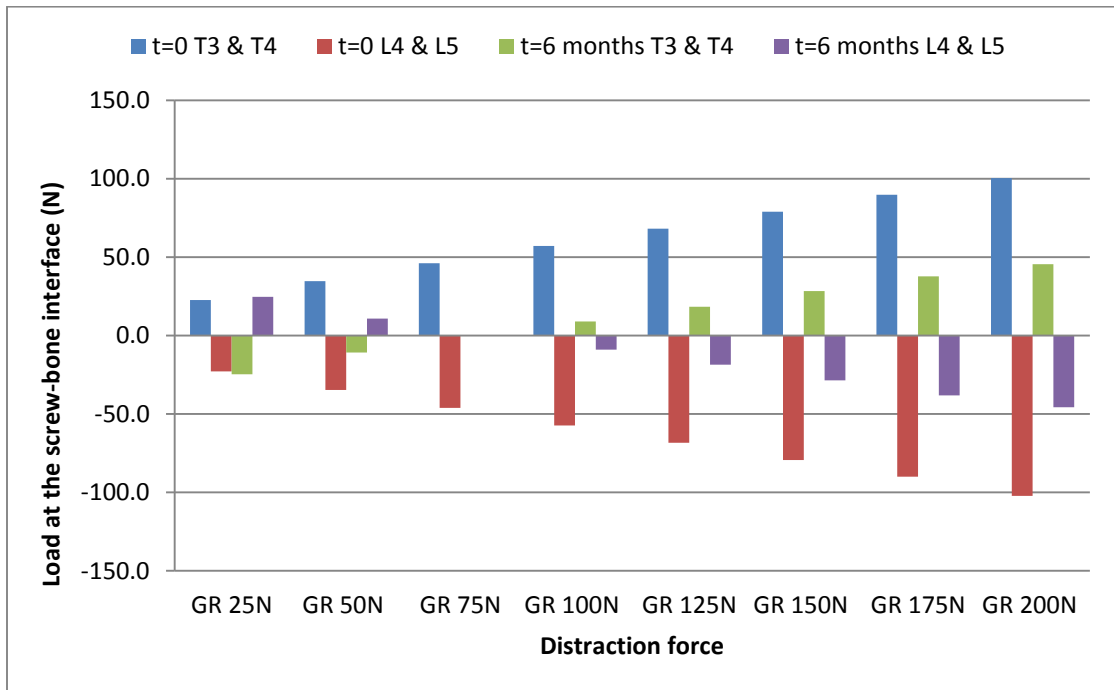


Figure 5-7: Average load (N) at the screw-bone interface after distraction (t=0) and after 6 months of growth (t=6 months) with different distraction forces. The positive values correspond to caudal-cranial direction and the negatives in cranial-caudal direction.

Table 5.1: The table below gives numerical value of forces in the rod (axial direction) with different distraction forces. Negative values are tensile forces and positives are compressive forces.

	Net force developed in the rod (N)	
	after distraction (t=0)	after growth (t=6 months)
GR 25N	45.5	-50.3
GR 50N	69.4	-22.0
GR 75N	92.3	-0.1
GR 100N	114.5	17.9
GR 125N	136.5	36.9
GR 150N	158.2	56.9
GR 175N	179.6	75.8
GR 200N	201.2	91.1

### 5.3 Effect of Distraction Frequency on Normal Juvenile Spine

Using a normal juvenile spine instrumented with growth rods, four time interval simulations over a 24 month period were performed, each with a different frequency of distraction (a. 2 @ 12 months, b. 4 @ 6 months, c. 8 @ 3 months, and d. 12 @ 2 months).

It was seen that the maximum von Mises stress on the rod for a single growth period was always highest immediately after distraction and thereafter decreased with growth until the next distraction (Figure 5-8, Figure 5-9, Figure 5-10, & Figure 5-11). The maximum von Mises stress was always higher on the subsequent distractions, and hence the last distraction showed the highest von Mises stresses on the rod (Figure 5-12). For the simulation with 2 distractions at 12-month interval, the highest maximum von Mises stress on the rod for the period of 24 months was 738 MPa. Whereas, the lowest maximum von Mises stress on the rods for this case was 111 MPa (Figure 5-12). For the simulation with a distraction period of 6 months, the highest maximum von Mises stress on the rod for the period of 24 months was 601 MPa and the lowest maximum von Mises stress was 67 MPa (Figure 5-12). A distraction period of 3 months showed a highest maximum von Mises stress of 526 MPa and a lowest von Mises stress of 21 MPa on the rod for the period of 24 months (Figure 5-12). For the distraction period of 2 months the highest and lowest von Mises stresses on the rod for the period of 24 months were 313 MPa and 18 MPa respectively (Figure 5-12).

To analyze the differences in stress produced by change in material of the rod, we reran all the simulations with cobalt-chromium and with stainless steel as rod materials. The highest maximum von Mises stresses increased with both cobalt-chromium and stainless steel. The increase was 14%, 13%, 12.7%, and 8.8% for stainless steel with distractions at 12 month, 6 month, 3 month, and 2 month intervals, respectively (Figure 5-13). With cobalt-chromium the percentage increases were 15.7%, 14.6%, 14%, and 9.6% with distractions at 12 monthly, 6 monthly, 3 monthly, and 2 monthly distractions intervals, respectively (Figure 5-14).

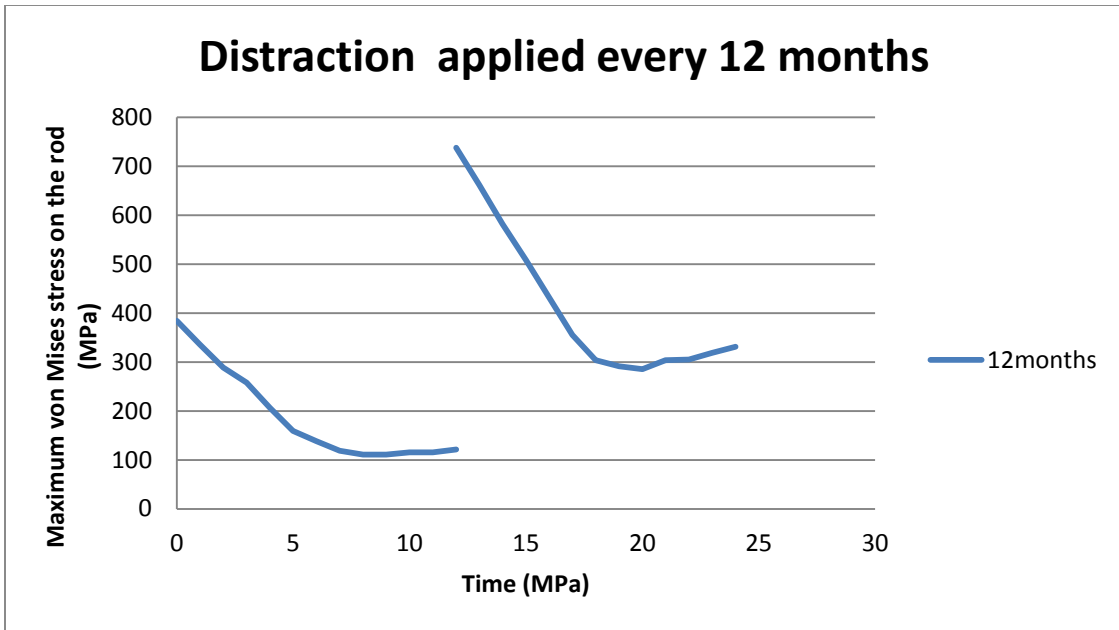


Figure 5-8: The maximum von Mises stress on the rod for the period of 24 months with distraction every 12 months. The first curve is for the growth period from 1<sup>st</sup> distraction (at 0 months) to 12 months (just before distraction). The second curve is for the growth period from 2<sup>nd</sup> distraction (at 12 months) to 24 months (just before distraction)

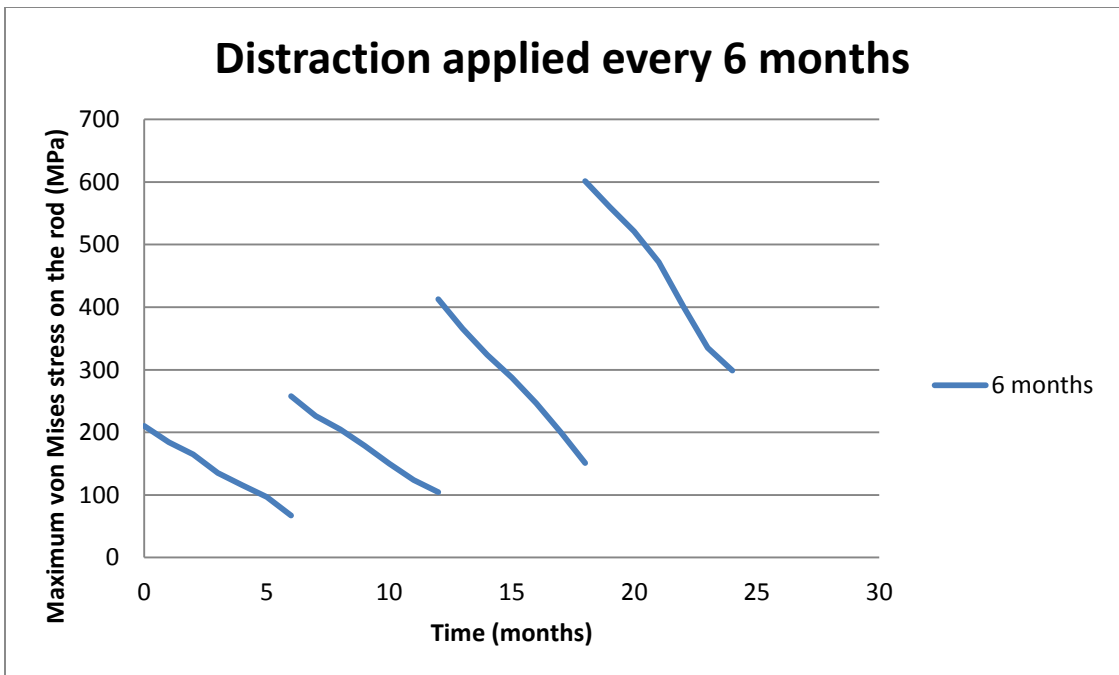


Figure 5-9: The maximum von Mises stress on the rod for the period of 24 months with distraction every 6 months. The first curve, second curve, third curve and fourth curve are for the growth period 1<sup>st</sup> distraction to 6 months, 2<sup>nd</sup> distraction to 12 months, 3<sup>rd</sup> distraction to 18 months and 4<sup>th</sup> distraction to 24 months respectively.

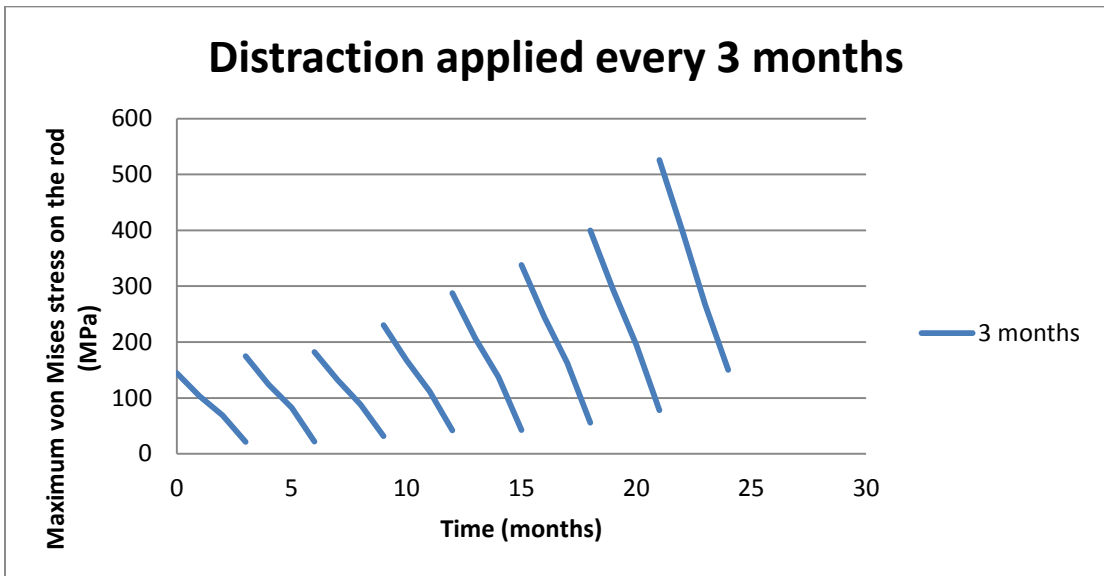


Figure 5-10: The maximum von Mises stress on the rod for the period of 24 months with distraction every 3 months. The first curve represents 1<sup>st</sup> distraction and 3 months of growth following it. Each subsequent curve relates to the subsequent distraction and its growth period of 3 months.

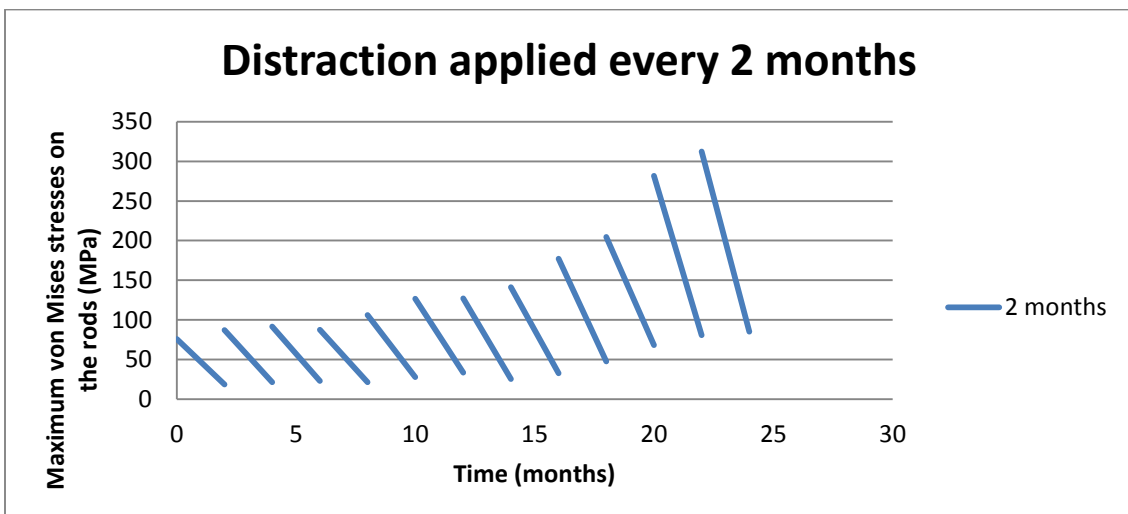


Figure 5-11: The maximum von Mises stress on the rod for the period of 24 months with distraction every 2 months. The first curve represents 1<sup>st</sup> distraction and 2 months of growth following it. Each subsequent curve relates to the subsequent distraction and its growth period of 2 months.

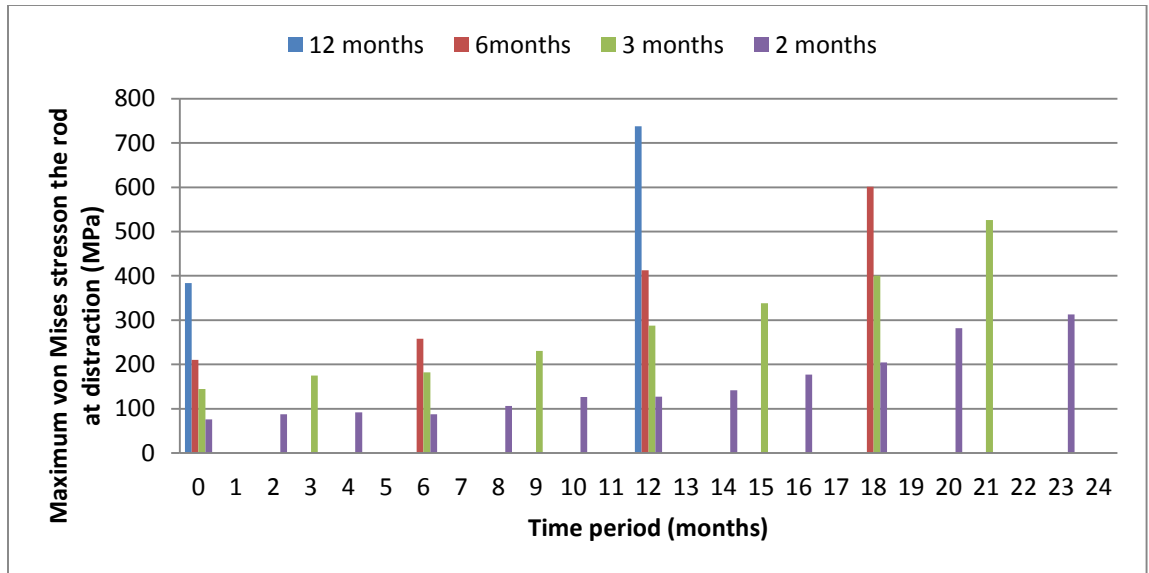


Figure 5-12: The graph shows the maximum von Mises stress on the rod immediately after distraction with different frequency of distraction for the duration of 24 months. For 12 monthly distraction there are two peaks (at 0 and at 12 months). For 6 monthly distraction there are four peaks (at 0, 6, 12, and 18 months). For 3 monthly distraction there are eight peaks (at 0, 3, 6, 9, 12, 15, 18, and 21 months). For 2 monthly distraction there are twelve peaks (at 0, 2, 4, 6, 8, 10, 12, 14, 16, 18, 20, and 22 months).

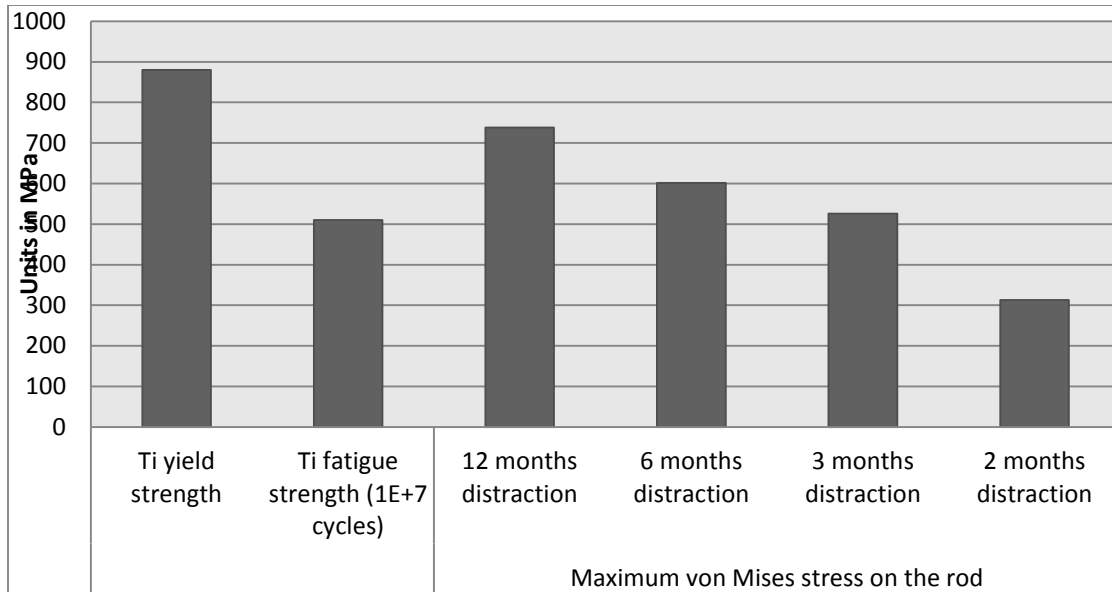


Figure 5-13: The graph compares the highest value of the maximum von Mises stress on the rod seen with different frequency of distraction for the duration of 24 months. These highest values pertain to last distraction in each case. For 12 monthly distraction it is the distraction at the 12<sup>th</sup> month. For 6 monthly distraction it is at the 18<sup>th</sup> month. For 3 monthly distraction it is at the 21<sup>st</sup> month. For 2 monthly distraction it is at the 22<sup>nd</sup> month.

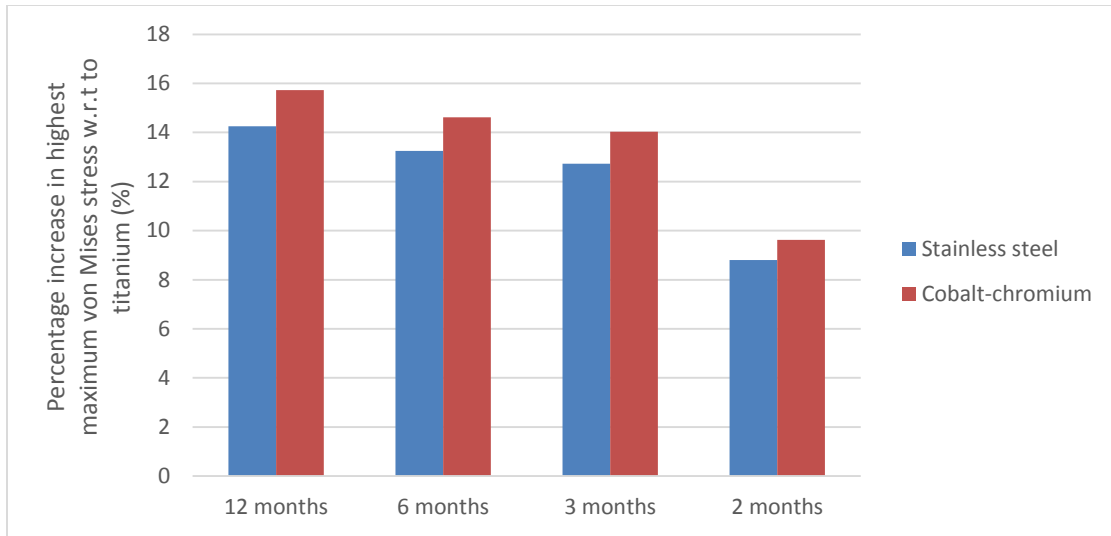


Figure 5-14: The graph shows the percentage increase in highest maximum von Mises stress by using cobalt-chromium and stainless steel with respect to titanium for different intervals of distraction.



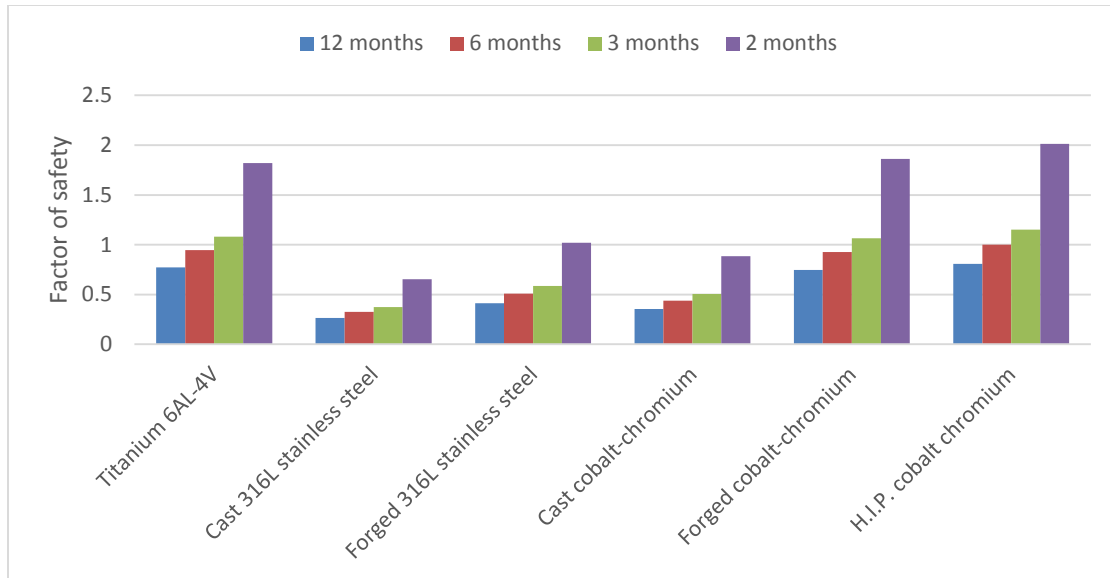


Figure 5-15: The graph compares the factor of safety with different materials like titanium, cobalt-chromium and stainless steel for different intervals of distraction. The factor of safety was calculated as fatigue strength of the material divided by the highest maximum von Mises stress on the rod in 24 months.

#### 5.4 Effect of Distraction Force on Representative Juvenile Spines

For the scoliotic model 1A, T1-S1 height increased by 6.1 mm, 6.9 mm, 8.8 mm, 9.9 mm, 11.3 mm, and 12.7 mm with 50-25, 50all, 100-75, 100all, 150-125 and 150all of distraction force after 6 months of growth. For intact spine the T1-S1 height increases by 8.6 mm (for 9 year old) in 6 months as reported in the literature, Figure 5-16. Cobb's angle was 35 degrees before distraction, it decreased from 24.0 degrees with 50-25 to 11.5 degrees with 150all at 0 months period, thereafter increasing in the subsequent 6 months

of growth period. 100-75 resulted in the least change in Cobb's angle with 33.2 degrees at 6 months, Figure 5-17. Kyphosis angle was 38 degrees before distraction, it decreased from 36.6 degrees with 50-25 to 25.8 degrees with 150all at 0 months period, thereafter increasing in the subsequent 6 months of growth period. 100all resulted in the least change in kyphosis with 37.4 degrees at 6 months period, Figure 5-18. Lordosis angle was 39 degrees before distraction, it decreased from 37.6 degrees with 50-25 to 27.5 degrees with 150all at 0 months period, thereafter increasing in the subsequent 6 months of growth period. 100-75 resulted in the least change in lordosis with 39.5 degrees at 6 months period, Figure 5-19. The maximum von Mises stresses increased with increase in distraction force; 50-25, 50all, 100-75, 100all, 150-125 and 150all resulted in 126.9 MPa, 189.4 MPa, 290.6 MPa, 351.8 MPa, 493.2 MPa, and 541.7 MPa stresses on the rods respectively. However the stresses changed to 97.3 MPa, 73.2 MPa, 37.3 MPa, 10.2 MPa, 89.6 MPa, and 113.2 MPa respectively at 6 months period, Figure 5-20. The total unilateral screw-bone interface load increased with increase in distraction force; 50-25, 50all, 100-75, 100all, 150-125 and 150all resulted in 45.0 N, 51.3 N, 86.1 N, 100.2 N, 126.5 N, and 153.0 N of load at the interface respectively. However similar to stress on the rods, the loads changed to 42.1 N, 37.8 N, 12.4 N, 25.3 N, 73.2 N, and 106.3 N respectively at 6 months period, Figure 5-21.

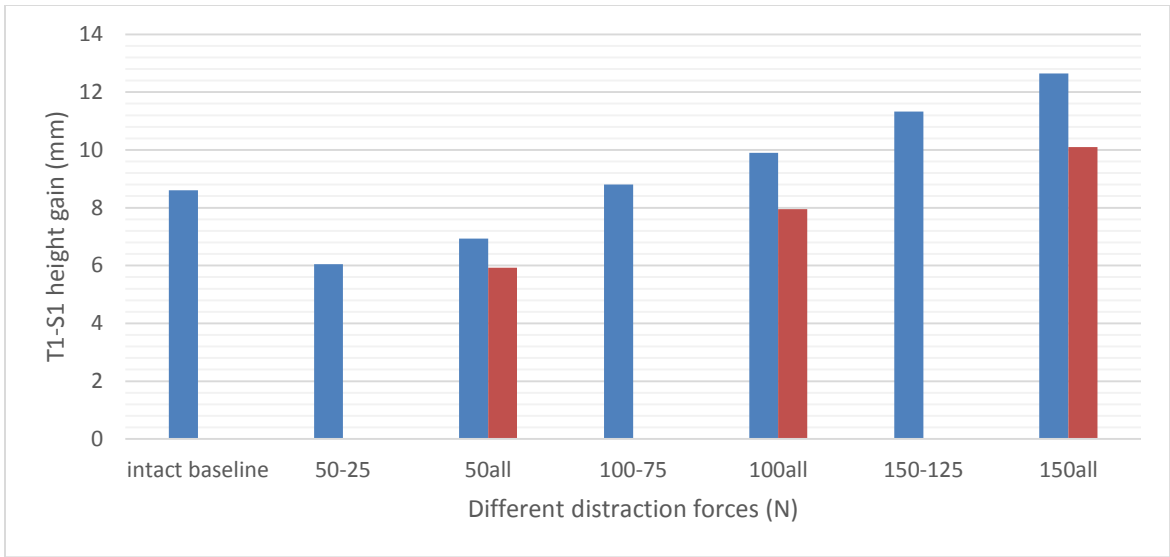


Figure 5-16: Height increase across T1-S1 (in mm) during the growth period of 6 months following distraction for representative scoliotic model 1A. The data from non-scoliotic normal spine instrumented with growth rod is shown in red.

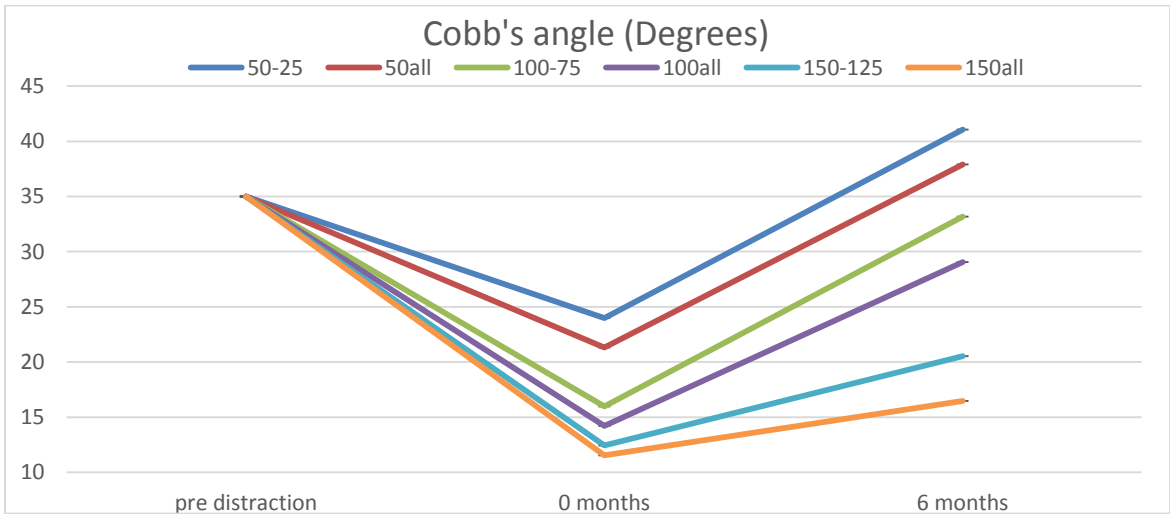


Figure 5-17: The thoracic Cobb's angle (in degrees) after distraction (t=0) and following 6 months (t=6 months) of growth for representative scoliotic model 1A.

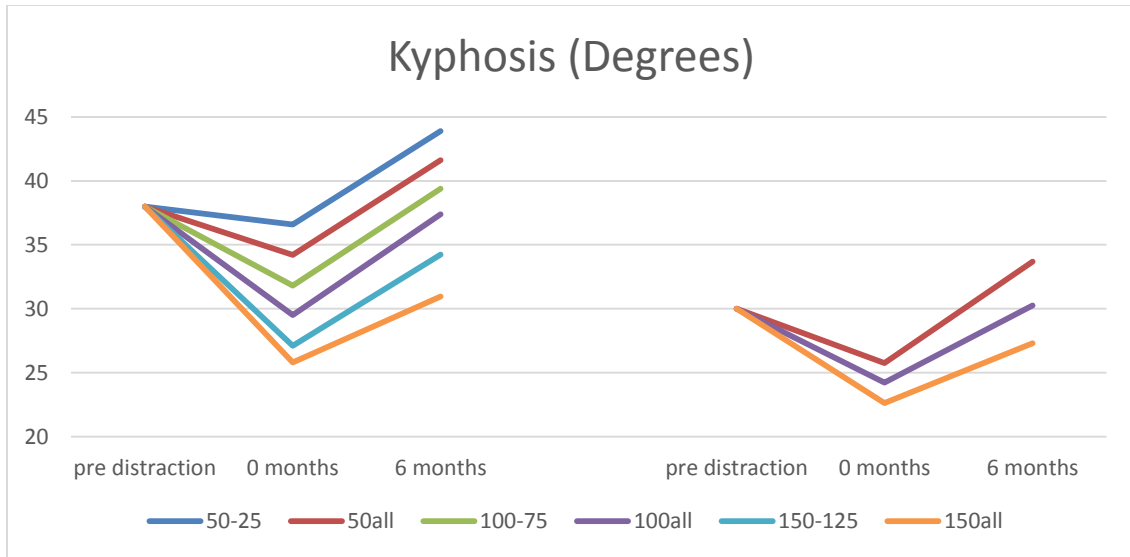


Figure 5-18: The kyphosis (in degrees) after distraction (t=0) and following 6 months (t=6 months) of growth for representative scoliotic model 1A. The data from non-scoliotic normal spine instrumented with growth rod is shown on the right.

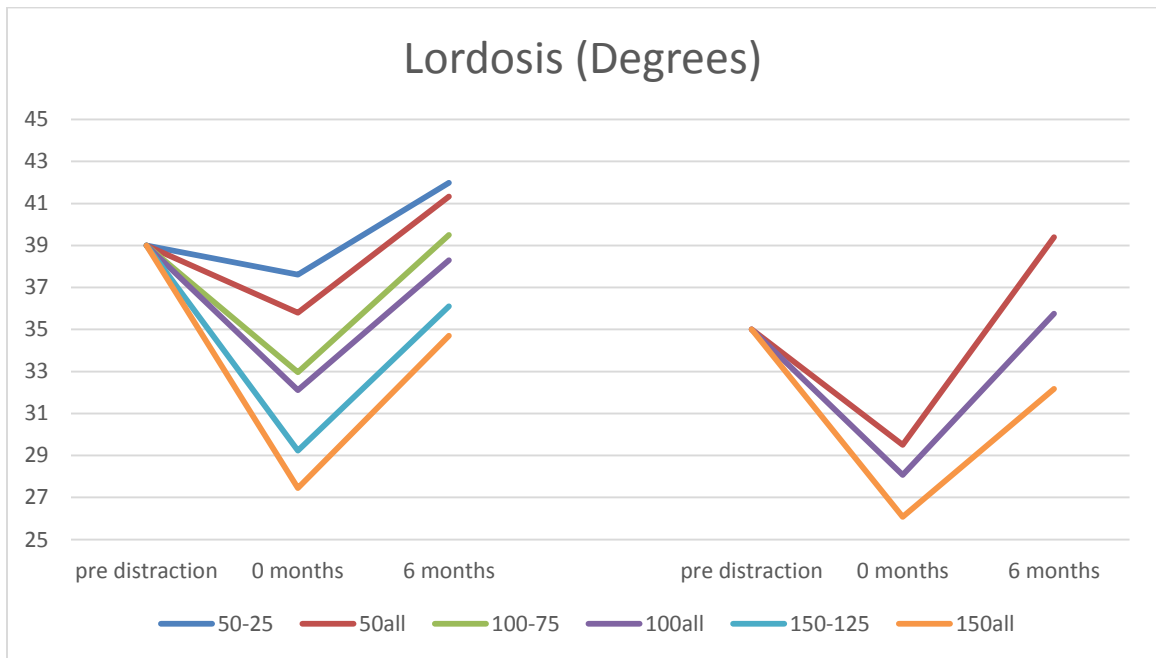


Figure 5-19: The lordosis (in degrees) after distraction (t=0) and following 6 months (t=6 months) of growth for representative scoliotic model 1A. The data from non-scoliotic normal spine instrumented with growth rod is shown on the right.

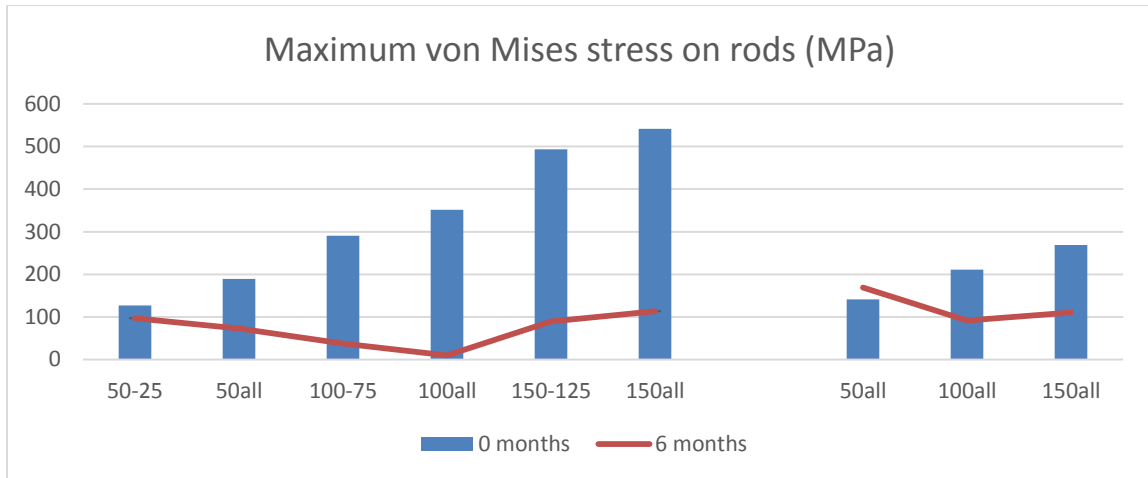


Figure 5-20: Maximum von Mises stress (in MPa) in the growth rod after distraction ( $t=0$ ) and after 6 months of growth ( $t=6$  months) for representative scoliotic model 1A. The data from non-scoliotic normal spine instrumented with growth rod is shown on the right.

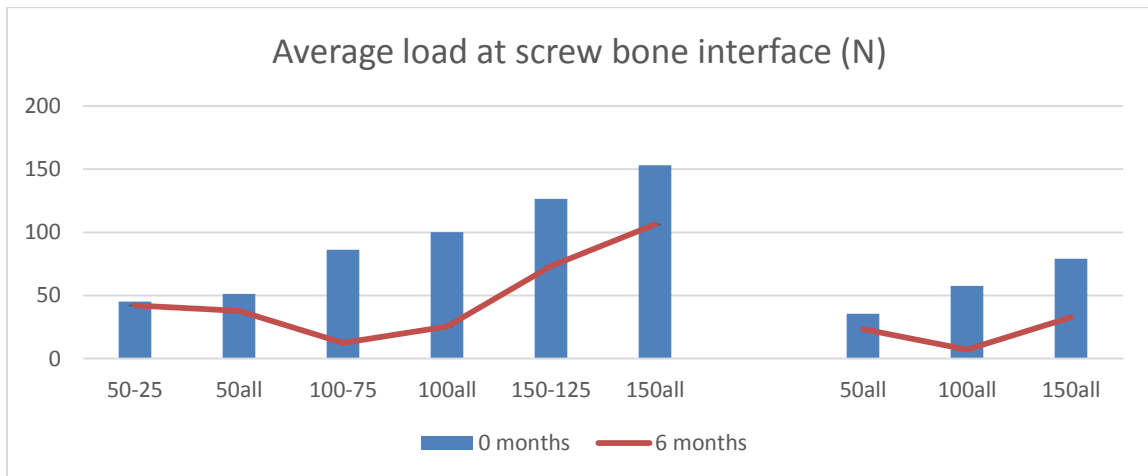


Figure 5-21: Total unilateral average load (N) at the screw-bone interface after distraction ( $t=0$ ) and after 6 months of growth ( $t=6$  months) for representative scoliotic model 1A. The average load data from non-scoliotic normal spine instrumented with growth rod is shown on the right.

For group 1B scoliotic model, T1-S1 height increased by 6.4 mm, 7.3 mm, 9 mm, 10.2 mm, 11.8 mm, 13.3 mm with 50-25, 50all, 100-75, 100all, 150-125 and 150all of distraction force after 6 months of growth. For intact spine the T1-S1 height increases by 8.6 mm (for 9 year old) in 6 months as reported in the literature, Figure 5-22. Cobb's angle was 35 degrees before distraction, it decreased from 25.2 degrees with 50-25 to 13.0 degrees with 150all at 0 months period, thereafter increasing in the subsequent 6 months of growth period. 100-75 resulted in the least change in Cobb's angle with 35.2 degrees at 6 months, Figure 5-23. Kyphosis angle was 38 degrees before distraction, it decreased from 35.9 degrees with 50-25 to 25.4 degrees with 150all at 0 months period, thereafter increasing in the subsequent 6 months of growth period. 100all resulted in the least change in kyphotic angle with 39.0 degrees at 6 months period, Figure 5-24. Lordosis angle was 39 degrees before distraction, it decreased from 37.1 degrees with 50-25 to 27.1 degrees with 150all at 0 months period, thereafter increasing in the subsequent 6 months of growth period. 100-75 resulted in the least change in lordotic angle with 37.9 degrees at 6 months period, Figure 5-25. The maximum von Mises stresses increased with increase in distraction force; 50-25, 50all, 100-75, 100all, 150-125 and 150all resulted in 140.0 MPa, 201.7 MPa, 310.0 MPa, 391.2 MPa, 518.7 MPa, and 550.3 MPa stresses on the rods respectively. However the stresses changed to 111.1 MPa, 87.3 MPa, 54.0 MPa, 31.1 MPa, 102.2 MPa, and 133.2 MPa respectively at 6 months period, Figure 5-26. The total unilateral screw-bone interface load increased with increase in distraction force; 50-25, 50all, 100-75, 100all, 150-125 and 150all resulted in 47.6 N, 54.4 N, 91.8 N, 105.2 N, 134.2 N, and 163.4 N of load at the interface respectively. However similar to stress on the

rods, the loads changed to 44.3 N, 39.6 N, 10.5 N, 22.6 N, 75.5 N, and 111.9 N respectively at 6 months period, Figure 5-27.

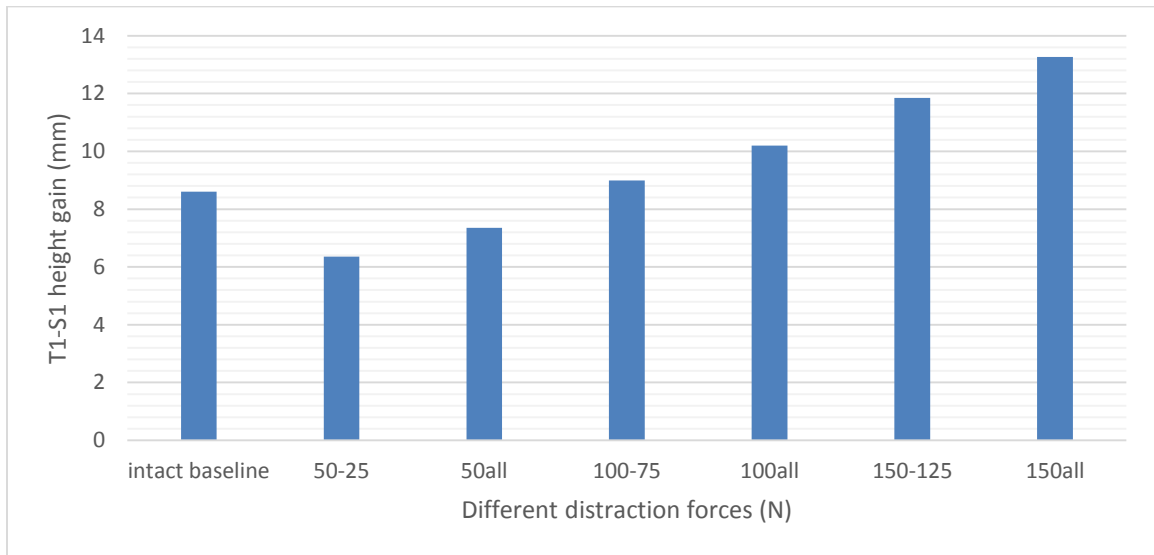


Figure 5-22: Height increase across T1-S1 (in mm) during the growth period of 6 months following distraction for representative scoliotic model 1B.

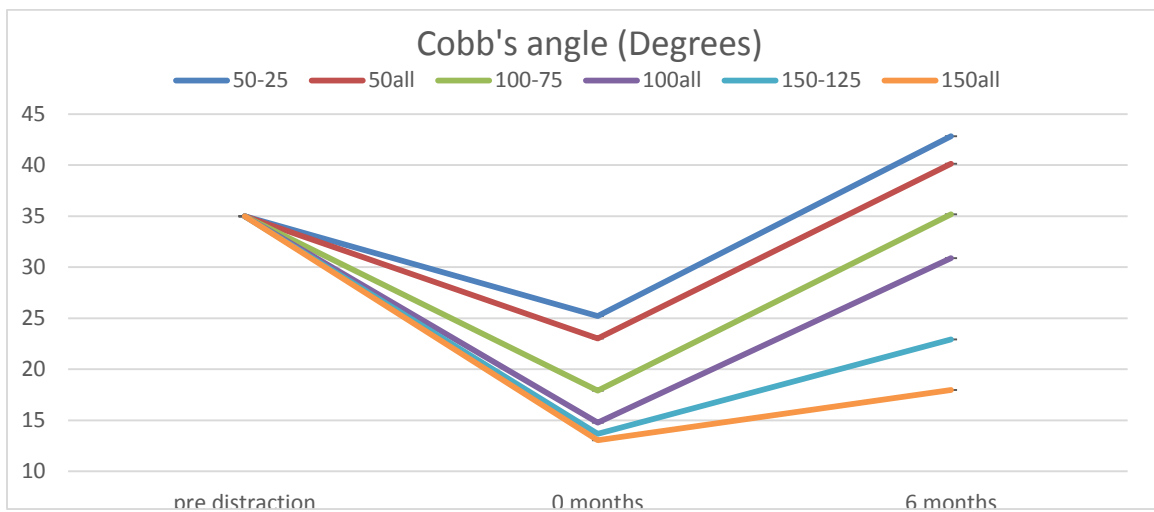


Figure 5-23: The thoracic Cobbs's angle (in degrees) after distraction (t=0) and following 6 months (t=6 months) of growth for representative scoliotic model 1B.

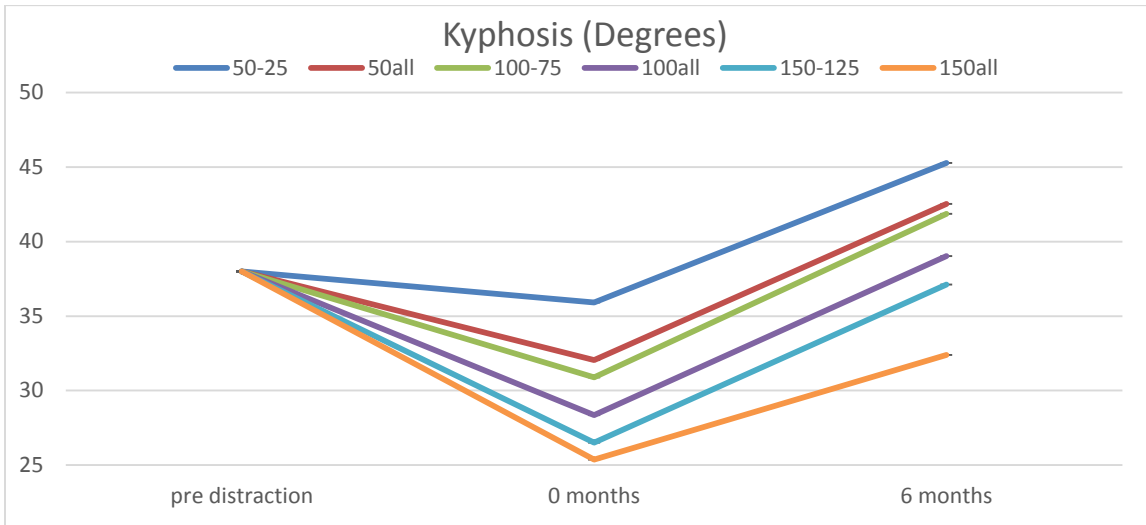


Figure 5-24: The kyphosis (in degrees) after distraction (t=0) and following 6 months (t=6 months) of growth for representative scoliotic model 1B.

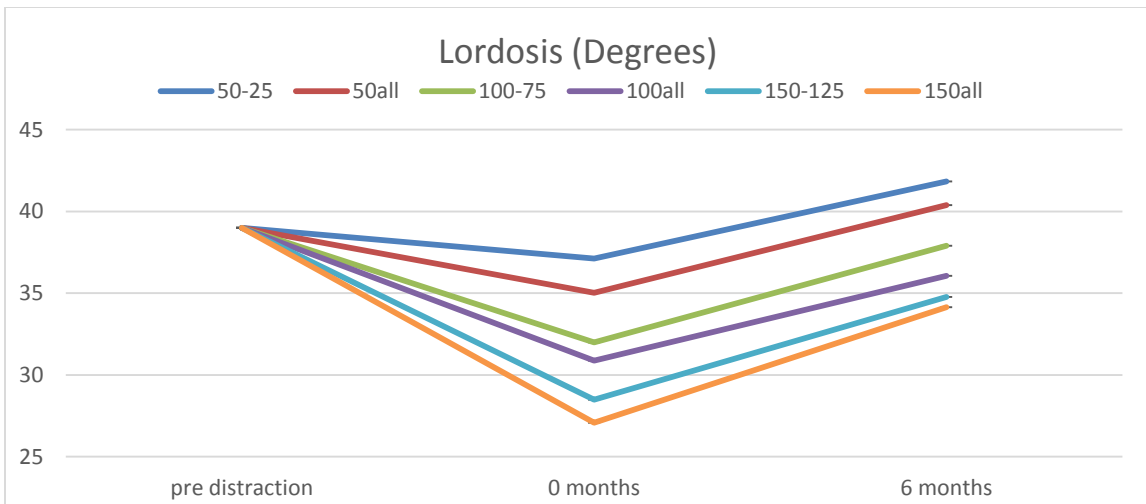


Figure 5-25: The lordosis (in degrees) after distraction (t=0) and following 6 months (t=6 months) of growth for representative scoliotic model 1B.



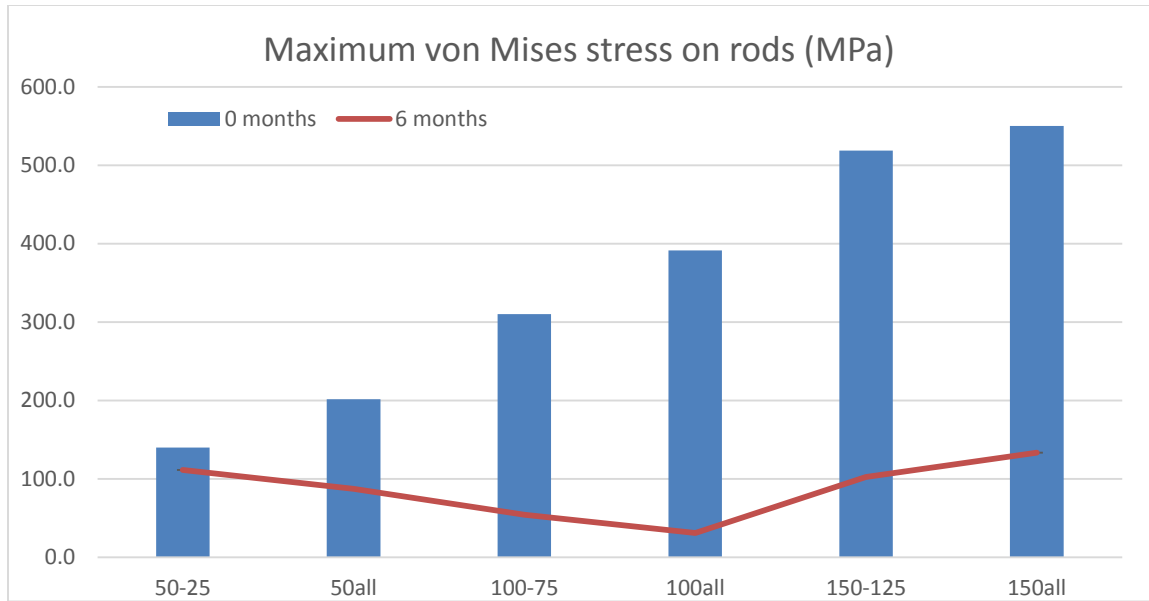


Figure 5-26: Maximum von Mises stress (in MPa) in the growth rod after distraction (t=0) and after 6 months of growth (t=6 months) for representative scoliotic model 1B.

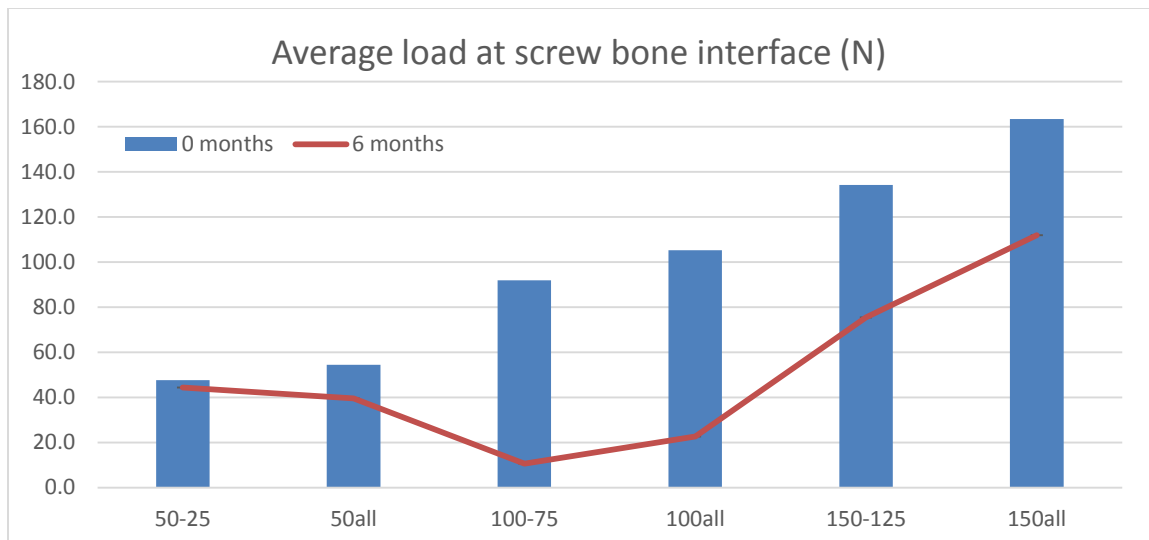


Figure 5-27: Total unilateral average load (N) at the screw-bone interface after distraction (t=0) and after 6 months of growth (t=6 months) for representative scoliotic model 1B.

For the scoliotic model 2, T1-S1 height increased by 6.2 mm, 7.1 mm, 8.7 mm, 9.8 mm, 11.2 mm, 12.6 mm with 50-25, 50all, 100-75, 100all, 150-125 and 150all of

distraction force after 6 months of growth. For intact spine the T1-S1 height increases by 8.6 mm (for 9 year old) in 6 months as reported in the literature, Figure 5-28. Cobb's angle was 35 degrees before distraction, it decreased from 27.5 degrees with 50-25 to 14.2 degrees with 150all at 0 months period, thereafter increasing in the subsequent 6 months of growth period. 100all resulted in the least change in Cobb's angle with 35.2 degrees at 6 months, Figure 5-29. Kyphosis angle was 38 degrees before distraction, it decreased from 32.7 degrees with 50-25 to 22.9 degrees with 150all at 0 months period, thereafter increasing in the subsequent 6 months of growth period. 100-75 resulted in the least change in kyphotic angle with 38.5 degrees at 6 months period, Figure 5-30. Lordosis angle was 39 degrees before distraction, it decreased from 35.5 degrees with 50-25 to 25.4 degrees with 150all at 0 months period, thereafter increasing in the subsequent 6 months of growth period. 100-75 resulted in the least change in lordotic angle with 37.9 degrees at 6 months period, Figure 5-31. The maximum von Mises stresses increased with increase in distraction force; 50-25, 50all, 100-75, 100all, 150-125 and 150all resulted in 127.3 MPa, 168.1 MPa, 254.1 MPa, 340.2 MPa, 415.0 MPa, and 466.4 MPa stresses on the rods respectively. However the stresses changed to 101.0 MPa, 72.7 MPa, 44.3 MPa, 27.0 MPa, 81.8 MPa, and 112.9 MPa respectively at 6 months period, Figure 5-32. The total unilateral screw-bone interface load increased with increase in distraction force; 50-25, 50all, 100-75, 100all, 150-125 and 150all resulted in 43.2 N, 52.0 N, 75.3 N, 91.5 N, 107.4 N, and 138.5 N of load at the interface respectively. However similar to stress on the rods, the loads changed to 41.0 N, 47.2 N, 35.3 N, 9.9 N, 92.9 N, and 121.6 N respectively at 6 months period, Figure 5-33.

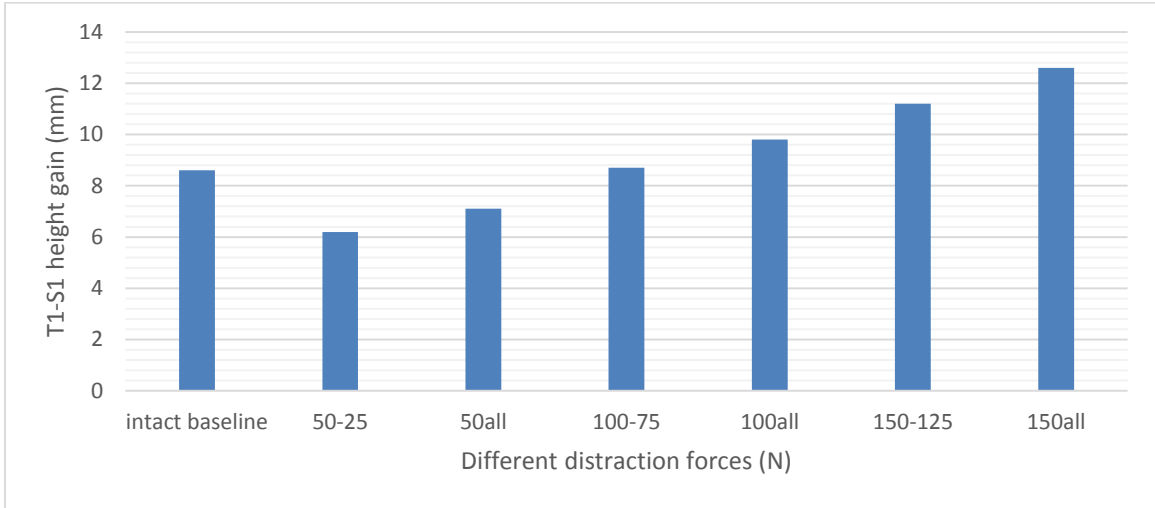


Figure 5-28: Height increase across T1-S1 (in mm) during the growth period of 6 months following distraction for representative scoliotic model 2.

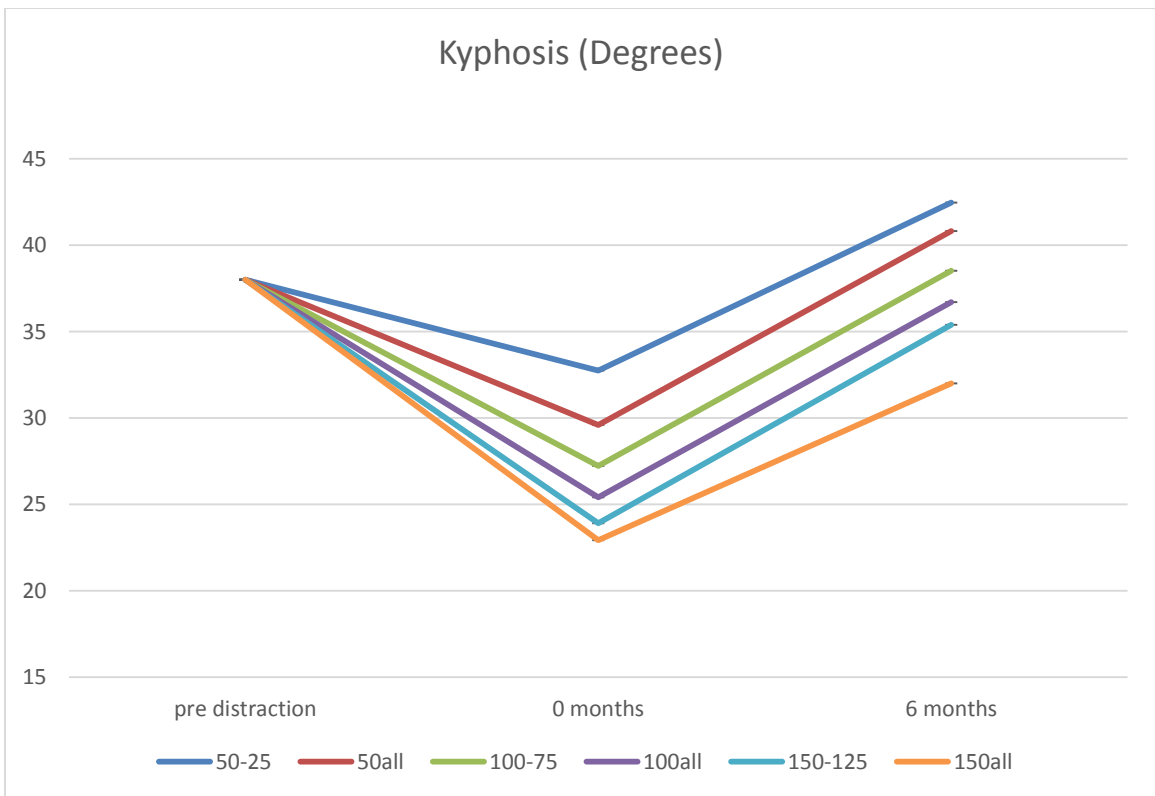


Figure 5-29: The kyphosis (in degrees) after distraction (t=0) and following 6 months (t=6 months) of growth for representative scoliotic model 2.

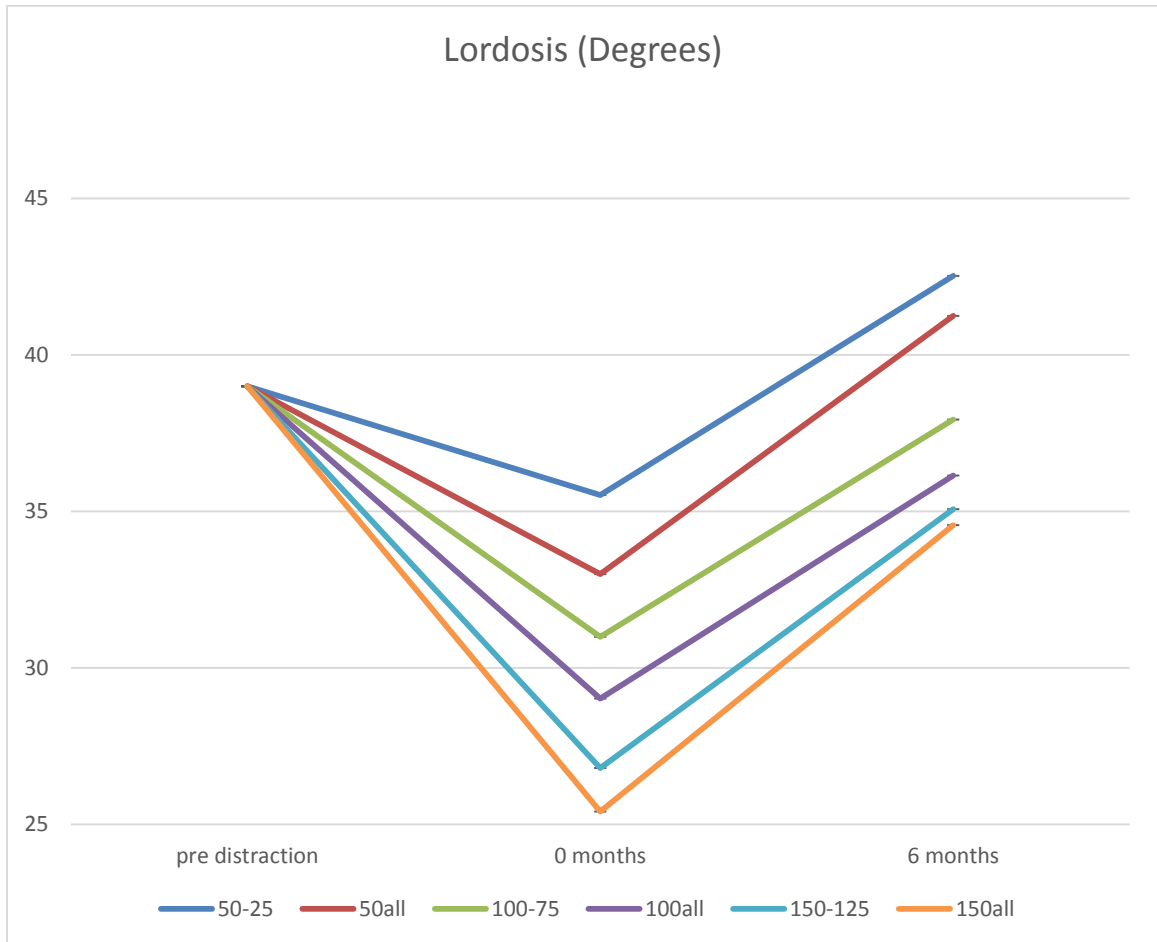


Figure 5-30: The lordosis (in degrees) after distraction (t=0) and following 6 months (t=6 months) of growth for representative scoliotic model 2.

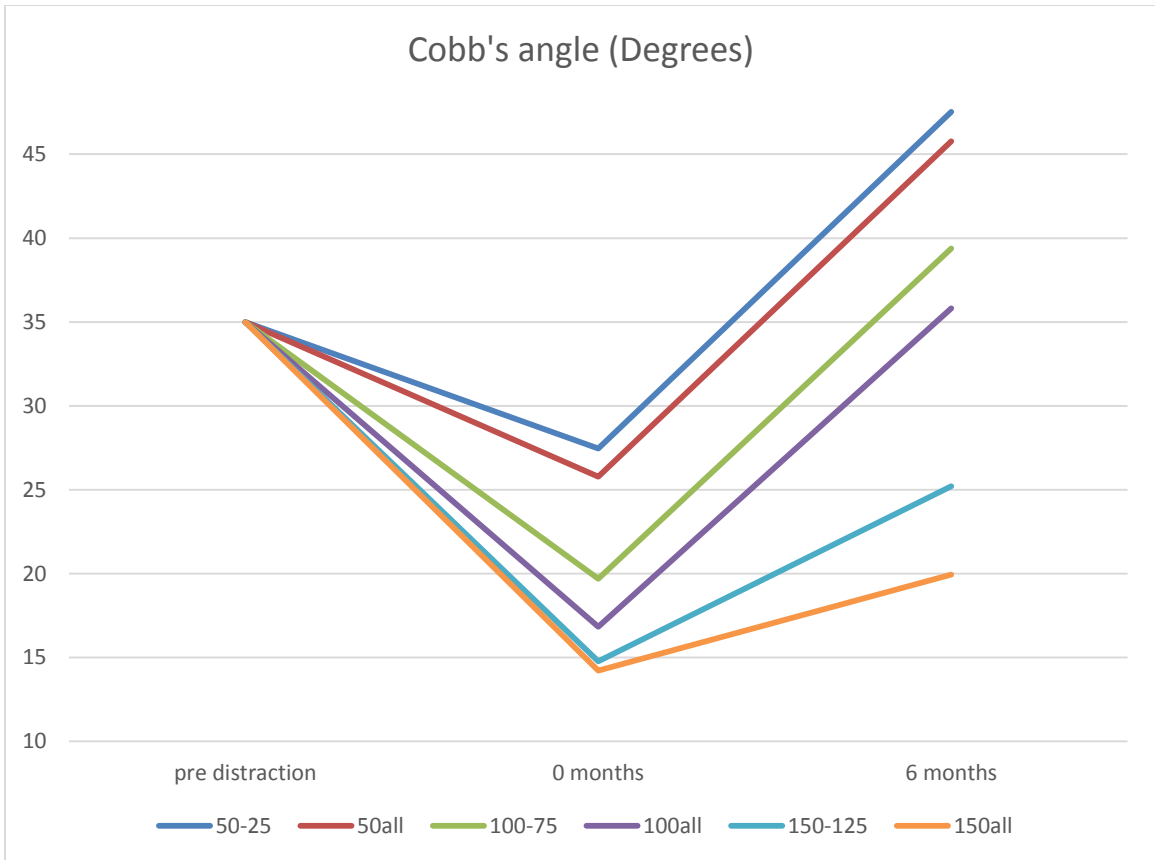


Figure 5-31: The thoracic Cobb's angle (in degrees) after distraction (t=0) and following 6 months (t=6 months) of growth for representative scoliotic model 2.

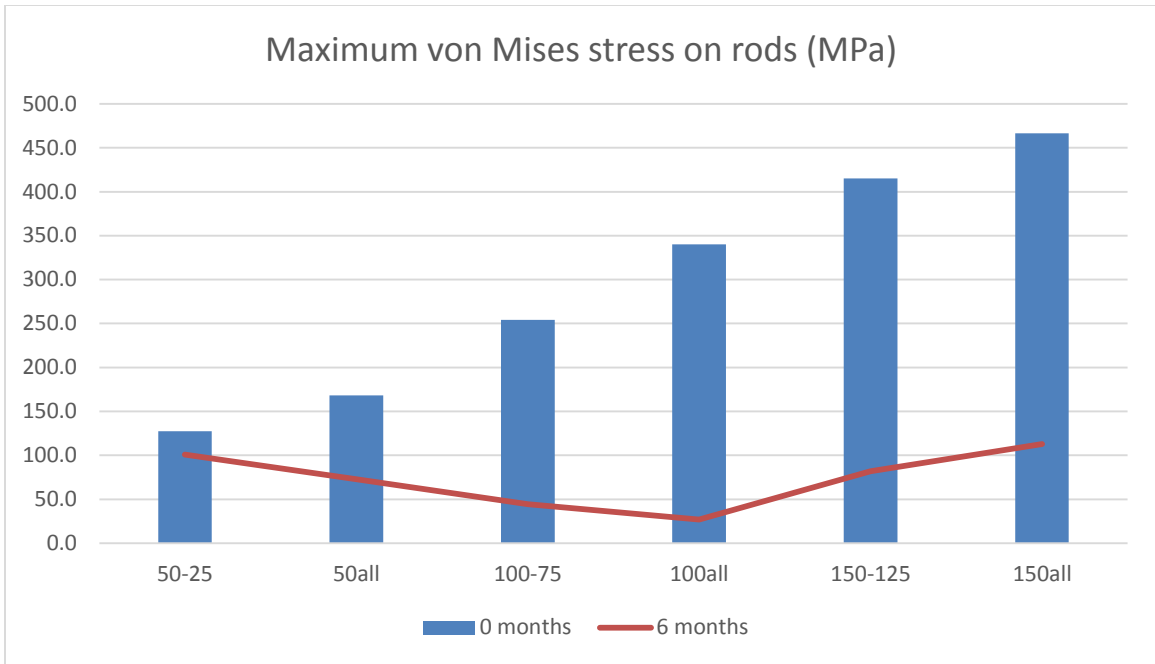


Figure 5-32: Maximum von Mises stress (in MPa) in the growth rod after distraction (t=0) and after 6 months of growth (t=6 months) for representative scoliotic model 2.

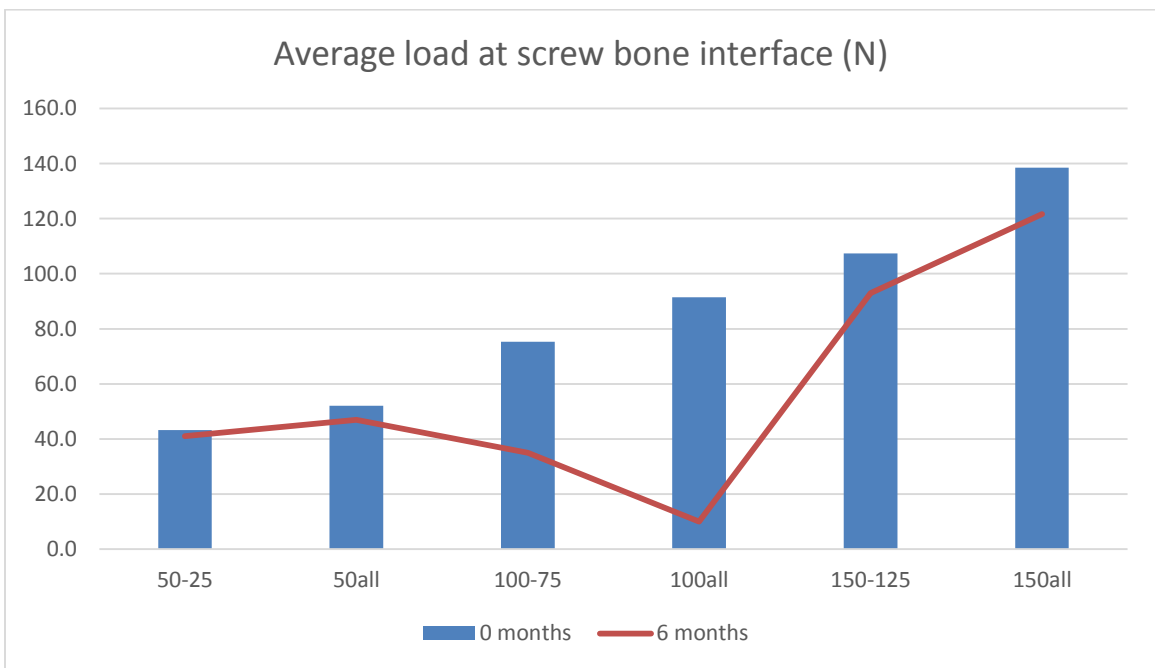


Figure 5-33: Total unilateral average load (N) at the screw-bone interface after distraction (t=0) and after 6 months of growth (t=6 months) for representative scoliotic model 2.

For the group 3 scoliotic model, T1-S1 height increased by 6.1 mm, 7.3 mm, 8.5 mm, 9.9 mm, 10.8 mm, 12.8 mm with 50-25, 50all, 100-75, 100all, 150-125 and 150all of distraction force after 6 months of growth. For intact spine the T1-S1 height increases by 8.6 mm (for 9 year old) in 6 months as reported in the literature, Figure 5-34. Cobb's angle was 35 degrees before distraction, it decreased from 28.0 degrees with 50-25 to 14.5 degrees with 150all at 0 months period, thereafter increasing in the subsequent 6 months of growth period. 100all resulted in the least change in Cobb's angle with 36.5 degrees at 6 months, Figure 5-35. Kyphosis angle was 38 degrees before distraction, it decreased from 29.4 degrees with 50-25 to 20.1 degrees with 150all at 0 months period, thereafter increasing in the subsequent 6 months of growth period. 50all resulted in the least change in kyphotic angle with 37.1 degrees at 6 months period, Figure 5-36. Lordosis angle was 39 degrees before distraction, it decreased from 33 degrees with 50-25 to 24.1 degrees with 150all at 0 months period, thereafter increasing in the subsequent 6 months of growth period. 100-75 resulted in the least change in lordotic angle with 39.0 degrees at 6 months period, Figure 5-37. The maximum von Mises stresses increased with increase in distraction force; 50-25, 50all, 100-75, 100all, 150-125 and 150all resulted in 130.5 MPa, 173.1 MPa, 261.9 MPa, 349.6 MPa, 428.5 MPa, and 479.9 MPa stresses on the rods respectively. However the stresses changed to 113.1 MPa, 103.5 MPa, 93.7 MPa, 69.4 MPa, 174.7 MPa, and 186.6 MPa respectively at 6 months period, Figure 5-38. The total unilateral screw-bone interface load increased with increase in distraction force; 50-25,

50all, 100-75, 100all, 150-125 and 150all resulted in 46.3 N, 53.1 N, 70.1 N, 95.3 N, 118.5 N, and 143.2 N of load at the interface respectively. However similar to stress on the rods, the loads changed to 42.3 N, 30.7 N, 20.5 N, 60.7 N, 76.6 N, and 105.5 N respectively at 6 months period, Figure 5-39.

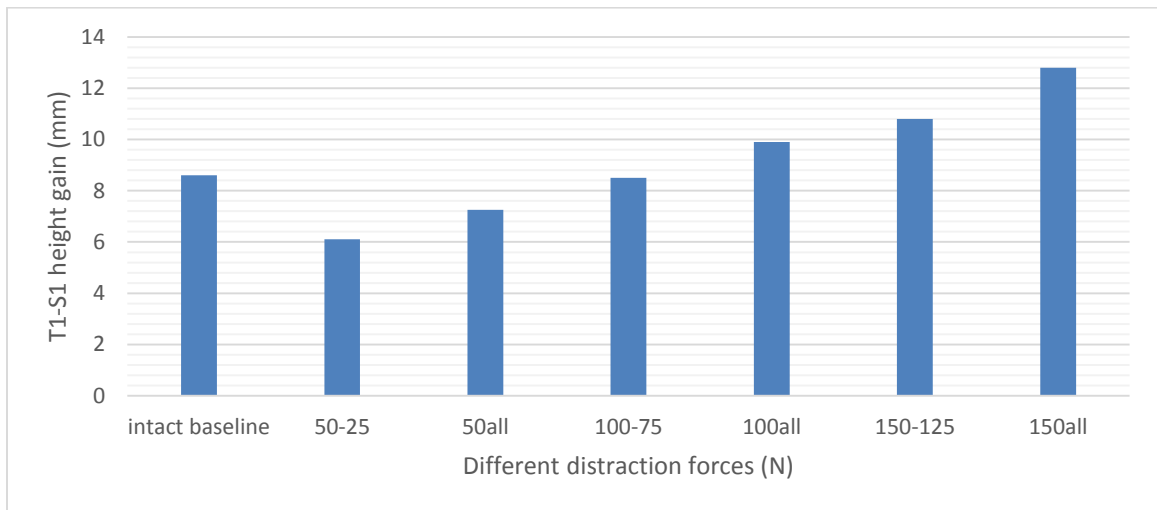


Figure 5-34: Height increase across T1-S1 (in mm) during the growth period of 6 months following distraction for representative scoliotic model 3.



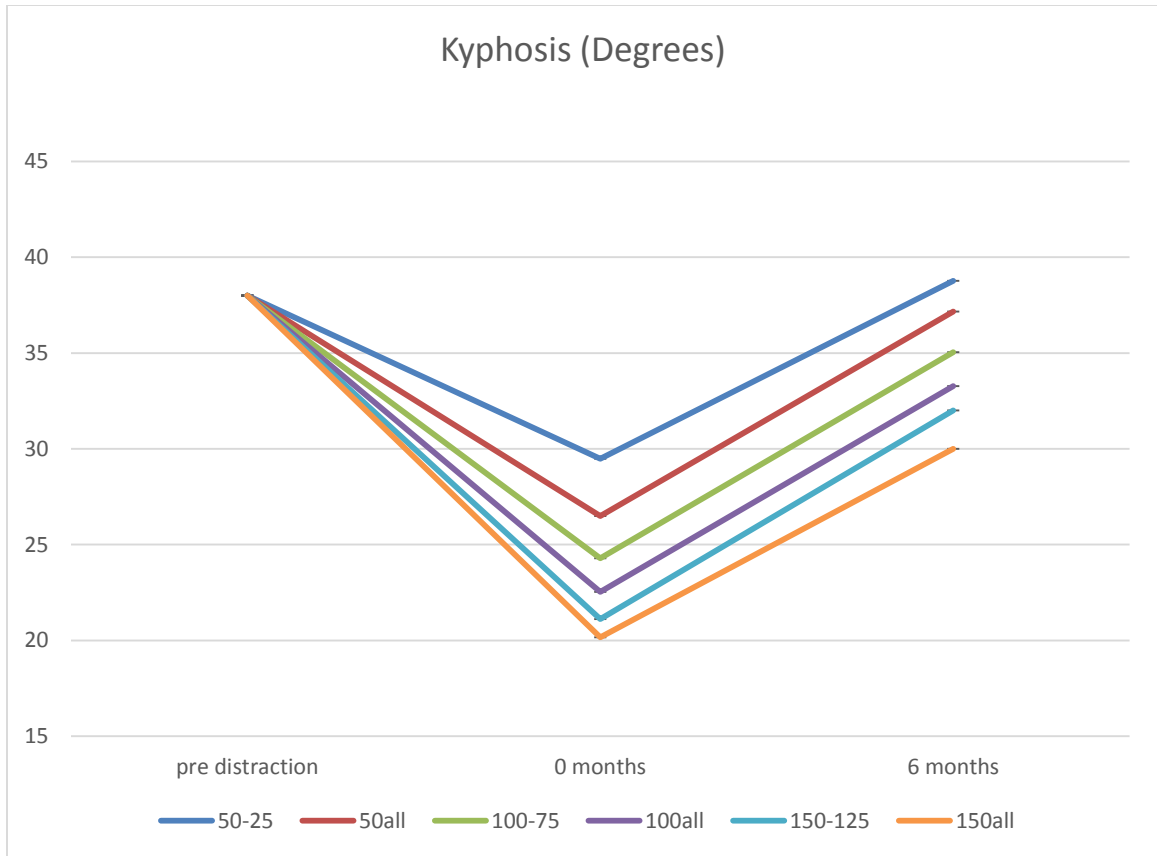


Figure 5-35: The kyphosis (in degrees) after distraction (t=0) and following 6 months (t=6 months) of growth for representative scoliotic model 3.

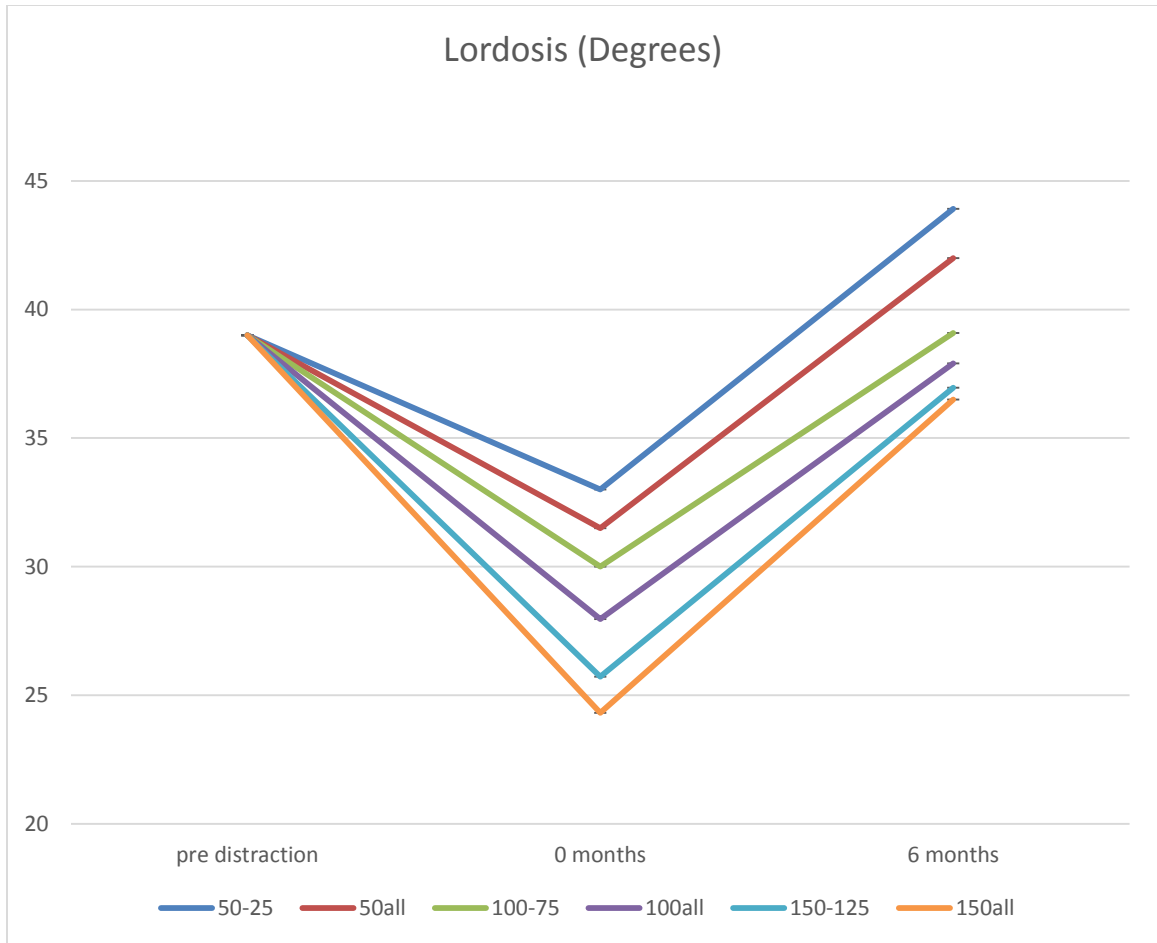


Figure 5-36: The lordosis (in degrees) after distraction ( $t=0$ ) and following 6 months ( $t=6$  months) of growth for representative scoliotic model 3.

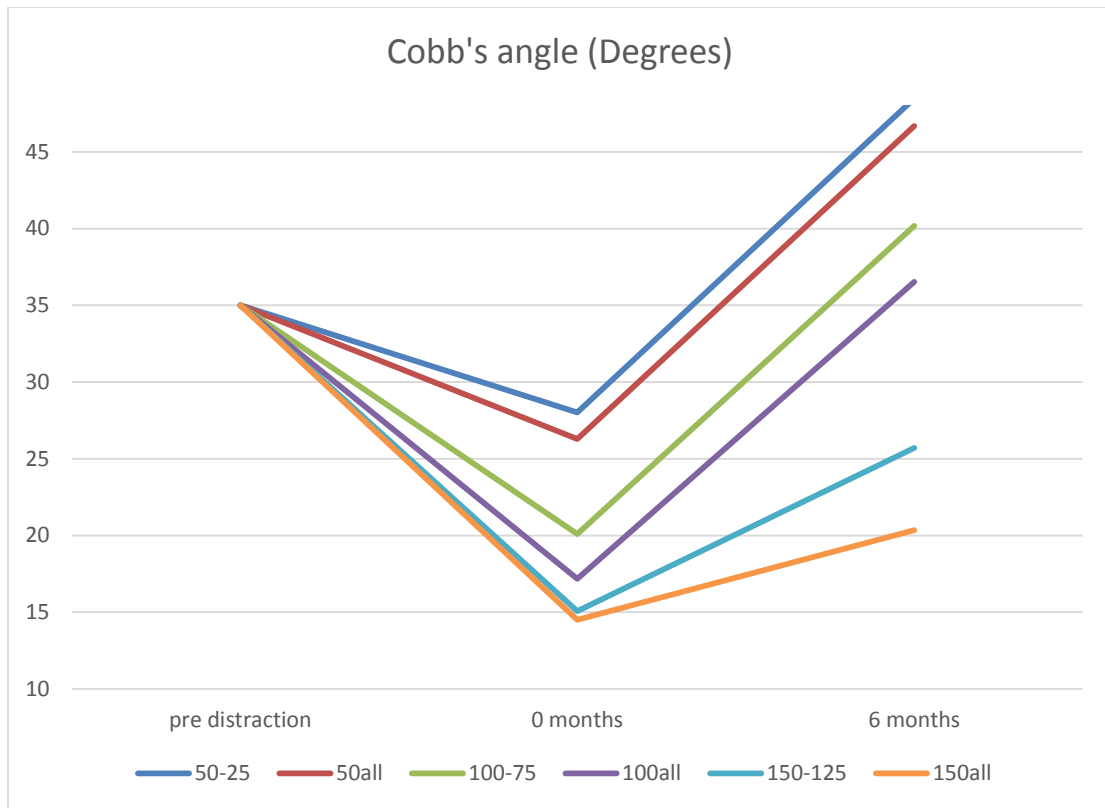


Figure 5-37: The thoracic Cobbs's angle (in degrees) after distraction (t=0) and following 6 months (t=6 months) of growth for representative scoliotic model 1B.

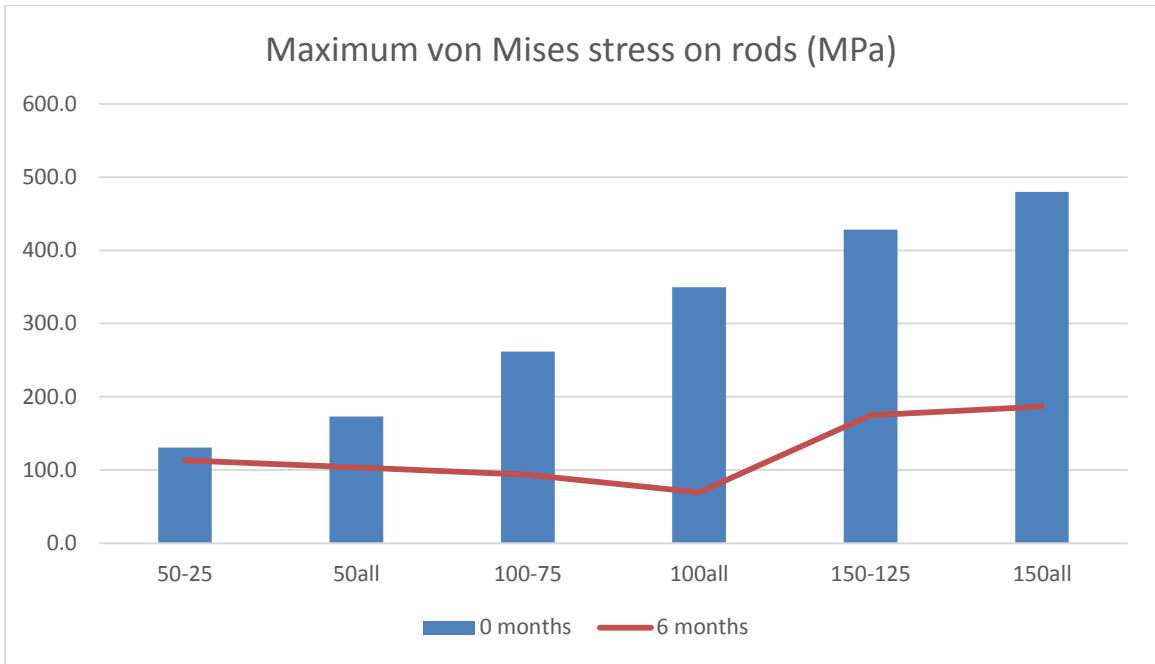


Figure 5-38: Maximum von Mises stress (in MPa) in the growth rod after distraction ( $t=0$ ) and after 6 months of growth ( $t=6$  months) for representative scoliotic model 3.

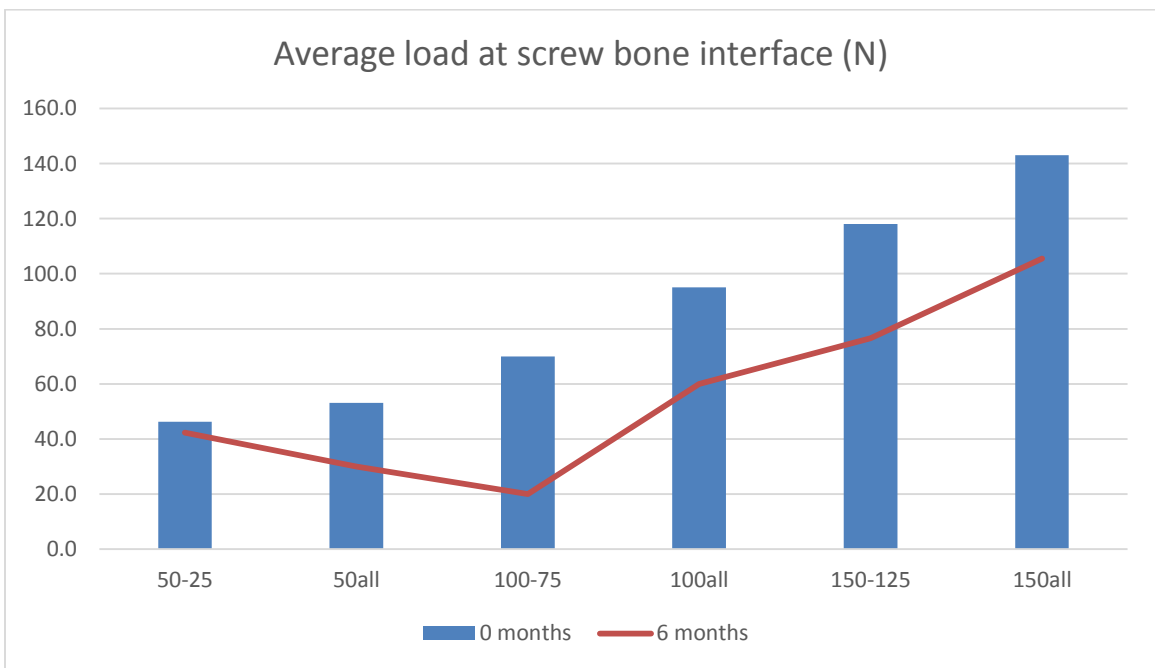


Figure 5-39: Total unilateral average load (N) at the screw-bone interface after distraction (t=0) and after 6 months of growth (t=6 months) for representative scoliotic model 3.

For the scoliotic model 4, T1-S1 height increased by 6.8 mm, 7.9 mm, 9.4 mm, 10.5 mm, 12.6 mm, 14.1 mm with 50-25, 50all, 100-75, 100all, 150-125 and 150all of distraction force after 6 months of growth. For intact spine the T1-S1 height increases by 8.6 mm (for 9 year old) in 6 months as reported in the literature, Figure 5-40. Cobb's angle was 35 degrees before distraction, it decreased from 23.8 degrees with 50-25 to 12.3 degrees with 150all at 0 months period, thereafter increasing in the subsequent 6 months of growth period. 100-75 resulted in the least change in Cobb's angle with 32.3 degrees at 6 months, Figure 5-41. Kyphosis angle was 38 degrees before distraction, it decreased from 34.4 degrees with 50-25 to 24.3 degrees with 150all at 0 months period, thereafter increasing in the subsequent 6 months of growth period. 100all resulted in the least change in kyphotic angle with 37.9 degrees at 6 months period, Figure 5-42. Lordosis angle was 39 degrees before distraction, it decreased from 37.0 degrees with 50-25 to 29.1 degrees with 150all at 0 months period, thereafter increasing in the subsequent 6 months of growth period. 100-75 resulted in the least change in lordotic angle with 39 degrees at 6 months period, Figure 5-43. The maximum von Mises stresses increased with increase in distraction force; 50-25, 50all, 100-75, 100all, 150-125 and 150all resulted in 147.5 MPa, 198.2 MPa, 300.6 MPa, 397.8 MPa, 493.4 MPa, and 590.0 MPa stresses on the rods respectively. However the stresses changed to 109.5 MPa, 89.3 MPa, 61.8 MPa, 25.1 MPa, 122.5 MPa, and 180.0 MPa respectively at 6 months period, Figure 5-44. The total unilateral screw-bone interface load increased with increase in distraction force; 50-25,

50all, 100-75, 100all, 150-125 and 150all resulted in 42.3 N, 55.2 N, 102.6 N, 111.3 N, 130.7 N, and 140.9 N of load at the interface respectively. However similar to stress on the rods, the loads changed to 40.3 N, 49.0 N, 30.6 N, 20.3 N, 110.4 N, and 199.8 N respectively at 6 months period, Figure 5-45.

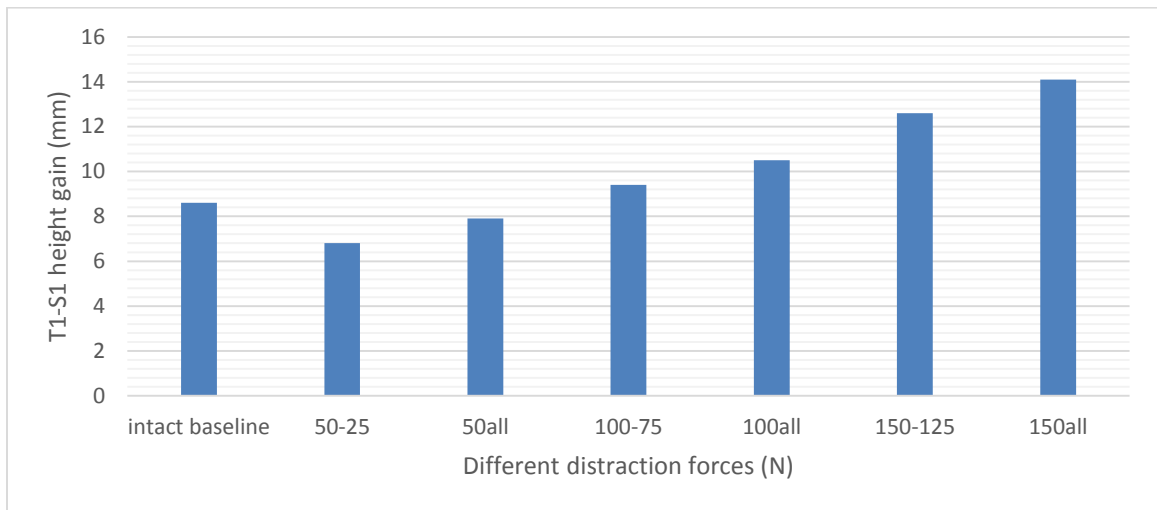


Figure 5-40: Height increase across T1-S1 (in mm) during the growth period of 6 months following distraction for representative scoliotic model 4.

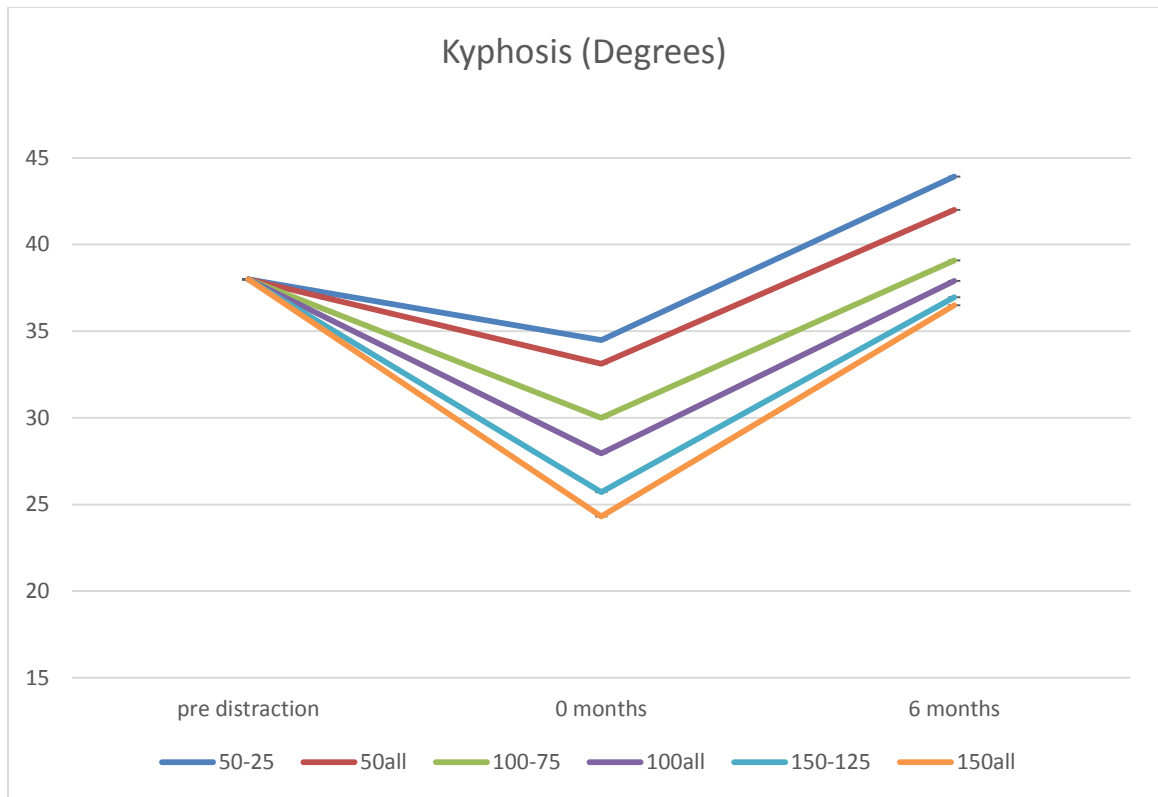


Figure 5-41: The kyphosis (in degrees) after distraction (t=0) and following 6 months (t=6 months) of growth for representative scoliotic model 4.

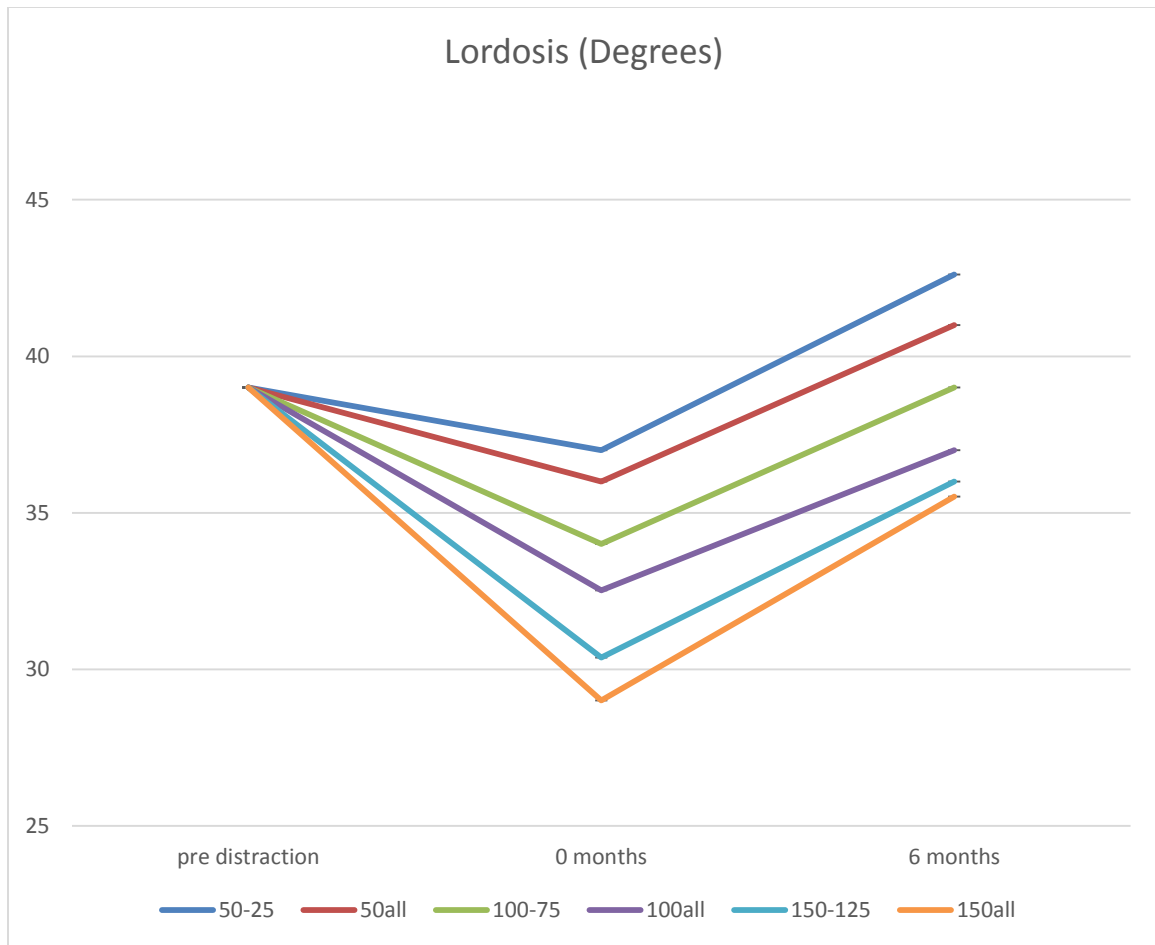


Figure 5-42: The lordosis (in degrees) after distraction ( $t=0$ ) and following 6 months ( $t=6$  months) of growth for representative scoliotic model 4.



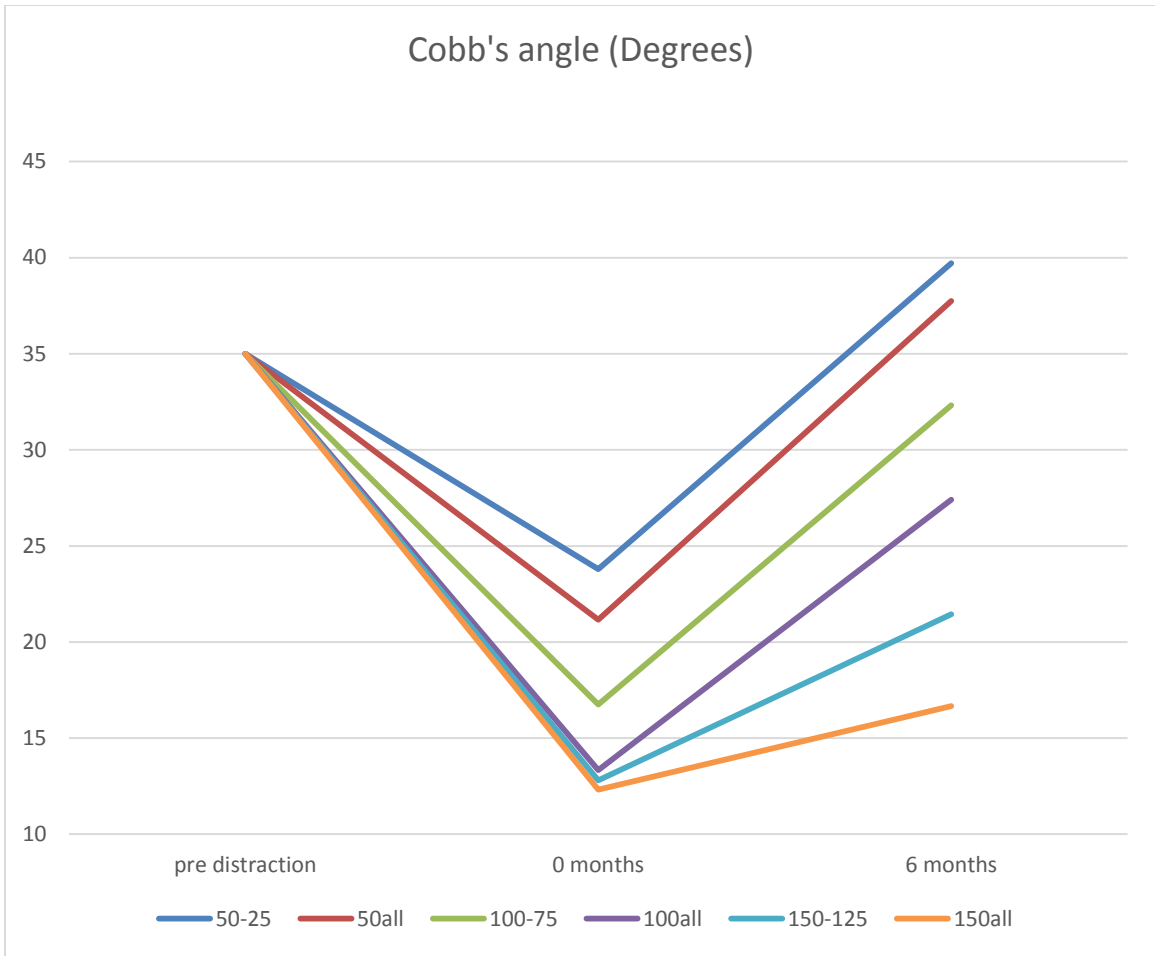


Figure 5-43: The lumbar Cobb's angle (in degrees) after distraction ( $t=0$ ) and following 6 months ( $t=6$  months) of growth for representative scoliotic model 4.

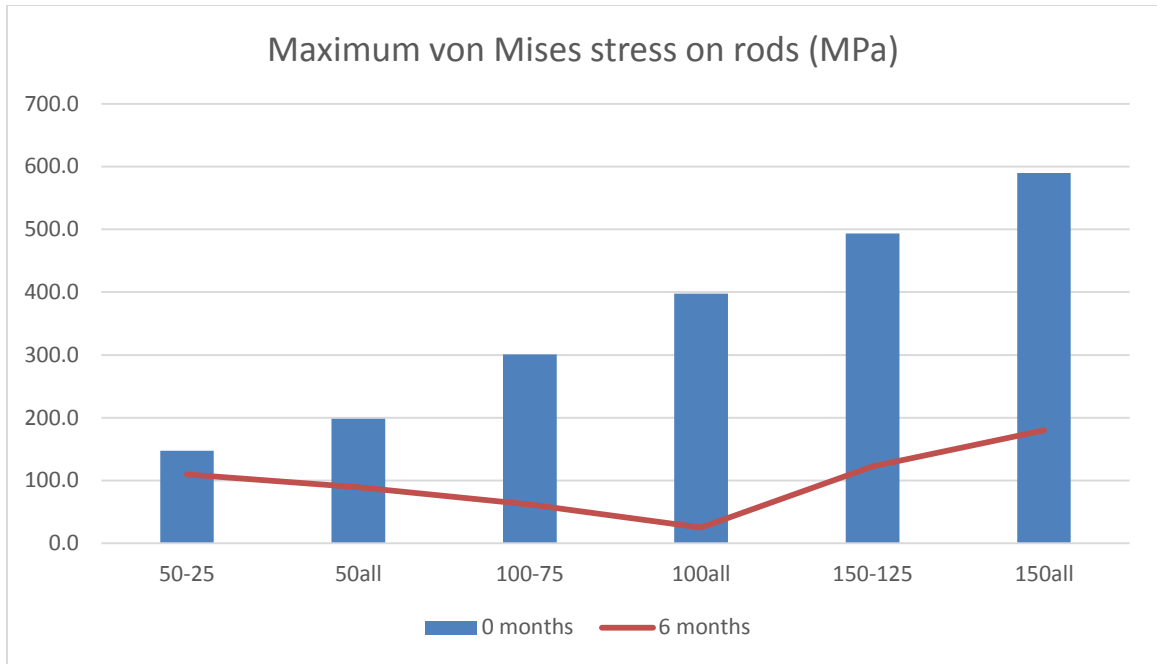


Figure 5-44: Maximum von Mises stress (in MPa) in the growth rod after distraction ( $t=0$ ) and after 6 months of growth ( $t=6$  months) for representative scoliotic model 4.

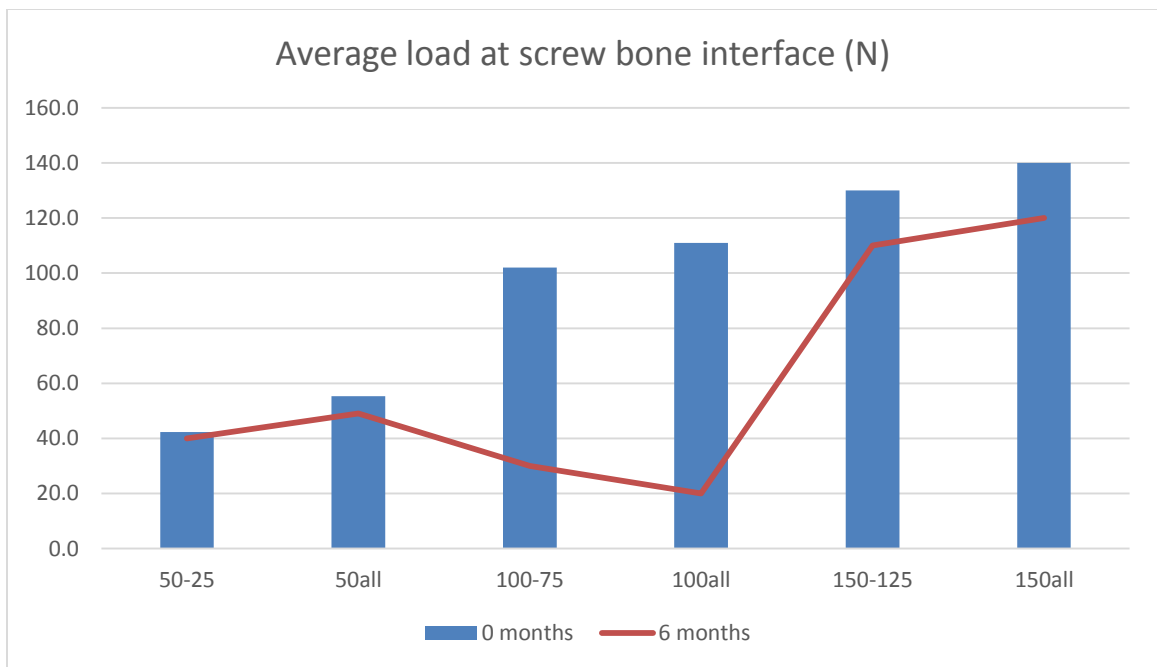


Figure 5-45: Total unilateral average load (N) at the screw-bone interface after distraction ( $t=0$ ) and after 6 months of growth ( $t=6$  months) for representative scoliotic model 4.

## **5.5 Effect of Distraction Frequency on Representative Juvenile Spines**

For the group 1A scoliotic model, the simulation with a distraction period of 2 months, the maximum von Mises stress on the rod during distraction ranged from 79.2 MPa (1<sup>st</sup> distraction) to 391.9 MPa (last distraction). For the simulation with a distraction period of 3 months, the maximum von Mises stress on the rod during distraction ranged from 178.0 MPa (1<sup>st</sup> distraction) to 609.0 MPa (last distraction). For the simulation with a distraction period of 6 months, the maximum von Mises stress on the rod during distraction ranged from 290.6 MPa (1<sup>st</sup> distraction) to 611.6 MPa (last distraction). For the simulation with a distraction period of 12 months, the maximum von Mises stress on the rod during distraction ranged from 421.7 MPa (1<sup>st</sup> distraction) to 735.1 MPa (last distraction) (Figure 5-46).

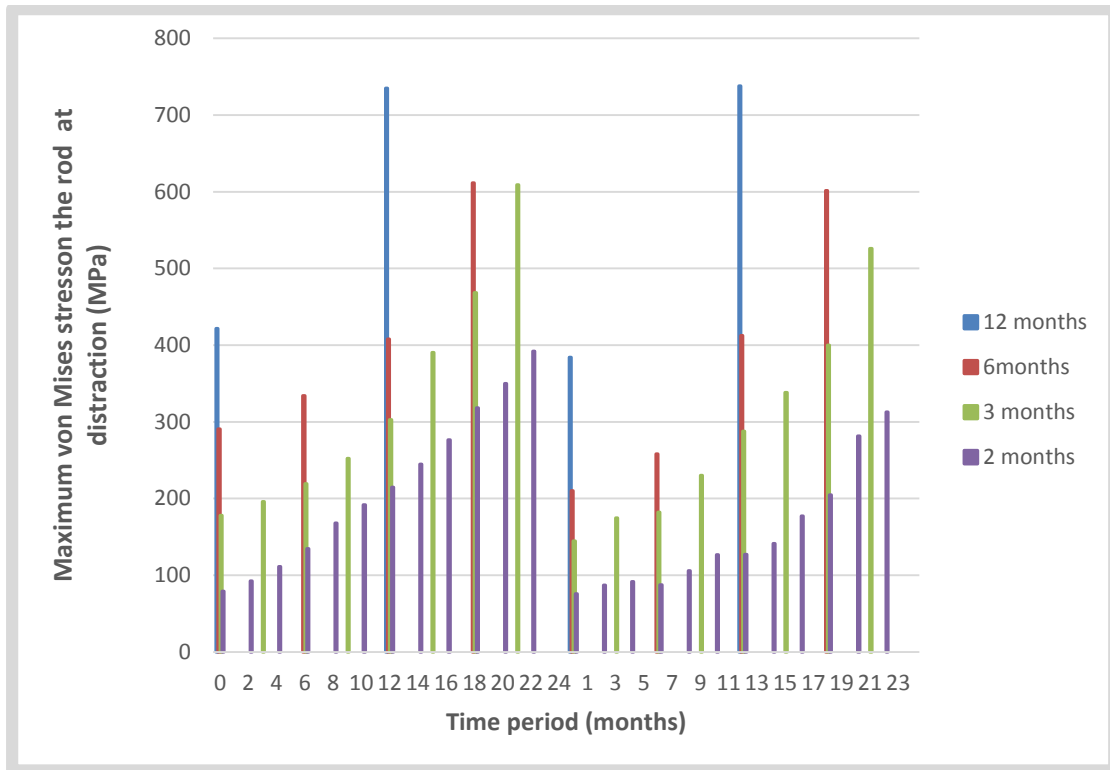


Figure 5-46: The graph shows the maximum von Mises stress on the rod immediately after distraction with different frequency of distraction for the duration of 24 months (for representative scoliotic model 1A). For 12 monthly distractions there are two peaks (at 0 and at 12 months). For 6 monthly distractions there are four peaks (at 0, 6, 12, and 18 months). For 3 monthly distractions there are eight peaks (at 0, 3, 6, 9, 12, 15, 18, and 21 months). For 2 monthly distractions there are twelve peaks (at 0, 2, 4, 6, 8, 10, 12, 14, 16, 18, 20, and 22 months). The data from non-scoliotic normal spine instrumented with growth rod is shown on the right.

For the group 1B, the simulation with a distraction period of 2 months, the maximum von Mises stress on the rod during distraction ranged from 85.3 MPa (1<sup>st</sup> distraction) to 452.6 MPa (last distraction). For the simulation with a distraction period of 3 months, the

maximum von Mises stress on the rod during distraction ranged from 201.0 MPa (1<sup>st</sup> distraction) to 647.2 MPa (last distraction). For the simulation with a distraction period of 6 months, the maximum von Mises stress on the rod during distraction ranged from 310.0 MPa (1<sup>st</sup> distraction) to 630.5 MPa (last distraction). For the simulation with a distraction period of 12 months, the maximum von Mises stress on the rod during distraction ranged from 436.4 MPa (1<sup>st</sup> distraction) to 781.8 MPa (last distraction), Figure 5-47.

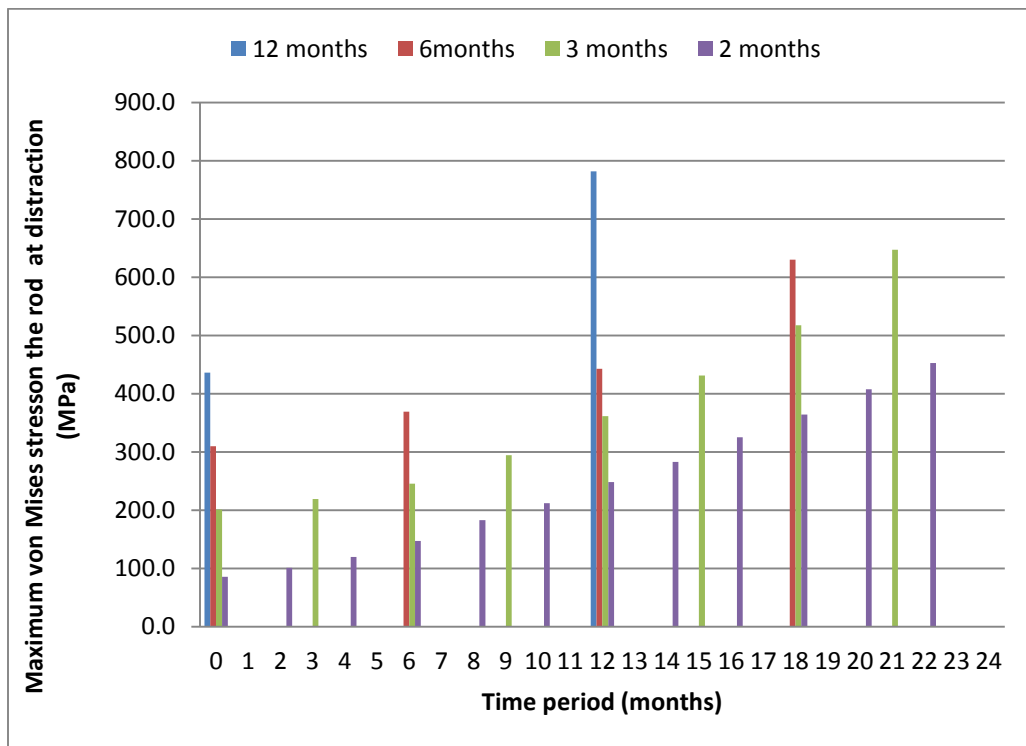


Figure 5-47: The graph shows the maximum von Mises stress on the rod immediately after distraction with different frequency of distraction for the duration of 24 months (for representative scoliotic model 1B). For 12 monthly distractions there are two peaks (at 0 and at 12 months). For 6 monthly distractions there are four peaks (at 0, 6, 12, and 18 months). For 3 monthly distractions there are eight peaks (at 0, 3, 6, 9, 12, 15, 18, and 21

months). For 2 monthly distractions there are twelve peaks (at 0, 2, 4, 6, 8, 10, 12, 14, 16, 18, 20, and 22 months).

For the group 2, the simulation with a distraction period of 2 months, the maximum von Mises stress on the rod during distraction ranged from 99.2 MPa (1<sup>st</sup> distraction) to 521.1 MPa (last distraction). For the simulation with a distraction period of 3 months, the maximum von Mises stress on the rod during distraction ranged from 201.9 MPa (1<sup>st</sup> distraction) to 687.7 MPa (last distraction). For the simulation with a distraction period of 6 months, the maximum von Mises stress on the rod during distraction ranged from 254.1 MPa (1<sup>st</sup> distraction) to 647.1 MPa (last distraction). For the simulation with a distraction period of 12 months, the maximum von Mises stress on the rod during distraction ranged from 451.6 MPa (1<sup>st</sup> distraction) to 781.3 MPa (last distraction), Figure 5-48.

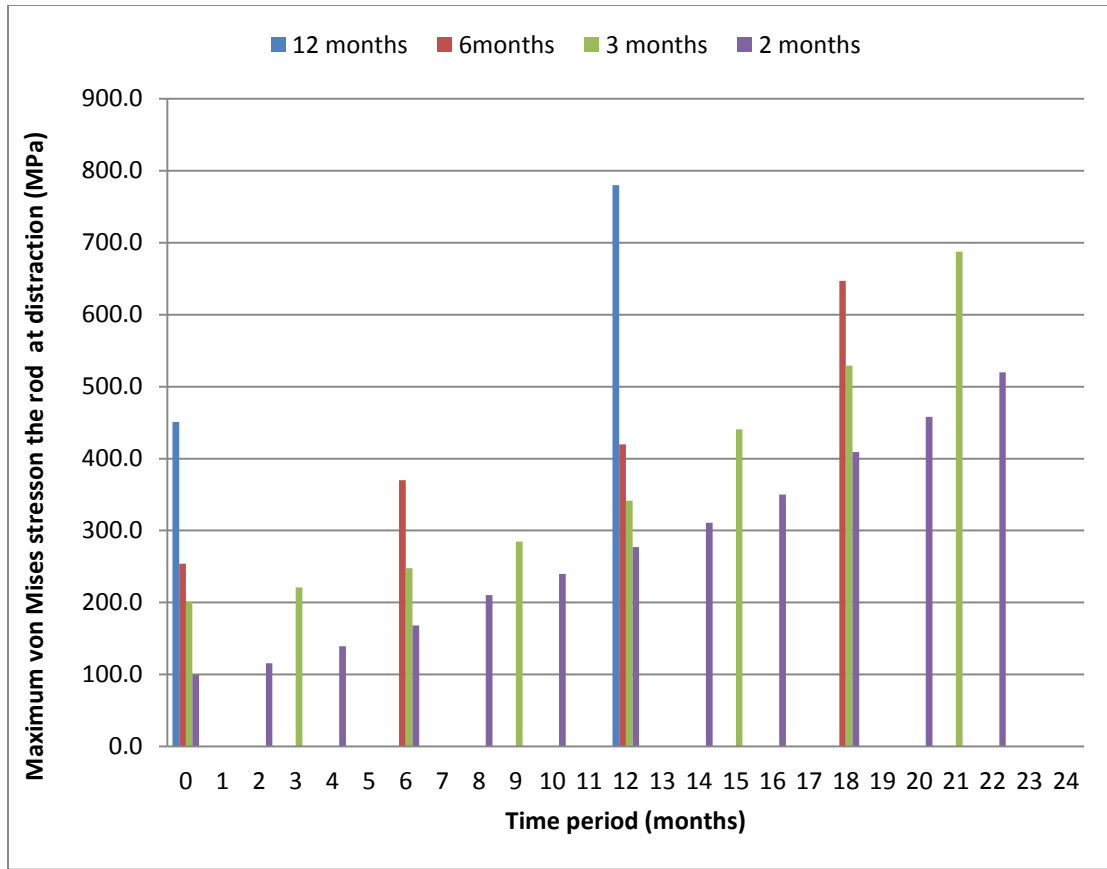


Figure 5-48: The graph shows the maximum von Mises stress on the rod immediately after distraction with different frequency of distraction for the duration of 24 months (for representative scoliotic model 2). For 12 monthly distractions there are two peaks (at 0 and at 12 months). For 6 monthly distractions there are four peaks (at 0, 6, 12, and 18 months). For 3 monthly distractions there are eight peaks (at 0, 3, 6, 9, 12, 15, 18, and 21 months). For 2 monthly distractions there are twelve peaks (at 0, 2, 4, 6, 8, 10, 12, 14, 16, 18, 20, and 22 months).

For the group 3, the simulation with a distraction period of 2 months, the maximum von Mises stress on the rod during distraction ranged from 102.5 MPa (1<sup>st</sup> distraction) to 532.9 MPa (last distraction). For the simulation with a distraction period of 3 months, the

maximum von Mises stress on the rod during distraction ranged from 198.2 MPa (1<sup>st</sup> distraction) to 677.4 MPa (last distraction). For the simulation with a distraction period of 6 months, the maximum von Mises stress on the rod during distraction ranged from 261.9 MPa (1<sup>st</sup> distraction) to 669.4 MPa (last distraction). For the simulation with a distraction period of 12 months, the maximum von Mises stress on the rod during distraction ranged from 468.6 MPa (1<sup>st</sup> distraction) to 798.8 MPa (last distraction), Figure 5-49.

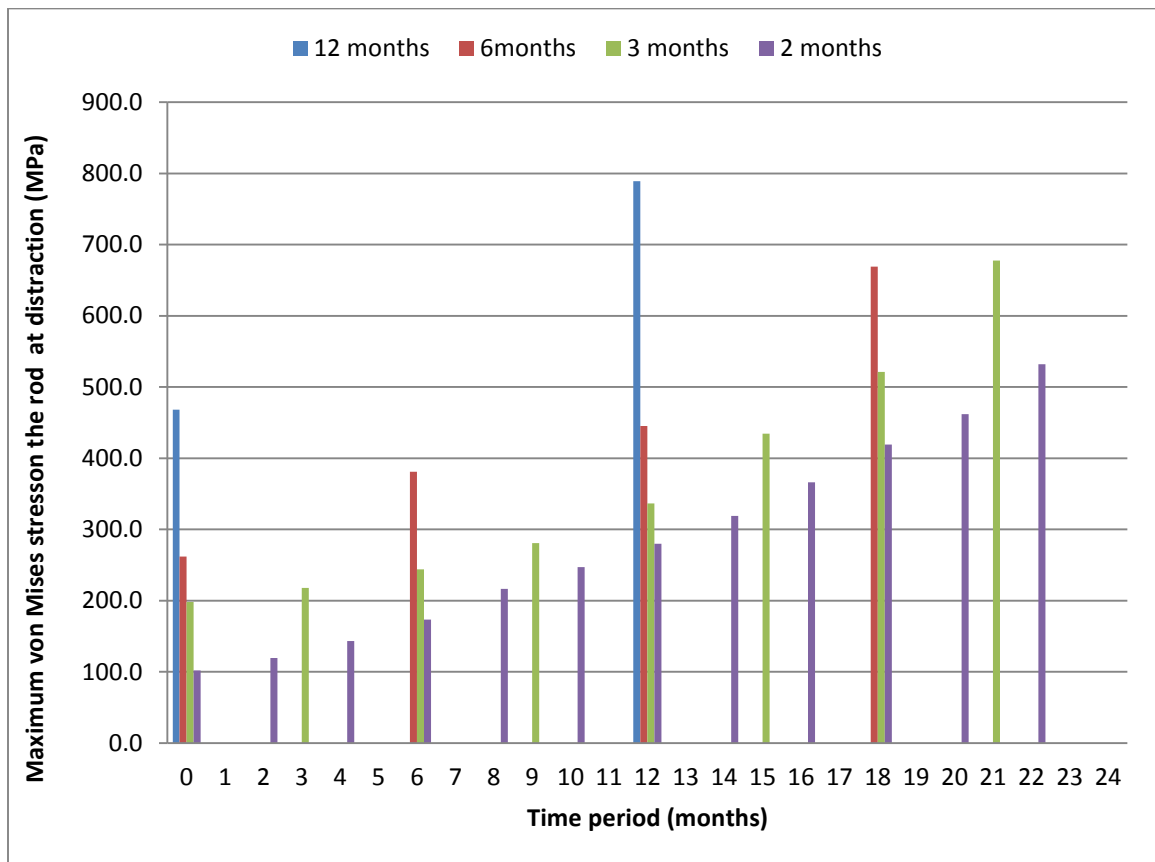


Figure 5-49: The graph shows the maximum von Mises stress on the rod immediately after distraction with different frequency of distraction for the duration of 24 months (for



representative scoliotic model 3). For 12 monthly distractions there are two peaks (at 0 and at 12 months). For 6 monthly distractions there are four peaks (at 0, 6, 12, and 18 months). For 3 monthly distractions there are eight peaks (at 0, 3, 6, 9, 12, 15, 18, and 21 months). For 2 monthly distractions there are twelve peaks (at 0, 2, 4, 6, 8, 10, 12, 14, 16, 18, 20, and 22 months).

For the group 4, the simulation with a distraction period of 2 months, the maximum von Mises stress on the rod during distraction ranged from 120.6 MPa (1<sup>st</sup> distraction) to 550.2 MPa (last distraction). For the simulation with a distraction period of 3 months, the maximum von Mises stress on the rod during distraction ranged from 219.1 MPa (1<sup>st</sup> distraction) to 749.3 MPa (last distraction). For the simulation with a distraction period of 6 months, the maximum von Mises stress on the rod during distraction ranged from 305.3 MPa (1<sup>st</sup> distraction) to 707.9 MPa (last distraction). For the simulation with a distraction period of 12 months, the maximum von Mises stress on the rod during distraction ranged from 551.4 MPa (1<sup>st</sup> distraction) to 813.2 MPa (last distraction), Figure 5-50.

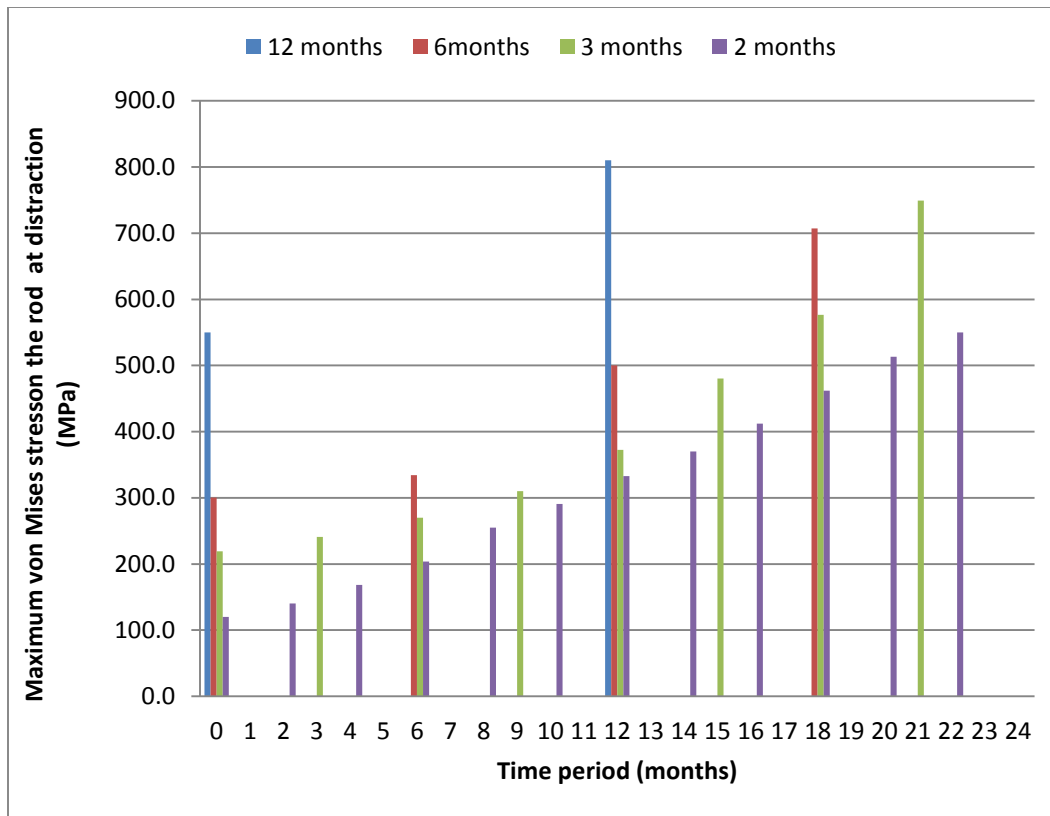


Figure 5-50: The graph shows the maximum von Mises stress on the rod immediately after distraction with different frequency of distraction for the duration of 24 months (for representative scoliotic model 4). For 12 monthly distractions there are two peaks (at 0 and at 12 months). For 6 monthly distractions there are four peaks (at 0, 6, 12, and 18 months). For 3 monthly distractions there are eight peaks (at 0, 3, 6, 9, 12, 15, 18, and 21 months). For 2 monthly distractions there are twelve peaks (at 0, 2, 4, 6, 8, 10, 12, 14, 16, 18, 20, and 22 months).

## 5.6 Sensitivity Study

Figure 5-51 shows the relationship between the axial stiffness and the percentage correction in Cobb's angle due to gravity alone. Figure 5-52 shows the relationship between

the percentage correction in Cobb's angle due to gravity alone and the required distraction interval for limiting the maximum von Mises stress to 255 Mpa on the growth rods.

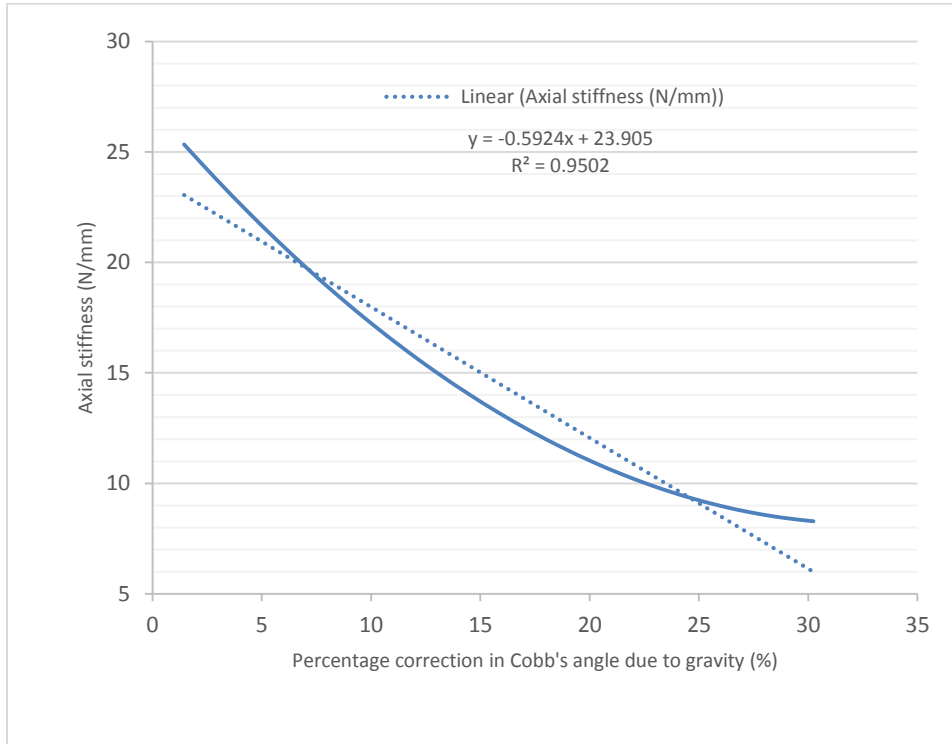


Figure 5-51: The graph shows the relation between the axial stiffness of Group 1A FE model and percentage correction obtained at that given stiffness with gravitational loads.

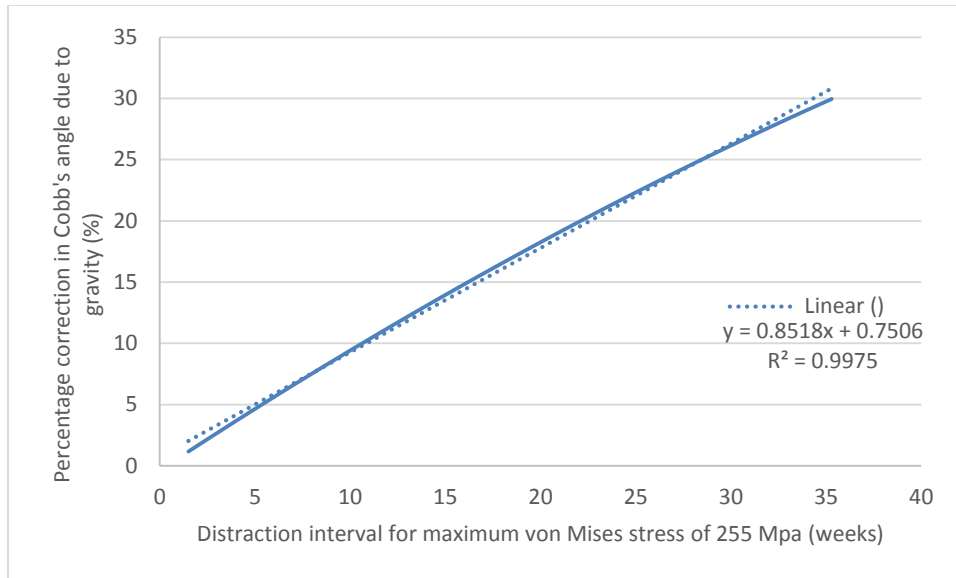


Figure 5-52: The graph established relationship between maximum allowed distraction interval (for maximum von Mises stress up to 255 MPa) on the rod for a given percentage of Cobb's angle correction observed (related to axial stiffness) under gravitational loads.

### 5.7 *In vitro* evaluation of screw loosening

Group 1 specimens with optimal distraction force had a peak force values, during pull-out, of 979.5 N (T1-left pedicle), 1013.7 N (T1-right pedicle), 973.9 N (T2-left pedicle), 911.13 N (T2-right pedicle), 1201.2 N (T3-left pedicle) and 980.5 N (T3- right pedicle), while the group 2 specimens with high distraction force had a peak force values of 608.6 N (T4-left pedicle), 775.3 N (T4-right pedicle), 763.4 N (T10-left pedicle), 701.2 N (T10-right pedicle), 679.2 N (T11-left pedicle), and 944.7 N (T11-right pedicle). The mean values were 1009.9 N and 745.4 N for optimal and high distraction force respectively. The P-value for unpaired t-test (one sided and unequal variance) was 0.0008.

# Chapter 6

## Discussion

### 6.1 Overview

The effects of distraction force on T1-S1 growth, sagittal contours, the loads at the screw-bone interface and maximum von Mises stresses on the rods were studied. Both normal and scoliotic juvenile spine models were chosen for the study. A normal juvenile spine model was first used to isolate the effect of distraction force and frequency on spinal growth, sagittal contours, and maximum von Mises stresses on the rods, thus producing results independent of the severity of deformity and curve rigidity. This study was the first of its kind and provided insight into the effect of the distraction force and frequency on a normal juvenile spine. Next, multiple scoliotic spine models were developed to corroborate the trends in results observed using a normal juvenile spine and to analyze the accompanied changes to the Cobb's angle. To further investigate the effects on the results with changes in material properties a sensitivity analysis was performed. Additionally *in vitro* study was undertaken to relate the results of high loads at screw-bone interface to screw loosening.

## **6.2 Effect of distraction force**

Using a normal juvenile spine, the thoracic kyphosis and lumbar lordosis decreased consistently with increases in distraction force resulting in hypo-kyphosis at thoracic and hypo-lordosis at lumbar regions, immediately after distraction. This decrease in kyphosis at thoracic and lordosis at lumbar regions is a result of distraction but was recovered to a varying extent during the growth period. Distraction forces of 150 N, 200 N and 250 N recovered the thoracic kyphosis close to the intact baseline. Similarly, the lumbar lordosis recovered close to the intact baseline with 200 N, 250 N, and 300 N of distraction forces. The current study suggests that final kyphosis after 6 months increases with lower initial distraction force. On the contrary, lower final kyphosis was observed with higher distraction forces. The optimal range for proper conservation of sagittal balance was 200-250 N for this normal juvenile spine model. Using representative scoliotic spine models, it was found that the Cobb's angle correction achieved with optimal distraction force was able to prevent the progression of deformity although higher distraction force did result in better correction. Desired Cobb's angle correction is a factor that is dependent on the extent of deformity, in extreme cases, higher distraction forces may be the only option available for the surgeons, although, in mild cases, a compromise could be made to reduce propensity towards rod fracture. Maintenance of sagittal contour is another important factor, and like the results obtained from normal juvenile spine, representative scoliotic spine models also showed that the changes in kyphosis and lordosis were minimum for optimal distraction forces.

Rod fracture is a common complication of growing rod treatments as has been highlighted in several studies<sup>10-12</sup>. Therefore, lowering the stresses on the rods will help in reducing the occurrence of failure. For the normal juvenile spine the maximum von Mises stress on the rod, immediately after distraction, increased unidirectional from 50 N to 400 N of distraction force. It can be seen that the distraction force of 200 N to 250 N resulted in the lowest maximum von Mises stress at 6 months post op. The factor of safety (fatigue strength of medical grade titanium is 510 MPa at 10 million cycle) is 11 at 6 months with 250 N of distraction force, while it is 2.7 and 5.3 with 50 N and 400 N of distraction forces respectively. Similarly using representative scoliotic spines, the maximum von Mises stress was lowest in the vicinity of optimal distraction force at 6 months period. It was found that for these spine models, forces greater than 100N on concave side and 75 N on convex side resulted in unnecessary growth in expense of increased complication, i.e. higher stresses on the rod.

Screw loosening is one of the other common complications that is often clinically observed.[3, 4] The average load at the screw-bone interface, at the end of 6 months, was lowest for 150 N, 200 N and 250 N with the normal juvenile spine model. Additionally, the loads exerted increased bi-directionally with either increase or decrease of distraction forces, i.e. either side of this range. The load at the screw-bone interface was also analysed for representative scoliotic spine and it followed the same trend as that for the maximum von Mises's stress on the rod at both 0 and 6 months.

T1-S1 height increased with increase in distraction force. For normal juvenile spine, the distraction force of 250 N resulted in optimal growth.[14] Distraction forces above 250N stimulated the growth (more than 8.6 mm) while distraction forces below that stunted the

growth (less than 8.6 mm). Recent clinical literature suggest that distractive forces stimulate apophyseal growth of the axial skeleton with growth rods, compared to normal growth rate.[5, 6] This could have occurred through applying a higher distraction force than optimal amount. Similarly for representative scoliotic spines the distraction force of 100-75 sustained the growth i.e., it caused the growth equal to that of the intact baseline, while distraction forces of 100all, 150-125, and 150all stimulated the growth i.e., it resulted in higher growth than intact baseline. This trend is similar to what was observed in clinical studies.[51, 99, 126]

As discussed above for this normal juvenile spine of 9 year old child, 250 N of distraction force resulted in growth sustenance with overall minimum stresses on the rod, minimum forces on vertebrae by pedicle screws and minimum changes in sagittal contours. Similar trend was observed with multiple representative scoliotic spine models with optimal force of 100-75 and 100all. The trends observed in this study indicate that there might also exist an optimal force for a scoliotic spine. Although the optimal force values may be very different depending upon the rigidity of the curves.

### **6.3 Effect of distraction frequency**

As mentioned previously, rod breakage is the main issue with the use of growth rods in patients. However there is limited literature that sheds light on the failure mechanism though [15-17, 20, 21, 124, 127] Yang et al. found that the risk of rod fracture increases with single rods, stainless steel rods and smaller diameter rods. They also found that rod fracture was more prevalent among patient preoperative ability of ambulation.[20] However, rod fracture has been reported in non-ambulatory patients too. The mean time



reported for rod fracture was  $25 \pm 21$  months and the mean time after distraction was  $5.8 \pm 3$  months. Hence fracture could occur anytime; earlier or at a later stage.[20]

Previous section demonstrated the effect of distraction forces on the biomechanics and growth modulation of a juvenile normal spine under a dual growth rod intervention for the period of 6 months. They highlight the importance of selection of optimal distraction force magnitude for better surgical outcome like sustained T1-S1 growth, unaltered sagittal contours, minimum stresses on the rods and lower load at the bone-screw interface.[125]

In this section discussion on frequency of distraction of growth rods on stresses on the rod up to a period of 2 years has been presented. For normal juvenile spine model, the maximum stress on the rod was highest immediately after distraction and decreases non-linearly during the period between two distractions. The highest maximum von Mises stresses on the rod for the duration of 24 months decreased with increase in frequency of rod distraction. It is known that 6 months of low intensity activity like walking accounts for about 900,000-1,350,000 cycles of stress.[128] The fatigue strength of titanium shown in Figure 5-13 is for 10,000,000 cycles of stress. This means that for an ambulatory patient with low intensity activity like walking, the titanium rod may fracture in 7 years period if the stresses on the rod exceed the fatigue strength of titanium (i.e. 510 MPa). Distraction frequencies of 12 months, 6 months and 3 months the fatigue failure stress value of 510 MPa on the rod is attained by 12 months, 18 months and 21 months respectively. The stresses could be of higher or lower magnitudes than the ones shown in the figures depending upon the stiffness of the spine. The main finding of this study is that reduction of stresses by means of frequent distraction could be a means of reducing the occurrence of rod failure. Additionally, as an instance it can be seen in Figure 5-12 that first two

distractions at 6 months interval produces stresses well below the fatigue strength of titanium. However the third distraction at 6 months produces stresses close to fatigue strength of titanium. This implies that infrequent distractions could still be used in the beginning and after few distraction it should then be followed by more frequent distraction. With traditional dual growth rods, frequent distraction is not an option, but with the use of MCGR it is feasible. In addition to analyzing the frequency of distraction, the effect of change in material (cobalt-chromium and stainless steel) of the rod was also analyzed. There was a 9-15% increase in the highest maximum von Mises stresses on the rods as compared to titanium. This is attributed to the higher elastic modulus of the cobalt chromium (210 GPa) and stainless steel (190 GPa) than titanium (115 GPa). For comparison between these three materials we used the fatigue strength divided by the highest stress observed on the rod, i.e. factor of safety. H.I.P cobalt chromium, forged cobalt-chromium and Titanium 6AL-4V showed the highest factor of safety for all intervals of distraction, while cast cobalt-chromium, forged 316L stainless steel, and cast 316L stainless steel showed the lowest factor of safety (Figure 5-15). This was due to higher fatigue strength of H.I.P cobalt chromium, forged cobalt-chromium and Titanium 6AL-4V and lower fatigue strength of cast cobalt-chromium, forged 316L stainless steel, and cast 316L stainless steel. Another factor that would affect the result of the study is rod diameter. The rod diameter used in the study was 4.5 mm, however a larger diameter rod will reduce the maximum stresses on the rod. Although using a larger diameter rod may increase the surface strain on the rod during preoperative rod contouring resulting in higher propensity of fatigue crack initiation. This might be mitigated by using pre-contoured rod. Besides this, various other studies have investigated and compared the fatigue performance of

spinal rods made of different materials. Dick et al tested 6.35 mm diameter rod of titanium alloy, pure titanium, and stainless steel using four point bending.[129] They found that the stainless steel rods achieved one million cycles regardless of treatment, whereas the fatigue life of titanium alloy rods was reduced by bender marks and bolt interconnection and that of pure titanium rods was reduced by bender marks and set screw marks. Following this, Lindsey et al performed a bilateral vertebrectomy constructs using straight and contoured (using a French bender) 5.5 and 6.0 mm diameter rods of titanium alloy, pure titanium, and 316L stainless steel.[130] Their results showed that contouring reduces the low cycle fatigue life of titanium (pure and alloy) without changing the endurance limit. Furthermore, the fatigue performance of contoured stainless steel rods were similar and superior to both contoured titanium rod types even with a smaller rod diameter. Similar to the previous author, Nguyen et al with the same experimental setup concluded that the fatigue life of contoured 6 mm cobalt chrome rods was similar to 5.5 mm stainless steel rods, whereas it was greater than the 6.0 mm titanium alloy rods.[131] Slivka et al later performed a comparative experiment (using unilateral vertebrectomy constructs) between 6.35 mm diameter titanium alloy rods and pure titanium rods, and found that the endurance limit of the contoured titanium alloy rods was the same as the contoured pure titanium rods even though straight titanium alloy rods had an endurance limit that was twice as high as the pure titanium rods.[132] The author then extended the study by using four different rod materials of 4.5 mm diameter each.[132] It was found that the endurance limits of titanium alloy, standard stainless steel and ultra stainless steel were reduced between 20% and 40% after bending (to a radius of 100 mm). However, titanium alloy rods, standard stainless steel rods and ultra stainless steel rods showed higher endurance limits after over bending

(to a radius of 50 mm) and then re-bending (to a radius of 100 mm) compared to single bending (to a radius of 100 mm). They also found that in all conditions, the endurance limit of the CoCr rods was at least 25% higher than the other materials. Other than the use of various materials, coating of implant in population with contact dermatitis to metal has a high prevalence. Nickel is the most common allergen in United States with up to 17% and 3% allergic responses in women and in men respectively. This is followed by cobalt and chromium, with 1% to 9% allergic responses respectively.[133] Titanium alloys and pure titanium are often used in patients with nickel and cobalt chrome allergies. Moreover, pure titanium is reported to be inert in the human body, immune to body fluid attack, and strong and flexible. Therefore, coating of spinal rods in fusionless instrumentation is not a common practice, However, Zielinski et al recently published a retrospective case report of a single patient with hypersensitivity to titanium, niobium, molybdenum, iron, high-grade stainless-steel implants and aluminum, among others.[134] For this special case a plasma-spray carbon-coated Vertical Expandable Prosthetic Titanium Ribs (VEPTR) rods were engineered and supplied (Synthes, Inc., West Chester, PA). They achieved good results with no sensitivity after 4.5 years of follow-up. To further analyse failure of rods we can use known fatigue tensile strength of titanium and compare it with the maximum von Mises stresses on the rod (at different frequency and at different distraction) to conclude if fracture or yield of the rod would occur. The fatigue strength of titanium is 510 MPa and therefore for the given FE model there is a high propensity for rod failure to occur at 12 months (for 12 monthly distraction), at 18 months (for 6 monthly distraction) and at 21 months (for 3 monthly distraction) because the maximum von Mises stress in these three cases are higher than 550 MPa.

Along with normal juvenile spine, five multiple representative scoliotic were also simulated to look at the frequency of distraction of growth rods and its effect on the stresses on the rod generated over a period of two years. For each case, the maximum von Mises stress was always higher on the subsequent distraction and hence, the last distraction showed the highest maximum von Mises stress on the rod. The highest maximum von Mises stress on the rod for the duration of 24 months decreased with an increase in frequency of rod distraction. The shorter distraction period may not be required in all patients but it may prove tremendously helpful for patients with stiffer spines or patients who need higher magnitude of distraction to improve lung function (by stimulation of growth). The results of the study also implied that to reduce the stresses on the rods, the frequency of distraction could be increased on consecutive distraction (as the spine is stiffening due to autofusion) as opposed to the very beginning itself. The current scoliotic spine data shows similar trends to the normal juvenile spine data, which showed that frequent distractions would require smaller distraction forces and thus, will induce lower stresses in the rods.[135]

#### **6.4 Sensitivity Study**

In the current study we have analyzed a method to translate clinically significant information obtained from our previous finite element studies on lowering the incidence of growth rod fracture. Discussion in previous sections highlights that a shorter distraction

intervals lower the stresses on the rod by reducing the amount of distraction required at each increment. The results from the sensitivity study helps translate this information into clinical practice. We developed and simulated multiple models varying in materials properties (to account for stiffness variation among the scoliotic patient) to establish a relationship between axial stiffness of the spine, percentage correction in Cobb's angle due to gravity, and required distraction interval, for factor of safety equal to two. The result of the study shows that by measuring the percentage correction before the surgery, a specific distraction interval could be chosen based on the required factor of safety for the growth rods.

The idea behind using a graphical representation, instead of a single number for the ideal distraction frequency is based on existence of variance in spinal stiffness among the patients. As with all surgical procedure, patient selection is an important factor that affects the efficacy of any technique. A frequency that is ideal for one patient may not be suitable for the other. Therefore this study refrains from selecting a particular distraction frequency as a cautionary measure. However we do recommend a higher frequencies of distraction (whenever possible) with the optimal distraction force as an ideal choice to reduce von Mises stresses on the rods. However proper understanding of assumptions is a prerequisite before using these numbers for the patients. These specific values and recommendations are limited to 9 year age group based on typical anatomical considerations (intervertebral disc height). Additionally the growth rods used in this study were 4.5 mm in diameter with Ti6Al4V as material type.

Spinal stiffness is another variable, and it changes over time (autofusion), therefore proper considerations are required to estimate the change in patient's stiffness and hence a

new distraction frequency. Distraction frequency and distraction forces are integrated, i.e. for every distraction frequency there is an optimal distraction force. Therefore, reducing distraction interval with the aim of reducing the propensity of rod fracture also requires a reduction in the distraction force. This optimal value is equivalent to the force required to distract the spine for the specific distraction interval. It is because of this reduction in optimal distraction force that the stresses on the rod reduces. Therefore, theoretically the distraction force of approximately zero magnitude would ideally mean a growth rod technology where the growth rods is able to sense the change in compressive stresses, and undergoes automated lengthening as a negative feedback mechanism.

### **6.5 *In Vitro* Screw Loosening**

The results of pull out study after 6 months of fatigue showed that the higher distraction forces combined with everyday cyclic motion could reduce the pull out load of the screw by 26% in average compared to an optimal distraction force combined with everyday cyclic motions. Based on this data, screw loosening is imminent with high loads at screw-bone interface due to high distraction forces.

### **6.6 Limitations**

Results acquired from this model, as with all biomechanical models, should be interpreted with consideration of certain limitations. First, there are no muscle forces in our model but this limitation is mitigated by using a follower load. As published by Patwardhan et al., using a follower load provides a similar kinematics response as in vivo.[136] Second, there is no material data available for juvenile scoliotic spine and hence, normal juvenile

spine data was used. As shown with the sensitivity analysis, change in material properties would affect the magnitude of stresses but the general trend would be similar. This implies that a spine that is more flexible would show lower stresses on the rods with the same distraction force magnitude. On the other hand, a stiffer spine would show higher stresses on the rods with the same distraction force magnitude. In addition to this, unavailability of cadaveric osteoligamentous juvenile spine range of motion data is a limitation. Nevertheless we compared the lumbar range of motion of the normal juvenile spine with another pediatric lumbar spine model. The differences in range of motion value between the current juvenile FE model and the previously published pediatric FE model ranged from -0.2 to 0.3 degrees. These differences are insignificant compared to the standard deviations that naturally exist among adult cadaveric studies i.e. about 8-12 degrees, 4-8 degrees and 3-6 degrees in flexion-extension, lateral bending and axial rotation respectively at individual lumbar functional spinal units.[137] Third, the surgical procedure of initial rod attachment was not simulated. The scoliotic curves are considerably larger before the surgery (more than 45-50 degrees), however the curves are corrected to about 40-50% percent by dual growth rod attachment, given their non-structural nature.[138] This requires a simulation step where the correction is achieved by simulating attachment of the rod to the spine model. Although biomechanical models based on the non-linear finite elements are profusely used in scoliosis, their discontinuous nature, large variations in displacements and element stiffness produces mathematical inconsistencies that cause convergence difficulties.[139] Considering this, most surgical simulations in scoliosis are simulated using kinematic models.[139] However for our purposes, biomechanical models were indispensable (output requirements of stresses on the rod surface and growth



simulation based on changing stresses on the growth plate layer), therefore a constant 35 degrees Cobb angle post initial surgery (after growth rod attachment) was simulated to account for the final curve. To estimate the percentage error in stresses generated on the rod, we applied 0.75 Nm of bending moment (suggestive of bending moment generated for 50% correction) on normal juvenile spine model after application of different distraction forces (250 N, 125 N, 63 N, and 32 N).[98] It was found that the maximum von Mises stresses on the rod increased by 18-23 MPa in extension and decreased by 5-11 MPa in flexion. For lateral bending and axial rotation, the maximum von Mises stresses on the rod increased by 9-26 MPa and 13-44 MPa respectively. These values constitute about 5-8% of the maximum von Mises stresses generated on the rods after application of distraction forces. Fourth, screw loosening study was performed for 6 months however with continued loading the loosening may or may not aggravate. However longer duration was not tested because it would be a major deviation from a physiological loading scenario because both bone resorption and formation are taking place at the interface and there could be a major change at the interface after periods longer than 6 months.[140, 141] Therefore to refrain from overestimating or underestimating the pullout strength a shorter duration of 6 months was chosen.

In addition to the above limitation, there is a need to interpret the results and how it would vary with change in basic assumptions used in the current study. Both, the intervertebral height and the axial stiffness are crucial inputs for the values obtained in the results section. Changes in intervertebral height would change the optimal distraction forces, for example a larger disc height would require a lower distraction force due to reduction in the required strain. Similarly axial stiffness affects the optimal distraction

forces as shown by the sensitivity analysis. The magnitude of  $\beta$ , the growth proportionality constant, was adopted from literature, and more or less might vary due to various biological factors or due to disturbed growth plate mechanotransduction in scoliotic patients.[81] The lower magnitude mean lower sensitivity at growth plates and this would raise the magnitude of required optimal distraction force, for a given distraction frequency. In contrary, higher magnitude mean higher sensitivity and this would reduce the magnitude of required optimal distraction force, for a given distraction frequency. The stresses observed on the rods would also vary with both material type (as previously discussed) and geometry. The current study uses the prevalent size of 4.5 mm rod, however changing the diameter would change the stresses generated on the rod. A higher stresses would be generated on the rods with smaller diameter and vice versa. Contouring of rod, using benders, is another factor that might result in lower fatigue strength with Ti6AL4V. This could be mitigated by using a stainless steel or cobalt-chrome rods. However, this predisposes the growth rods to galvanic corrosion, due to dissimilarity in material type between pedicle screws (usually Ti6AL4V) and rods. Although clinical data are lacking, the use of titanium alloy screws and Co-Cr rods appears to be justified from explant analysis and in vitro electrochemical experiments.[142]

Lastly, there are few recommendation for future work. Surgical planning and decision consists of several variables like, preoperative flexibility, age, height, weight, intervertebral disc height, preoperative coronal, axial and sagittal contours, size and type of growth rods etc. Therefore, development and validation of a technique to consistently generate a simplified patient specific model (either beam element or volumetric model), based on the above inputs, could assist in the surgeon's decision making. This would help

the surgeon make informed decisions, to achieve the require growth and halt the progression of scoliosis without major complications. Another avenue of research could be a growth rod that could sense the minute changes in stresses generated at the growth plate, and result in automated distraction. Understanding growth and finding better mechanism to predict growth could also prove beneficial to several patients. Some patients might not grow in height, and the misjudgment of using growth rods in such patient might put them in unnecessary socio-economic burden. Besides these recommendations, the current study could be furthered by in vivo studies using suitable animal models and also by controlled prospective clinical research involving higher frequency (along with lower distraction) than standard for one group of patients.

## **6.7 Conclusions**

The effects of distraction force on T1-S1 growth, sagittal contours, the loads at the screw-bone interface and maximum von Mises stresses on the rods were analyzed. In addition to that, the effects of frequency of distraction on maximum von Mises stresses on the rods for different loading conditions were also studied. The study satisfies all the hypotheses as outlined earlier. It was found that an optimal distraction force exists for which the growth is sustained with least maximum von Mises stresses on the rod, lowest load on the screw-bone interface and altered sagittal contours at the end of 6 months.

Additionally the result of this study signifies the importance of shorter distraction period in reducing the stresses on the rods. The results of the study also implied that to reduce the stresses on the rods, the distraction interval can be shortened as a function of time, i.e. using

standard distraction period (6 months) for first 2-3 distractions, followed by shorter distraction intervals (1-2 months) on consecutive ones as per patient's requirements.

The current study also highlighted a method of translating fundamental information from finite element modeling to clinical arena for mitigating the occurrence of growth rod fracture, besides establishing a relationship between optimal distraction interval and curve rigidity. Lastly, the *in vitro* results corroborates the significance of reduction of high loads at screw-bone interface by using an optimal distraction force or a shorter distraction interval to lower the incidence of screw loosening.

## References

1. Thompson, G.H., et al., *Comparison of single and dual growing rod techniques followed through definitive surgery: a preliminary study*. Spine (Phila Pa 1976), 2005. **30**(18): p. 2039-44.
2. Yang, J.S., et al., *Growing rod fractures: risk factors and opportunities for prevention*. Spine (Phila Pa 1976), 2011. **36**(20): p. 1639-44.
3. ZHAO, Y., et al., *Comparison of initial efficacy between single and dual growing rods in treatment of early onset scoliosis*. Chinese Medical Journal, 2012. **125**(16): p. 2862-2866.
4. Li, Q.Y., et al., *Primary effect of dual growing rod technique for the treatment of severe scoliosis in young children*. Chin Med J (Engl), 2010. **123**(2): p. 151-5.
5. Olgun, Z.D., et al., *Vertebral Body Growth During Growing Rod Instrumentation: Growth Preservation or Stimulation?* Journal of Pediatric Orthopaedics, 2012. **32**(2): p. 184-189.
6. Demirkiran, G., et al., *Effects of the Fusionless Instrumentation on the Disks and Facet Joints of the Unfused Segments: A Pig Model*. Journal of Pediatric Orthopaedics, 2013.

7. Akbarnia, B.A., et al., *Dual growing rod technique for the treatment of progressive early-onset scoliosis: a multicenter study*. Spine, 2005. **30**(17S): p. S46-S57.
8. Lonstein, J.E. and J.M. Carlson, *The prediction of curve progression in untreated idiopathic scoliosis during growth*. J Bone Joint Surg Am, 1984. **66**(7): p. 1061-71.
9. Wiggins, G.C., et al., *Pediatric spinal deformities*. Neurosurg Focus, 2003. **14**(1): p. e3.
10. Gillingham, B.L., R.A. Fan, and B.A. Akbarnia, *Early onset idiopathic scoliosis*. J Am Acad Orthop Surg, 2006. **14**(2): p. 101-12.
11. Green, N.E., *Part-time bracing of adolescent idiopathic scoliosis*. J Bone Joint Surg Am, 1986. **68**(5): p. 738-42.
12. Gomez, J.A., et al., *"Growth friendly" spine surgery: management options for the young child with scoliosis*. Journal of the American Academy of Orthopaedic Surgeons, 2011. **19**(12): p. 722-727.
13. Akbarnia, B.A., M. Yazici, and G.H. Thompson, *The growing spine: Management of spinal disorders in young children*. 2011: Springer.
14. Stokes, I.A.F. and L. Windisch, *Vertebral height growth predominates over intervertebral disc height growth in adolescents with scoliosis*. Spine, 2006. **31**(14): p. 1600-1604.
15. Akbarnia, B.A., et al., *Fusionless procedures for the management of early-onset spine deformities in 2011: what do we know?* Journal of children's orthopaedics, 2011. **5**(3): p. 159-172.

16. Yang, J.S., et al., *Growing rods for spinal deformity: characterizing consensus and variation in current use*. Journal of Pediatric Orthopaedics, 2010. **30**(3): p. 264-270.
17. Akbarnia, B.A., et al., *Dual growing rod technique followed for three to eleven years until final fusion: the effect of frequency of lengthening*. Spine, 2008. **33**(9): p. 984-990.
18. Thompson, G.H., B.A. Akbarnia, and R.M. Campbell Jr, *Growing rod techniques in early-onset scoliosis*. Journal of Pediatric Orthopaedics, 2007. **27**(3): p. 354-361.
19. Sankar, W.N., D.C. Acevedo, and D.L. Skaggs, *Comparison of complications among growing spinal implants*. Spine, 2010. **35**(23): p. 2091-2096.
20. Yang, J.S., et al., *Growing rod fractures: risk factors and opportunities for prevention*. Spine, 2011. **36**(20): p. 1639-1644.
21. Bess, S., et al., *Complications of Growing-Rod Treatment for Early-Onset Scoliosis Analysis of One Hundred and Forty Patients*. The Journal of Bone & Joint Surgery, 2010. **92**(15): p. 2533-2543.
22. Klemme, W.R., et al., *Spinal instrumentation without fusion for progressive scoliosis in young children*. Journal of Pediatric Orthopaedics, 1997. **17**(6): p. 734-742.
23. Sakai, D.S., L.A. Tomlinson, and J.P. Dormans, *Distraction Phenomenon After Lengthening of Spinal Growing Rods A Case Report*. The Journal of Bone & Joint Surgery Case Connector, 2012. **2**(3): p. e45 1-4.

24. Noordeen, H.M., et al., *In Vivo Distraction Force and Length Measurements of Growing Rods: Which Factors Influence the Ability to Lengthen?* Spine, 2011. **36**(26): p. 2299.
25. Akbarnia, B.A., et al., *Innovation in growing rod technique: a study of safety and efficacy of a magnetically controlled growing rod in a porcine model.* Spine (Phila Pa 1976), 2012. **37**(13): p. 1109-1114.
26. Chen, W.J., P.L. Lai, and L.H. Chen, *Adjacent instability after instrumented lumbar fusion.* Chang Gung Med J, 2003. **26**(11): p. 792-8.
27. Bogduk, N., *Clinical anatomy of the lumbar spine and sacrum.* 2005: Elsevier Health Sciences.
28. Panjabi, M.M., et al., *Human lumbar vertebrae: quantitative three-dimensional anatomy.* Spine, 1992. **17**(3): p. 299-306.
29. Hirsch, C., B.-E. Ingelmark, and M. Miller, *The anatomical basis for low back pain: studies on the presence of sensory nerve endings in ligamentous, capsular and intervertebral disc structures in the human lumbar spine.* Acta orthopaedica, 1963. **33**(1-4): p. 1-17.
30. Rissanen, P.M., *The surgical anatomy and pathology of the supraspinous and interspinous ligaments of the lumbar spine with special reference to ligament ruptures.* Acta Orthopaedica, 1960. **31**(S46): p. 3-100.
31. Nachemson, A.L. and J.H. Evans, *Some mechanical properties of the third human lumbar interlaminar ligament (ligamentum flavum).* Journal of biomechanics, 1968. **1**(3): p. 211-220.



32. Panjabi, M.M., *The stabilizing system of the spine. Part I. Function, dysfunction, adaptation, and enhancement.* Journal of spinal disorders & techniques, 1992. **5**(4): p. 383-389.
33. MAYER, T.G., et al., *Quantification of Lumbar Function: Part 2: Sagittal Plane Trunk Strength in Chronic Low-Back Pain Patients.* Spine, 1985. **10**(8): p. 765-772.
34. Roaf, R., *Vertebral growth and its mechanical control.* J Bone Joint Surg Br, 1960. **42**(1): p. 40-59.
35. Panjabi, M.M. and A.A. White III, *Basic biomechanics of the spine.* Neurosurgery, 1980. **7**(1): p. 76-93.
36. Mehta, M.H., *Growth as a corrective force in the early treatment of progressive infantile scoliosis.* J Bone Joint Surg Br, 2005. **87**(9): p. 1237-47.
37. Koumbourlis, A.C., *Scoliosis and the respiratory system.* Paediatr Respir Rev, 2006. **7**(2): p. 152-60.
38. Goldberg, C.J., et al., *Respiratory function and cosmesis at maturity in infantile-onset scoliosis.* Spine (Phila Pa 1976), 2003. **28**(20): p. 2397-406.
39. Karol, L.A., et al., *Pulmonary function following early thoracic fusion in non-neuromuscular scoliosis.* J Bone Joint Surg Am, 2008. **90**(6): p. 1272-81.
40. Akbarnia, B.A., *Pediatric spine fractures.* Orthop Clin North Am, 1999. **30**(3): p. 521-36, x.
41. Akbarnia, B.A., et al., *Dual growing rod technique for the treatment of progressive early-onset scoliosis: a multicenter study.* Spine (Phila Pa 1976), 2005. **30**(17 Suppl): p. S46-57.

42. Sponseller, P.D., et al., *Growing rods for infantile scoliosis in Marfan syndrome*. Spine (Phila Pa 1976), 2009. **34**(16): p. 1711-5.
43. Blakemore, L.C., et al., *Submuscular Isola rod with or without limited apical fusion in the management of severe spinal deformities in young children: preliminary report*. Spine (Phila Pa 1976), 2001. **26**(18): p. 2044-8.
44. Moe, J.H., et al., *Harrington instrumentation without fusion plus external orthotic support for the treatment of difficult curvature problems in young children*. Clin Orthop Relat Res, 1984(185): p. 35-45.
45. Klemme, W.R., et al., *Spinal instrumentation without fusion for progressive scoliosis in young children*. J Pediatr Orthop, 1997. **17**(6): p. 734-42.
46. Mineiro, J. and S.L. Weinstein, *Subcutaneous rodding for progressive spinal curvatures: early results*. J Pediatr Orthop, 2002. **22**(3): p. 290-5.
47. Skaggs, K.F., et al., *Upper thoracic pedicle screw loss of fixation causing spinal cord injury: a review of the literature and multicenter case series*. J Pediatr Orthop, 2013. **33**(1): p. 75-9.
48. Mahar, A.T., et al., *Biomechanical comparison of four different fixation techniques for pediatric tibial eminence avulsion fractures*. J Pediatr Orthop, 2008. **28**(2): p. 159-62.
49. Sakai, D.S., L.A. Tomlinson, and J.P. Dormans, *Distraction Phenomenon After Lengthening of Spinal Growing Rods*. JBJS Case Connector, 2012. **2**(3): p. e45.
50. Demirkiran, G., et al., *Effects of the Fusionless Instrumentation on the Disks and Facet Joints of the Unfused Segments: A Pig Model*. Journal of Pediatric Orthopaedics, 2014. **34**(2): p. 185-193.

51. Olgun, Z.D., et al., *Vertebral body growth during growing rod instrumentation: growth preservation or stimulation?* J Pediatr Orthop, 2012. **32**(2): p. 184-9.
52. Smith, J.T. and R.M. Campbell, Jr., *Magnetically controlled growing rods for spinal deformity.* Lancet, 2012. **379**(9830): p. 1930-1.
53. Kain, Z.N., et al., *Preoperative anxiety in children. Predictors and outcomes.* Arch Pediatr Adolesc Med, 1996. **150**(12): p. 1238-45.
54. Wick, J.M. and J. Konze, *A magnetic approach to treating progressive early-onset scoliosis.* AORN J, 2012. **96**(2): p. 163-73.
55. Akbarnia, B.A., et al., *Next generation of growth-sparing techniques: preliminary clinical results of a magnetically controlled growing rod in 14 patients with early-onset scoliosis.* Spine (Phila Pa 1976), 2013. **38**(8): p. 665-70.
56. Cheung, K.M.-C., et al., *Magnetically controlled growing rods for severe spinal curvature in young children: a prospective case series.* The Lancet, 2012. **379**(9830): p. 1967-1974.
57. Dannawi, Z., et al., *Early results of a remotely-operated magnetic growth rod in early-onset scoliosis.* Bone Joint J, 2013. **95-B**(1): p. 75-80.
58. Hickey, B.A., et al., *Early experience of MAGEC magnetic growing rods in the treatment of early onset scoliosis.* Eur Spine J, 2014. **23** Suppl 1: p. S61-5.
59. Hickey, B.A., et al., *Early experience of MAGEC magnetic growing rods in the treatment of early onset scoliosis.* Eur Spine J, 2014.
60. Akbarnia, B.A., et al., *Dual growing rod technique followed for three to eleven years until final fusion: the effect of frequency of lengthening.* Spine (Phila Pa 1976), 2008. **33**(9): p. 984-90.

61. Ghista, D.N., et al., *Biomechanical basis of optimal scoliosis surgical correction*. J Biomech, 1988. **21**(2): p. 77-88.
62. Viviani, G.R., et al., *Biomechanical analysis and simulation of scoliosis surgical correction*. Clin Orthop Relat Res, 1986(208): p. 40-7.
63. Subbaraj, K., D.N. Ghista, and G.R. Viviani, *Presurgical finite element simulation of scoliosis correction*. J Biomed Eng, 1989. **11**(1): p. 9-18.
64. Noone, G., et al., *Biomechanical simulations of scoliotic spinal deformity and correction*. Australas Phys Eng Sci Med, 1993. **16**(2): p. 63-74.
65. Martino, J., et al., *Biomechanical analysis of vertebral derotation techniques for the surgical correction of thoracic scoliosis. A numerical study through case simulations and a sensitivity analysis*. Spine (Phila Pa 1976), 2013. **38**(2): p. E73-83.
66. Brassey, C.A., et al., *Finite element modelling versus classic beam theory: comparing methods for stress estimation in a morphologically diverse sample of vertebrate long bones*. J R Soc Interface, 2013. **10**(79): p. 20120823.
67. Cheng, F.H., et al., *Finite element analysis of the scoliotic spine under different loading conditions*. Biomed Mater Eng, 2010. **20**(5): p. 251-9.
68. Mao, H., et al., *Development of high-quality hexahedral human brain meshes using feature-based multi-block approach*. Comput Methods Biomech Biomed Engin, 2013. **16**(3): p. 271-9.
69. Fok, J., S. Adeeb, and J. Carey, *FEM Simulation of Non-Progressive Growth from Asymmetric Loading and Vicious Cycle Theory: Scoliosis Study Proof of Concept*. Open Biomed Eng J, 2010. **4**: p. 162-9.

70. Azegami, H., et al., *Etiology of idiopathic scoliosis. Computational study*. Clin Orthop Relat Res, 1998(357): p. 229-36.
71. Berteau, J.P., et al., *Beyond the classic correction system: a numerical nonrigid approach to the scoliosis brace*. Spine J, 2011. **11**(5): p. 424-31.
72. Clin, J., et al., *A new method to include the gravitational forces in a finite element model of the scoliotic spine*. Med Biol Eng Comput, 2011. **49**(8): p. 967-77.
73. Abolaeha, O.A., J. Weber, and L.T. Ross, *Finite element simulation of a scoliotic spine with periodic adjustments of an attached growing rod*. Conf Proc IEEE Eng Med Biol Soc, 2012. **2012**: p. 5781-5.
74. Desbiens-Blais, F., et al., *New brace design combining CAD/CAM and biomechanical simulation for the treatment of adolescent idiopathic scoliosis*. Clin Biomech (Bristol, Avon), 2012. **27**(10): p. 999-1005.
75. Little, J.P. and C. Adam, *Towards determining soft tissue properties for modelling spine surgery: current progress and challenges*. Med Biol Eng Comput, 2012. **50**(2): p. 199-209.
76. Little, J.P., et al., *An FE investigation simulating intra-operative corrective forces applied to correct scoliosis deformity*. Scoliosis, 2013. **8**(1): p. 9.
77. Rohlmann, A., et al., *Flexible non-fusion scoliosis correction systems reduce intervertebral rotation less than rigid implants and allow growth of the spine: a finite element analysis of different features of orthobiom*. Eur Spine J, 2008. **17**(2): p. 217-23.

78. Lin, H., et al., *Mechanobiological bone growth: comparative analysis of two biomechanical modeling approaches*. Med Biol Eng Comput, 2009. **47**(4): p. 357-66.
79. Driscoll, M., et al., *The role of spinal concave-convex biases in the progression of idiopathic scoliosis*. Eur Spine J, 2009. **18**(2): p. 180-7.
80. Lalonde, N.M., et al., *Biomechanical modeling of the lateral decubitus posture during corrective scoliosis surgery*. Clin Biomech (Bristol, Avon), 2010. **25**(6): p. 510-6.
81. Shi, L., et al., *Biomechanical analysis and modeling of different vertebral growth patterns in adolescent idiopathic scoliosis and healthy subjects*. Scoliosis, 2011. **6**: p. 11.
82. Driscoll, M., et al., *Biomechanical comparison of fusionless growth modulation corrective techniques in pediatric scoliosis*. Med Biol Eng Comput, 2011. **49**(12): p. 1437-45.
83. Ji, S., et al., *Automated subject-specific, hexahedral mesh generation via image registration*. Finite Elem Anal Des, 2011. **47**(10): p. 1178-1185.
84. Shivanna, K.H., S.C. Tadepalli, and N.M. Grosland, *Feature-Based Multiblock Finite Element Mesh Generation*. Comput Aided Des, 2010. **42**(12): p. 1108-1116.
85. Li, Z., et al., *Development, validation, and application of a parametric pediatric head finite element model for impact simulations*. Ann Biomed Eng, 2011. **39**(12): p. 2984-97.
86. Sigal, I.A., M.R. Hardisty, and C.M. Whyne, *Mesh-morphing algorithms for specimen-specific finite element modeling*. J Biomech, 2008. **41**(7): p. 1381-9.

87. Sigal, I.A. and C.M. Whyne, *Mesh morphing and response surface analysis: quantifying sensitivity of vertebral mechanical behavior*. Ann Biomed Eng, 2010. **38**(1): p. 41-56.
88. Bah, M.T., P.B. Nair, and M. Browne, *Mesh morphing for finite element analysis of implant positioning in cementless total hip replacements*. Med Eng Phys, 2009. **31**(10): p. 1235-43.
89. Grassi, L., et al., *Evaluation of the generality and accuracy of a new mesh morphing procedure for the human femur*. Med Eng Phys, 2011. **33**(1): p. 112-20.
90. O'Reilly, M.A. and C.M. Whyne, *Comparison of computed tomography based parametric and patient-specific finite element models of the healthy and metastatic spine using a mesh-morphing algorithm*. Spine (Phila Pa 1976), 2008. **33**(17): p. 1876-81.
91. Salo, Z., M. Beek, and C.M. Whyne, *Evaluation of mesh morphing and mapping techniques in patient specific modeling of the human pelvis*. Int J Numer Method Biomed Eng, 2013. **29**(1): p. 104-13.
92. Carr, J.C., W.R. Fright, and R.K. Beatson, *Surface interpolation with radial basis functions for medical imaging*. IEEE Trans Med Imaging, 1997. **16**(1): p. 96-107.
93. Anderson, A.L., et al., *The effect of posterior thoracic spine anatomical structures on motion segment flexion stiffness*. Spine (Phila Pa 1976), 2009. **34**(5): p. 441-6.
94. Oda, I., et al., *An in vitro human cadaveric study investigating the biomechanical properties of the thoracic spine*. Spine (Phila Pa 1976), 2002. **27**(3): p. E64-70.
95. Goodwin, R.R., et al., *Distraction and compression loads enhance spine torsional stiffness*. J Biomech, 1994. **27**(8): p. 1049-57.

96. Engsberg, J.R., et al., *Methods to locate center of gravity in scoliosis*. Spine (Phila Pa 1976), 2003. **28**(23): p. E483-9.
97. Lopez-Valdes, F.J., et al., *The biomechanics of the pediatric and adult human thoracic spine*. Ann Adv Automot Med, 2011. **55**: p. 193-206.
98. Agarwal, A., et al., *Smaller Interval Distractions May Reduce Chances of Growth Rod Breakage Without Impeding Desired Spinal Growth: A Finite Element Study*. Spine Deformity, 2014. **2**(6): p. 430-436.
99. Agarwal, A., et al., *Effect of Distraction Force on Growth and Biomechanics of the Spine: A Finite Element Study on Normal Juvenile Spine With Dual Growth Rod Instrumentation*. Spine Deformity, 2014. **2**(4): p. 260-269.
100. Agarwal, A., et al., *Distraction magnitude and frequency affects the outcome in Juvenile Idiopathic Patients with Growth Rods: Finite Element Study Using a Representative Scoliotic Spine Model*. The Spine Journal, 2015.
101. Yoganandan, N.A., et al. *Pediatric and small female neck injury scale factors and tolerance based on human spine biomechanical characteristics*. in *Proceedings of the International Research Council on the Biomechanics of Injury conference*. 2000. International Research Council on Biomechanics of Injury.
102. Kumaresan, S., N. Yoganandan, and F.A. Pintar, *Age-specific pediatric cervical spine biomechanical responses: three-dimensional nonlinear finite element models*. 1997, SAE Technical Paper.
103. Liu, X. and J. Yang, *Development of child pedestrian mathematical models and evaluation with accident reconstruction*. Traffic Injury Prevention, 2002. **3**(4): p. 321-329.



104. Dong, L., et al., *Development and validation of a 10-year-old child ligamentous cervical spine finite element model*. Ann Biomed Eng, 2013. **41**(12): p. 2538-52.
105. Meijer, G.J.M., *Development of a non-fusion scoliosis correction device: numerical modelling of scoliosis correction*. 2011: University of Twente.
106. Stokes, I.A. and J.P. Laible, *Three-dimensional osseo-ligamentous model of the thorax representing initiation of scoliosis by asymmetric growth*. J Biomech, 1990. **23**(6): p. 589-95.
107. Villemure, I., et al., *Biomechanical simulations of the spine deformation process in adolescent idiopathic scoliosis from different pathogenesis hypotheses*. Eur Spine J, 2004. **13**(1): p. 83-90.
108. Watanabe, K., et al., *Vertebral derotation in adolescent idiopathic scoliosis causes hypokyphosis of the thoracic spine*. BMC Musculoskelet Disord, 2012. **13**: p. 99.
109. Little, J.P. and C.J. Adam, *The effect of soft tissue properties on spinal flexibility in scoliosis: biomechanical simulation of fulcrum bending*. Spine (Phila Pa 1976), 2009. **34**(2): p. E76-82.
110. Little, J.P., et al., *Investigating the change in three dimensional deformity for idiopathic scoliosis using axially loaded MRI*. Clin Biomech (Bristol, Avon), 2012. **27**(5): p. 415-21.
111. Gesbert, J.C., et al., *A new 3D geometrical modelling of adolescent idiopathic scoliosis*. Comput Methods Biomech Biomed Engin, 2011. **14**(S1): p. 221-222.
112. Palepu, V., *Doctor of Philosophy Degree in Biomedical Engineering*. 2013, The University of Toledo.

113. Kumaresan, S., et al., *Biomechanical study of pediatric human cervical spine: a finite element approach*. J Biomech Eng, 2000. **122**(1): p. 60-71.
114. Robinson, C.M. and M.J. McMaster, *Juvenile idiopathic scoliosis. Curve patterns and prognosis in one hundred and nine patients*. J Bone Joint Surg Am, 1996. **78**(8): p. 1140-8.
115. Kotwicki, T., M. Napiontek, and A. Nowakowski, *Transverse plane of apical vertebra of structural thoracic curve: vertebra displacement versus vertebral deformation*. Stud Health Technol Inform, 2006. **123**: p. 164-8.
116. Stokes, I., R.G. Burwell, and P.H. Dangerfield, *Biomechanical spinal growth modulation and progressive adolescent scoliosis-a test of the 'vicious cycle' pathogenetic hypothesis: Summary of an electronic focus group debate of the IBSE*. Scoliosis, 2006. **1**(16): p. 7161-1.
117. Kumaresan, S., et al., *Biomechanical study of pediatric human cervical spine: a finite element approach*. Journal of biomechanical engineering, 2000. **122**(1): p. 60-71.
118. Jebaseelan, D.D., et al. *Quantification of segmental flexibilities of juvenile lumbar spinal column using a three-dimensional finite element model (FEM)*. in *6th World Congress of Biomechanics (WCB 2010). August 1-6, 2010 Singapore*. 2010. Springer.
119. Jebaseelan, D.D., et al., *Validation efforts and flexibilities of an eight-year-old human juvenile lumbar spine using a three-dimensional finite element model*. Medical & biological engineering & computing, 2010. **48**(12): p. 1223-1231.

120. Jebaseelan, D.D., et al., *Sensitivity studies of pediatric material properties on juvenile lumbar spine responses using finite element analysis*. Medical & biological engineering & computing, 2012. **50**(5): p. 515-522.
121. Agarwal, A., et al., *Biomechanical evaluation of an endplate-conformed polycaprolactone-hydroxyapatite intervertebral fusion graft and its comparison with a typical nonconformed cortical graft*. J Biomech Eng, 2013. **135**(6): p. 61005-9.
122. Schultz, A., et al., *Analysis and quantitative myoelectric measurements of loads on the lumbar spine when holding weights in standing postures*. Spine, 1982. **7**(4): p. 390-397.
123. Villemure, I. and I.A. Stokes, *Growth plate mechanics and mechanobiology. A survey of present understanding*. J Biomech, 2009. **42**(12): p. 1793-803.
124. Thompson, G.H., et al., *Comparison of single and dual growing rod techniques followed through definitive surgery: a preliminary study*. Spine, 2005. **30**(18): p. 2039-2044.
125. Agarwal, A., et al., *Effect of Distraction Force on Growth and Biomechanics of the Spine: A Finite Element Study on Normal Juvenile Spine with Dual Growth Rod Instrumentation (In press: Manuscript Number: SDF-D-13-00133R2)*. Spine deformity, 2014.
126. Demirkiran, G., et al., *Effects of the fusionless instrumentation on the disks and facet joints of the unfused segments: a pig model*. J Pediatr Orthop, 2014. **34**(2): p. 185-93.

127. Farooq, N., et al., *Minimizing complications with single submuscular growing rods: a review of technique and results on 88 patients with minimum two-year follow-up.* Spine (Phila Pa 1976), 2010. **35**(25): p. 2252-2258.
128. Bergeron, A.J., A. Munk, and O. Surgeon, *SPINAL ROD FATIGUE TESTING AND ANALYSIS.*
129. Dick, J.C. and C.A. Bourgeault, *Notch sensitivity of titanium alloy, commercially pure titanium, and stainless steel spinal implants.* Spine (Phila Pa 1976), 2001. **26**(15): p. 1668-72.
130. Lindsey, C., et al., *The effects of rod contouring on spinal construct fatigue strength.* Spine (Phila Pa 1976), 2006. **31**(15): p. 1680-7.
131. Nguyen, T.Q., et al., *The fatigue life of contoured cobalt chrome posterior spinal fusion rods.* Proc Inst Mech Eng H, 2011. **225**(2): p. 194-8.
132. Slivka, M.A., Y.K. Fan, and J.C. Eck, *The Effect of Contouring on Fatigue Strength of Spinal Rods: Is it Okay to Re-bend and Which Materials Are Best?* Spine Deformity, 2013. **1**(6): p. 395-400.
133. Galetz, M.C., et al., *Abrasion resistance of oxidized zirconium in comparison with CoCrMo and titanium nitride coatings for artificial knee joints.* J Biomed Mater Res B Appl Biomater, 2010. **93**(1): p. 244-51.
134. Zielinski, J., T.A. Lacy, and J.H. Phillips, *Carbon Coated Implants as a New Solution for Metal Allergy in Early-Onset Scoliosis: A Case Report and Review of the Literature.* Spine Deformity, 2014. **2**(1): p. 76-80.

135. Agarwal, A., et al., *Smaller Interval Distractions may Reduce Chances of Growth Rod Breakage without Impeding the Desired Spinal Growth: A Finite Element Study*. Spine Deformity, 2014.
136. Patwardhan, A.G., et al., *Effect of compressive follower preload on the flexion-extension response of the human lumbar spine*. J Orthop Res, 2003. **21**(3): p. 540-6.
137. Cook, D.J., M.S. Yeager, and B.C. Cheng, *Range of motion of the intact lumbar segment: a multivariate study of 42 lumbar spines*. Int J Spine Surg, 2015. **9**: p. 5.
138. Flynn, J.M., et al., *Growing-rod graduates: lessons learned from ninety-nine patients who completed lengthening*. J Bone Joint Surg Am, 2013. **95**(19): p. 1745-50.
139. Aubin, C.E., et al., *Biomechanical modeling of posterior instrumentation of the scoliotic spine*. Comput Methods Biomech Biomed Engin, 2003. **6**(1): p. 27-32.
140. Chappard, D., et al., *The early remodeling phases around titanium implants: a histomorphometric assessment of bone quality in a 3-and 6-month study in sheep*. The International journal of oral & maxillofacial implants, 1998. **14**(2): p. 189-196.
141. Mavrogenis, A., et al., *Biology of implant osseointegration*. J Musculoskelet Neuronal Interact, 2009. **9**(2): p. 61-71.
142. Kummer, F.J. and R.M. Rose, *Corrosion of titanium/cobalt-chromium alloy couples*. J Bone Joint Surg Am, 1983. **65**(8): p. 1125-6.

## Appendix A

### The Matlab Codes

```
%Matlab Code for Group 1A

%reading the normal spine nodes

[node, X, Y, Z] = textread('thoraciclumbarnodes.txt','%d,%f,%f,%f',176555);

cobbangle1=39*(pi/180);

cobbangle2=0*(pi/180);

inflectionZ1=380.9009901;

inflectionZ2=347.5643564;

inflectionZ3=252.3168317;

inflectionZ4=147.5445545;

inflectionZ5=90.3960396;

maxdeltaX1=(((inflectionZ2-inflectionZ4)/2)/tan((pi/2)-(cobbangle1/2)));

maxdeltaX2=0;

%formatting matrices to solve for coefficient of the equation of locus of

%the scoliotic curve
```

```

A=[1 inflectionZ1 inflectionZ1^2 inflectionZ1^3 inflectionZ1^4 inflectionZ1^5
inflectionZ1^6 inflectionZ1^7;
0 1 2*inflectionZ1 3*inflectionZ1^2 4*inflectionZ1^3 5*inflectionZ1^4
6*inflectionZ1^5 7*inflectionZ1^6;
1 inflectionZ2 inflectionZ2^2 inflectionZ2^3 inflectionZ2^4 inflectionZ2^5
inflectionZ2^6 inflectionZ2^7;
1 inflectionZ3 inflectionZ3^2 inflectionZ3^3 inflectionZ3^4 inflectionZ3^5
inflectionZ3^6 inflectionZ3^7;
0 1 2*inflectionZ3 3*inflectionZ3^2 4*inflectionZ3^3 5*inflectionZ3^4
6*inflectionZ3^5 7*inflectionZ3^6;
1 inflectionZ4 inflectionZ4^2 inflectionZ4^3 inflectionZ4^4 inflectionZ4^5
inflectionZ4^6 inflectionZ4^7;
0 1 2*inflectionZ5 3*inflectionZ5^2 4*inflectionZ5^3 5*inflectionZ5^4
6*inflectionZ5^5 7*inflectionZ5^6;
1 inflectionZ5 inflectionZ5^2 inflectionZ5^3 inflectionZ5^4 inflectionZ5^5
inflectionZ5^6 inflectionZ5^7];
%boundary condition
B=[-11;0;0;maxdeltaX1;0;0;0;0];
%coefficients
C=A\B;
deltaX=size(X);
deltaZ=size(Z);
newX=size(X);

```

```

newZ=size(Z);
slope=size(Z);
fid=fopen('newthoraciclumbarnodes.txt','w');
for i=1:176555
    if(Z(i)>inflectionZ5&&Z(i)<inflectionZ1)
        deltaX(i)=C(1)+C(2)*(Z(i))+C(3)*(Z(i)^2)+C(4)*(Z(i)^3)+C(5)*(Z(i)^4)+C(6)*(Z(i)^5)
+C(7)*(Z(i)^6)+C(8)*(Z(i)^7);

slope(i)=C(2)+2*C(3)*(Z(i))+3*C(4)*(Z(i)^2)+4*C(5)*(Z(i)^3)+5*C(6)*(Z(i)^4)+6*C(7
)*(Z(i)^5)+7*C(8)*(Z(i)^6);

        newX(i)=X(i)+(deltaX(i)*(sin(pi/2-atan(slope(i))))^2);

slope(i)=(C(2)+2*C(3)*(Z(i))+3*C(4)*(Z(i)^2)+4*C(5)*(Z(i)^3)+5*C(6)*(Z(i)^4)+6*C(
7)*(Z(i)^5)+7*C(8)*(Z(i)^6));

        deltaZ(i)=((X(i)+deltaX(i))*(sin(pi/2-atan(slope(i))))*(cos(pi/2-atan(slope(i)))));
        newZ(i)=Z(i)-deltaZ(i);
    elseif(Z(i)>inflectionZ1)
        newX(i)=X(i)-11;
        newZ(i)=Z(i);
    else
        newZ(i)=Z(i);
        newX(i)=X(i);
    end
end

```



```

    fprintf(fid,'%d, %f, %f, %f\n', node(i), newX(i), Y(i), newZ(i));
end
fclose(fid);

%Matlab Code for Group 1B

%reading the normal spine nodes
[node, X, Y, Z] = textread('thoraciclumbarnodes.txt','%d,%f,%f,%f',176555);
cobbangle1=39*(pi/180);
cobbangle2=24*(pi/180);
inflectionZ1=380.9009901;
inflectionZ2=347.5643564;
inflectionZ3=252.3168317;
inflectionZ4=147.5445545;
inflectionZ5=47.53465347;
inflectionZ6=-63.9009901;
maxdeltaX1=((inflectionZ2-inflectionZ4)/2)/tan((pi/2)-(cobbangle1/2));
maxdeltaX2=(-(inflectionZ4-inflectionZ6)/2)/tan((pi/2)-(cobbangle2/2));
%formatting matrices to solve for coefficient of the equation of locus of
%the scoliotic curve
A=[1 inflectionZ1 inflectionZ1^2 inflectionZ1^3 inflectionZ1^4 inflectionZ1^5
inflectionZ1^6 inflectionZ1^7 inflectionZ1^8 inflectionZ1^9;
0 1 2*inflectionZ1 3*inflectionZ1^2 4*inflectionZ1^3 5*inflectionZ1^4 6*inflectionZ1^5
7*inflectionZ1^6 8*inflectionZ1^7 9*inflectionZ1^8];

```

```
1 inflectionZ2 inflectionZ2^2 inflectionZ2^3 inflectionZ2^4 inflectionZ2^5
inflectionZ2^6 inflectionZ2^7 inflectionZ2^8 inflectionZ2^9;
```

```
1 inflectionZ3 inflectionZ3^2 inflectionZ3^3 inflectionZ3^4 inflectionZ3^5
inflectionZ3^6 inflectionZ3^7 inflectionZ3^8 inflectionZ3^9;
```

```
0 1 2*inflectionZ3 3*inflectionZ3^2 4*inflectionZ3^3 5*inflectionZ3^4 6*inflectionZ3^5
7*inflectionZ3^6 8*inflectionZ3^7 9*inflectionZ3^8;
```

```
1 inflectionZ4 inflectionZ4^2 inflectionZ4^3 inflectionZ4^4 inflectionZ4^5
inflectionZ4^6 inflectionZ4^7 inflectionZ4^8 inflectionZ4^9;
```

```
1 inflectionZ5 inflectionZ5^2 inflectionZ5^3 inflectionZ5^4 inflectionZ5^5
inflectionZ5^6 inflectionZ5^7 inflectionZ5^8 inflectionZ5^9;
```

```
0 1 2*inflectionZ5 3*inflectionZ5^2 4*inflectionZ5^3 5*inflectionZ5^4 6*inflectionZ5^5
7*inflectionZ5^6 8*inflectionZ5^7 9*inflectionZ5^8;
```

```
1 inflectionZ6 inflectionZ6^2 inflectionZ6^3 inflectionZ6^4 inflectionZ6^5
inflectionZ6^6 inflectionZ6^7 inflectionZ6^8 inflectionZ6^9;
```

```
0 1 2*inflectionZ6 3*inflectionZ6^2 4*inflectionZ6^3 5*inflectionZ6^4 6*inflectionZ6^5
7*inflectionZ6^6 8*inflectionZ6^7 9*inflectionZ6^8];
```

```
%boundary condition
```

```
B=[-11;0;0;maxdeltaX1;0;0;maxdeltaX2;0;0;0];
```

```
%coefficients
```

```
C=A\B;
```

```
deltaX=size(X);
```

```
deltaZ=size(Z);
```

```
newX=size(X);
```

```

newZ=size(Z);
slope=size(Z);
fid=fopen('newthoraciclumbarnodes.txt','w');
for i=1:176555
    if(Z(i)<inflectionZ1&&Z(i)>inflectionZ6
        deltaX(i)=C(1)+C(2)*(Z(i))+C(3)*(Z(i)^2)+C(4)*(Z(i)^3)+C(5)*(Z(i)^4)+C(6)*(Z(i)^5)
+C(7)*(Z(i)^6)+C(8)*(Z(i)^7)+C(9)*(Z(i)^8)+C(10)*(Z(i)^9);

        slope(i)=C(2)+2*C(3)*(Z(i))+3*C(4)*(Z(i)^2)+4*C(5)*(Z(i)^3)+5*C(6)*(Z(i)^4)+6*C(7
)*C(8)*(Z(i)^5)+7*C(8)*(Z(i)^6)+8*C(9)*(Z(i)^7)+9*C(10)*(Z(i)^8);

        newX(i)=X(i)+(deltaX(i)*(sin(pi/2-atan(slope(i))))^2);

        slope(i)=(C(2)+2*C(3)*(Z(i))+3*C(4)*(Z(i)^2)+4*C(5)*(Z(i)^3)+5*C(6)*(Z(i)^4)+6*C(
7)*(Z(i)^5)+7*C(8)*(Z(i)^6)+8*C(9)*(Z(i)^7)+9*C(10)*(Z(i)^8));

        deltaZ(i)=((X(i)+deltaX(i))*(sin(pi/2-atan(slope(i))))*(cos(pi/2-atan(slope(i)))));

        newZ(i)=Z(i)-deltaZ(i);
    elseif(Z(i)>inflectionZ1)
        newX(i)=X(i)-11;
        newZ(i)=Z(i);
    elseif(Z(i)<inflectionZ6)
        newX(i)=X(i);
        newZ(i)=Z(i);
    else

```

```

newZ(i)=Z(i);
newX(i)=X(i);
end
fprintf(fid,'%d, %f, %f, %f\n', node(i), newX(i), Y(i), newZ(i));
end
fclose(fid);

```

%Matlab Code for Group 2

%reading the normal spine nodes

```
[node, X, Y, Z] = textread('thoraciclumbarnodes.txt','%d,%f,%f,%f',176555);
```

```
cobbangle1=40*(pi/180);
```

```
cobbangle2=0*(pi/180);
```

```
inflectionZ1=380.9009901;
```

```
inflectionZ2=223.7425743;
```

```
inflectionZ3=-23.9009901;
```

```
maxdeltaX1=(((inflectionZ1-inflectionZ3)/2)/tan((pi/2)-(cobbangle1/2)));
```

```
maxdeltaX2=0;
```

%formatting matrices to solve for coefficient of the equation of locus of

%the scoliotic curve

```
A=[1 inflectionZ1 inflectionZ1^2 inflectionZ1^3 inflectionZ1^4;
```

```
0 1 2*inflectionZ1 3*inflectionZ1^2 4*inflectionZ1^3;
```

```
1 inflectionZ2 inflectionZ2^2 inflectionZ2^3 inflectionZ2^4;
```

```
1 inflectionZ3 inflectionZ3^2 inflectionZ3^3 inflectionZ3^4;
```

```

0 1 2*inflectionZ3 3*inflectionZ3^2 4*inflectionZ3^3];

%boundary condition

B=[16;0;maxdeltaX1;0;0];

%coefficients

C=A\B;

deltaX=size(X);

deltaZ=size(Z);

newX=size(X);

newZ=size(Z);

slope=size(Z);

fid=fopen('newthoraciclumbarnodes.txt','w');

for i=1:176555

    if(Z(i)>inflectionZ3&&Z(i)<inflectionZ1)

        deltaX(i)=C(1)+C(2)*(Z(i))+C(3)*(Z(i)^2)+C(4)*(Z(i)^3)+C(5)*(Z(i)^4);

        slope(i)=C(2)+2*C(3)*(Z(i))+3*C(4)*(Z(i)^2)+4*C(5)*(Z(i)^3);

        newX(i)=X(i)+(deltaX(i)*(sin(pi/2-atan(slope(i))))^2);

        slope(i)=(C(2)+2*C(3)*(Z(i))+3*C(4)*(Z(i)^2)+4*C(5)*(Z(i)^3));

        deltaZ(i)=((X(i)+deltaX(i))*(sin(pi/2-atan(slope(i))))*(cos(pi/2-atan(slope(i)))));

        newZ(i)=Z(i)-deltaZ(i);

    elseif(Z(i)>inflectionZ1)

        newX(i)=X(i)+16;

        newZ(i)=Z(i);

    elseif(Z(i)<inflectionZ3)

```

```

        newX(i)=X(i);
        newZ(i)=Z(i);
    else
        newZ(i)=Z(i);
        newX(i)=X(i);
    end
    fprintf(fid,'%d, %f, %f, %f\n', node(i), newX(i), Y(i), newZ(i));
end
fclose(fid);

```

%Matlab Code for Group 3

%reading the normal spine nodes

```
[node, X, Y, Z] = textread('thoraciclumbarnodes.txt','%d,%f,%f,%f',176555);
```

```
cobbangle1=28*(pi/180);
```

```
cobbangle2=0*(pi/180);
```

```
inflectionZ1=380.9009901;
```

```
inflectionZ2=299.9405941;
```

```
inflectionZ3=147.5445545;
```

```
inflectionZ4=-23.9009901;
```

```
maxdeltaX1=((inflectionZ2-inflectionZ4)/2)/tan((pi/2)-(cobbangle1/2));
```

```
maxdeltaX2=0;
```

%formatting matrices to solve for coefficient of the equation of locus of

%the scoliotic curve

```

A=[1 inflectionZ1 inflectionZ1^2 inflectionZ1^3 inflectionZ1^4 inflectionZ1^5
inflectionZ1^6;
0 1 2*inflectionZ1 3*inflectionZ1^2 4*inflectionZ1^3 5*inflectionZ1^4
6*inflectionZ1^5;
1 inflectionZ2 inflectionZ2^2 inflectionZ2^3 inflectionZ2^4 inflectionZ2^5
inflectionZ2^6;
1 inflectionZ3 inflectionZ3^2 inflectionZ3^3 inflectionZ3^4 inflectionZ3^5
inflectionZ3^6;
0 1 2*inflectionZ3 3*inflectionZ3^2 4*inflectionZ3^3 5*inflectionZ3^4
6*inflectionZ3^5;
1 inflectionZ4 inflectionZ4^2 inflectionZ4^3 inflectionZ4^4 inflectionZ4^5
inflectionZ4^6;
0 1 2*inflectionZ4 3*inflectionZ4^2 4*inflectionZ4^3 5*inflectionZ4^4
6*inflectionZ4^5];
%boundary condition
B=[-16;0;0;maxdeltaX1;0;0;0];
%coefficients
C=A\B;
deltaX=size(X);
deltaZ=size(Z);
newX=size(X);
newZ=size(Z);
slope=size(Z);

```

```

fid=fopen('newthoraciclumbarnodes.txt','w');

for i=1:176555

    if(Z(i)>inflectionZ4&&Z(i)<inflectionZ1)

        deltaX(i)=C(1)+C(2)*(Z(i))+C(3)*(Z(i)^2)+C(4)*(Z(i)^3)+C(5)*(Z(i)^4)+C(6)*(Z(i)^5)
        +C(7)*(Z(i)^6);

        slope(i)=C(2)+2*C(3)*(Z(i))+3*C(4)*(Z(i)^2)+4*C(5)*(Z(i)^3)+5*C(6)*(Z(i)^4)+6*C(7)
        )*(Z(i)^5);

        newX(i)=X(i)+(deltaX(i)*(sin(pi/2-atan(slope(i))))^2);

        slope(i)=(C(2)+2*C(3)*(Z(i))+3*C(4)*(Z(i)^2)+4*C(5)*(Z(i)^3)+5*C(6)*(Z(i)^4)+6*C(
        7)*(Z(i)^5));

        deltaZ(i)=((X(i)+deltaX(i))*(sin(pi/2-atan(slope(i))))*(cos(pi/2-atan(slope(i)))));

        newZ(i)=Z(i)-deltaZ(i);

    elseif(Z(i)>inflectionZ1)

        newX(i)=X(i)-16;

        newZ(i)=Z(i);

    elseif(Z(i)<inflectionZ4)

        newX(i)=X(i);

        newZ(i)=Z(i);

    else

```



```

newZ(i)=Z(i);
newX(i)=X(i);
end
fprintf(fid,'%d, %f, %f, %f\n', node(i), newX(i), Y(i), newZ(i));
end
fclose(fid);

```

%Matlab Code for Group 4

%reading the normal spine nodes

```
[node, X, Y, Z] = textread('thoraciclumbarnodes.txt','%d,%f,%f,%f',176555);
```

```
cobbangle1=22*(pi/180);
```

```
cobbangle2=30*(pi/180);
```

```
inflectionZ1=380.9009901;
```

```
inflectionZ2=223.7425743;
```

```
inflectionZ3=171.3564356;
```

```
inflectionZ4=80.87128713;
```

```
inflectionZ5=-63.9009901;
```

```
maxdeltaX1=(((inflectionZ1-inflectionZ3)/2)/tan((pi/2)-(cobbangle1/2)));
```

```
maxdeltaX2=(-(inflectionZ3-inflectionZ5)/2)/tan((pi/2)-(cobbangle2/2));
```

%formatting matrices to solve for coefficient of the equation of locus of

%the scoliotic curve

```
A=[1 inflectionZ1 inflectionZ1^2 inflectionZ1^3 inflectionZ1^4 inflectionZ1^5
```

```
inflectionZ1^6;
```

```

0 1 2*inflectionZ1 3*inflectionZ1^2 4*inflectionZ1^3 5*inflectionZ1^4 6*inflectionZ1^5;
1 inflectionZ2 inflectionZ2^2 inflectionZ2^3 inflectionZ2^4 inflectionZ2^5
inflectionZ2^6;
1 inflectionZ3 inflectionZ3^2 inflectionZ3^3 inflectionZ3^4 inflectionZ3^5
inflectionZ3^6;
1 inflectionZ4 inflectionZ4^2 inflectionZ4^3 inflectionZ4^4 inflectionZ4^5
inflectionZ4^6;
1 inflectionZ5 inflectionZ5^2 inflectionZ5^3 inflectionZ5^4 inflectionZ5^5
inflectionZ5^6;
0 1 2*inflectionZ5 3*inflectionZ5^2 4*inflectionZ5^3 5*inflectionZ5^4
6*inflectionZ5^5];
%boundary condition
B=[11;0;maxdeltaX1;0;maxdeltaX2;0;0];
%coefficients
C=A\B;
deltaX=size(X);
deltaZ=size(Z);
newX=size(X);
newZ=size(Z);
slope=size(Z);
fid=fopen('newthoraciclumbarnodes.txt','w');

for i=1:176555

```

```

if(Z(i)<inflectionZ1&&Z(i)>inflectionZ5)

deltaX(i)=C(1)+C(2)*(Z(i))+C(3)*(Z(i)^2)+C(4)*(Z(i)^3)+C(5)*(Z(i)^4)+C(6)*(Z(i)^5)
+C(7)*(Z(i)^6);
slope(i)=C(2)+2*C(3)*(Z(i))+3*C(4)*(Z(i)^2)+4*C(5)*(Z(i)^3)+5*C(6)*(Z(i)^4)+6*C(7
)*(Z(i)^5);

newX(i)=X(i)+(deltaX(i)*(sin(pi/2-atan(slope(i))))^2);
slope(i)=(C(2)+2*C(3)*(Z(i))+3*C(4)*(Z(i)^2)+4*C(5)*(Z(i)^3)+5*C(6)*(Z(i)^4)+6*C(
7)*(Z(i)^5));

deltaZ(i)=((X(i)+deltaX(i))*(sin(pi/2-atan(slope(i))))*(cos(pi/2-atan(slope(i)))));
newZ(i)=Z(i)-deltaZ(i);
elseif(Z(i)>inflectionZ1)

newX(i)=X(i)+11;

newZ(i)=Z(i);

elseif(Z(i)<inflectionZ5)

newX(i)=X(i);

newZ(i)=Z(i);

else

newZ(i)=Z(i);

newX(i)=X(i);

end

fprintf(fid,'%d, %f, %f, %f\n', node(i), newX(i), Y(i), newZ(i));

end

```

```
fclose(fid);
```